Density Functional Theory:
Toward Better Understanding of Complex Systems in Chemistry and Physics

A Dissertation
SUBMITTED TO THE FACULTY OF
UNIVERSITY OF MINNESOTA
BY

Sije Luo

IN PARTIAL FULFILLMENT OF THE REQUIREMENTS
FOR THE DEGREE OF
DOCTOR OF PHILOSOPHY

Advisor: Professor Donald G. Truhlar

June 2014

Acknowledgements

I want to particularly thank Professor Donald G. Truhlar, whose continuous supports and encouragements made all the work presented here possible. One of the wisest and most aspiring human beings I have ever met, Don is a true mentor in both work and life.

I also want to thank Professor Laura Gagliardi for her helps in class, my fellowship applications, and collaborative research projects. I am grateful for all the other faculty members in my preliminary and thesis committee – Professor Sanford Lipsky, Professor Ilja Siepmann, and Professor Matteo Cococcioni.

I find it lucky to be surrounded by a body of brilliant researchers. My special thank you goes to my closet collaborators in various projects – Yan Zhao, Roberto Peverati, Xuefei Xu, Ke Yang, Boris Averkiev, Haoyu Yu, Shaohong Li, Wenjing Zhang, and Giovanni Li Manni.

I owe an unimaginable amount to my parents, without whose support I would not have travelled so far.

Finally, I feel more than blessed to have Chulan Qing, my fiancée, in my life for the past seven years. Her supports helped me through difficulties that would otherwise be insurmountable, and her love made every bit of my effort worthwhile.

Dedication

This dissertation is dedicated to Chulan Qing, for whom I try to be a better self.

Abstract

Density functional theory (DFT) has become the workhorse of computational chemistry and physics in the past two decades. The continuous developments of high-quality exchange-correlation functionals (xcFs) have enabled chemists and physicists to study complex as well as large systems with high accuracy at low-to-moderate computational expense. Although a wide range of normal systems have been well understood by DFT, there are still complex ones presenting particular challenges where most commonly used xcFs have failed due to the complex nature of the system, lack of or difficulty to obtain reliable reference data, or the practical limitations of the Kohn-Sham DFT (KS-DFT) formulation.

This thesis presents studies with various exchange-correlation functionals on a wide selection of complex systems in chemistry and solid-state physics, including large organic molecules, adsorption on metallic surfaces, transition states, as well as transition metal atoms, ions, and compounds, to (i) draw conclusions upon recommendations of xcFs for important practical applications; (ii) understand the root of errors to help design better xcFs or propose new theoretical schemes of DFT; (iii) explore the utility of noncollinear spin orbitals in KS-DFT for better description of multi-reference systems.

Table of Contents

List of Tables

List of Figures

Preface

The following are citations for previously published works reproduced in this thesis:

Chapter 2.

Adapted from Luo, S.; Zhao, Y.; Truhlar, D. G. Validation of electronic structure methods for isomerization reactions of large organic molecules, *Phys. Chem. Chem. Phys.* **2011**, *13*, 13683. –Reproduced by Permission of the PCCP Owner Societies.

Chapter 3.

Adapted with permission from Luo, S.; Zhao, Y.; Truhlar, D. G., Improved CO adsorption energies, site preferences, and surface formation energies from a meta-generalized-gradient-approximation exchange-correlation functional, M06-L, *J. Phys. Chem. Lett.*. **2012**, *3*, 2975.© 2012 American Chemical Society.

Chapter 4.

Adapted with permission from Luo, S.; Averkiev, B.; Yang, K. R.; Xu, X.; Truhlar, D. G., Density Functional Theory of Open-Shell Systems. The 3d-Series Transition Metal Atoms and Their Cations, *J. Chem. Theory Comput.*. **2014**, *10*, 102.© 2014 American Chemical Society.

Chapter 5.

Adapted with permission from Luo, S; Truhlar, D. G., How Evenly Can Approximate Density Functionals Treat the Different Multiplicities and Ionization States of 4d Transition Metal Atoms?, *J. Chem. Theory Comput.*. **2012**, *8*, 4112.© 2012 American Chemical Society.

Chapter 6.

Adapted with permission from Luo, S; Truhlar, D. G., Noncollinear Spin States for Density Functional Calculations of Open-Shell and Multi-Configurational Systems: Dissociation of MnO and NiO and Barrier Heights of O_3, BeH_2, and H_4, *J. Chem. Theory Comput.*. **2013**, *9*, 5439.© 2013 American Chemical Society.

Chapter 7.

Adapted with permission from Luo, S.; Rivalta, I.; Batista, V.; Truhlar, D. G., Noncollinear Spins Provide a Self-Consistent Treatment of the Low-Spin State of a Biomimetic Oxomanganese Synthetic Trimer Inspired by the Oxygen Evolving Complex of Photosystem II, *J. Phys. Chem. Lett.*. **2011**, *2*, 2629.© 2011 American Chemical Society.

Chapter 1

Introduction

1.1 Density Functional Theory (DFT)

1.1.1 Kohn-Sham Density Functional Theory (KS-DFT)

Density functional theory (DFT) has become the workhorse of computational chemistry and physics in the past two decades. DFT gained its popularity mainly due to its simple theory and low computational cost. The continuous developments of high-quality exchange-correlation functionals (xcFs) have enabled chemists and physicists to study complex as well as large systems with high accuracy at low-to-moderate computational expense.

DFT is based on the theorem[1] that all properties of the molecular systems can be determined by its electron density $\rho(\boldsymbol{r})$, where $\boldsymbol{r}$ is the spatial coordinates. At present, DFT is almost always applied in its Kohn-Sham formalism (KS-DFT)[2], which represents the density of the system under consideration by a single Slater determinant[3] (see Eq. 1.1) of a fictitious non-interacting system.

$$\Psi^{SD} = \frac{1}{\sqrt{N!}} \begin{vmatrix} \chi_1(\mathbf{x}_1) & \chi_2(\mathbf{x}_1) & \cdots & \chi_N(\mathbf{x}_1) \\ \chi_1(\mathbf{x}_2) & \chi_2(\mathbf{x}_2) & \cdots & \chi_N(\mathbf{x}_2) \\ \vdots & \vdots & \vdots & \vdots \\ \chi_1(\mathbf{x}_N) & \chi_2(\mathbf{x}_N) & \cdots & \chi_N(\mathbf{x}_N) \end{vmatrix} \tag{1.1}$$

Here N is the number of electrons, χ_i is the ith spin-orbital (see Section 1.3), and $\mathbf{x} = (\mathbf{r}, \omega)$, where $\mathbf{r}$ denotes the spatial coordinates, and ω represents the spin.

The energy of the system would then be written as

$$E[\rho] = E_{Ne}[\rho] + T[\rho] + J[\rho] + E_{xc}[\rho] \tag{1.2}$$

where E_{Ne}, T, and J are the nuclei-electron attraction, the kinetic energy, and electron-electron repulsion respectively. E_{xc} is the exchange-correlation energy, which represents all the remaining parts of the energy.

By finding the varational minimum of the energy with respect to the electron density, one arrives at the Kohn-Sham equations

$$\hat{f}_i \chi_i = \varepsilon_i \chi_i \tag{1.3}$$

where the Fock operator is written as

$$\hat{f}_i(\mathbf{r}_1) = -\sum_A^M \frac{Z_A}{r_{iA}} - \frac{1}{2}\nabla_i^2 + \int \frac{\rho(\mathbf{r}_2)}{r_{12}} d\mathbf{r}_2 + V_{xc}(\mathbf{r}_1) \tag{1.4}$$

Here the four terms on the right-hand side of the equation correspond to their counterparts in Eq. (1.1.2), and the exchange-correlation potential is defined as

$$V_{xc} = \frac{\delta E_{xc}}{\delta \rho} \tag{1.5}$$

Equations (1.2) to (1.4) can be solved by the self-consistent field (SCF) method, where the electron density and terms in eq. (1.4) are iteratively updated until convergence is achieved, and the total energy is obtained by integrating Eq. (1.2).

Here we only discuss KS-DFT for systems with an even number of electrons where all the orbitals are doubly occupied, e.g., closed-shell systems. A calculation of this type is called a restricted Kohn-Sham (RKS) calculation. It is, however, also possible to extend DFT to systems with singly-occupied orbitals, namely, open-shell systems. The extension can be accomplished by using of spin densities ρ_α and ρ_β instead of ρ, and is

called an unrestricted Kohn-Sham (UKS) calculation.[4] It can also be accomplished by using noncollinear spin-orbitals, as explained Section 1.3.

One appeal of DFT is that it is a strictly correct theory – the only unknown part in eq. (1.2) is the xcF. If the exact xcF were known, DFT could calculate the exact electronic energy of molecular systems. Nevertheless, one should bear in mind that:

(i) The Kohn-Sham orbitals χ are merely an imaginary design for facilitating calculations of electron densities, and they should not be over-interpreted.

(ii) Although DFT can solve the Schrödinger equation exactly with the unknown exact xcF, the resulting Slater determinant is not necessarily an eigenfunction of operators other than the Hamiltonian. For example, the SD may not be an eigenfunction of the $\boldsymbol{S}^2$ operator; thus a DFT solution with the correct energetics may not present the correct spin symmetry, e.g. a broken-symmetry (BS) solution is possible.

1.1.2 Exchange-correlation Functionals

As discussed in the previous section, the quest for the exact exchange-correlation functional is the ultimate goal in density functional theory. The success of DFT in the past two decades is mostly due to the emergence of high-quality approximate xcFs, and the approximate nature of xcFs also partially accounts for the errors of DFT in practical applications.

In a general way, xc functionals may be divided into two groups: hybrid, in which some local exchange is replaced by a percentage X of nonlocal Hartree-Fock exchange, and local, in which the xc functional depends only on local variables, in particular on the local values of spin-labeled electron density, ρ_σ, where σ is α or β, on optionally also

on the local values of the square of the reduced density gradient[5], s_σ^2 , which is defined as $\left|\nabla\rho_\sigma\right|^2 \Big/ \rho_\sigma^{8/3}$, and on the local values of the spin-labeled kinetic energy densities τ_α and τ_β . They can be further divided into 14 subtypes as follows:

Local exchange-correlation functionals

- LSDA: a functional that depends only on ρ_σ (for closed shells, this is sometimes called LDA)
- GGA: a functional that also depends on s_σ^2, with the separability requirement that the exchange functional for each spin component σ is expressed as a product of a function of ρ_σ time a function of s_σ^2 (the correlation functional also depends only on ρ_σ and s_σ^2)
- NGA: a functional that depends on the same variables as a GGA, but without the separability requirement[6]
- meta-GGA: a functional like a GGA, but that also depends on spin-labeled kinetic energy densities τ_α and τ_β
- range-separated meta-GGA: a functional like a meta-GGA, but the parameters of the functional depend on interelectronic separation
- meta-NGA: a functional like an NGA, but that also depends on τ_α and τ_β

Hybrid exchange-correlation functionals

- global-hybrid GGA: a hybrid GGA where the percentage X of local exchange that is replaced by Hartree-Fock exchange is a global constant, that is, it is independent of point in space, ρ_σ, $\nabla\rho_\sigma$, τ_σ , or interelectronic separation
- global-hybrid meta-GGA: a hybrid meta-GGA where the percentage X of local exchange that is replaced by Hartree-Fock exchange is a global constant
- long-range-corrected GGA: a hybrid GGA in which X increases as a function of interelectronic separation
- long-range-corrected meta-GGA: a hybrid meta-GGA in which X increases as a function of interelectronic separation
- screened exchange GGA: a hybrid GGA in which X decreases to zero as interelectronic separation increases
- screened exchange NGA: a hybrid NGA in which X decreases to zero as interelectronic separation increases
- screened exchange meta-NGA: like a screened-exchange NGA except the local part also depends on τ_α and τ_β (same as a long-range-corrected hybrid meta-GGA but using a meta-NGA rather than a meta-GGA and X decreases rather than increases with interelectronic separation)

The wide variety of exchange-correlation functionals equips chemists and physicists with numerous tools for studying a particular system, and the computational accuracy also heavily depends on the xcF in use. xcFs are designed with different philosophies and purposes – some aim for good across-the-board performances for broad applications in chemistry and physics, whereas others target at specific problems such as

weak interactions, surface science, or transition metal chemistry, etc. Although a wide ranges of normal systems have been studied and understood quite well with DFT, there are still complex ones presenting particular challenges where most commonly used xcFs have failed. It could be due to the complex nature of the system, lack of or difficulty to obtain reliable reference data, or the practical limitations of KS-DFT formulation. Hence one of the major topics of this thesis is to test the performances of xcFs for these complex systems to (i) draw conclusions upon recommendations of xcFs for important practical applications; (ii) understand the root of errors to help design better xcFs or propose new theoretical schemes of DFT.

1.2 Multi-Reference Systems

When solving the many-electron Schrödinger equation of the system, one usually starts with a zero-order wave function called the reference wave function[7]. It serves as a foundation for describing the correlation behavior of electrons by excitation or de-excitation of electrons from the zero-order wave function.

One possible choice of the reference wave function is to use a single configuration – a single Slater determinant (Eq. 1.1), or a spin-adapted linear combination of a fixed number of SDs called a configuration state function (CSF)[8]. Electronic structure methods using a single SD or CSF as the reference wave function are called single-reference methods. KS-DFT uses a single SD as the reference wave function, and thus is a single-reference method. The most commonly used method to obtain a single-configuration wave function to use as the single-configuration reference wave function in single-reference methods is the Hartree-Fock method[9].

Alternatively, if a set of degenerate or near-degenerate configurations is used as the reference wave function, the method is called a multi-configuration method. In these calculations, the molecular orbitals (MOs) and the weight of each configuration in the reference function are usually variationally optimized simultaneously, and the computational expense sometimes grows factorially with respect to the system size. Hence in contrast to DFT, which can treats systems of hundreds or even thousands of electrons readily with considerable accuracy, the application of multi-reference methods is often limited by their high computational cost.

Nevertheless, there are many systems that cannot be appropriately treated by single-reference methods; these are called multi-reference systems. They are widely observed in radicals with π bonds, transition metals, some transition states, and most electronically excited states.[7, 10-11] Multi-reference systems are particularly challenging for DFT, and frequently the problem of lacking an appropriate multi-configuration reference wave function is further complicated by the approximate nature of the exchange-correlation functionals in use. Therefore, another important task of this thesis is to study a wide selection of multi-reference systems, ranging from transition metal atoms and compounds to transition states, with DFT, to understand both the qualities of various xcFs and theoretical improvements that could be used for better description of multi-reference systems.

1.3 Noncollinear Density Functional Theory (NC-DFT)

When one is restricted to the single reference configuration of DFT, a possible option for introducing extra flexibilities for treating multi-reference systems arises from using more general spin orbitals. Spin orbitals are used for describing one electron in the

many-electron system, and contain both a spatial part, also called the molecular orbital (MO), and a spin part. For a closed-shell system with an even number (*2N*) of electrons, one can choose to use *N* MOs, each occupied by an α electron and a β electron, e.g.

$$\chi_i = \varphi_i(\mathrm{r})\sigma(\omega) \qquad \sigma(\omega) = \alpha \text{ or } \beta, \quad i = 1, 2, ..., N \tag{1.6}$$

Spin orbitals in the form of eq. (1.6) are called restricted spin orbitals.

Alternatively, one can choose to have different spatial parts for each α and β electron, and they are called unrestricted spin orbitals.

$$\chi_i = \varphi_i(\mathrm{r})\sigma(\omega) \qquad \sigma(\omega) = \alpha \text{ or } \beta, \quad i = 1, 2, ..., 2N \tag{1.7}$$

Obviously, unrestricted spin orbitals are necessary for systems with an odd number of electrons, or singly-occupied orbitals, e.g., open-shell systems.

Both restricted and unrestricted spin orbitals are called collinear spin orbitals, for the spin of an electron can be only be pointing "up" (α electron) or "down" (β electron) along a pre-defined quantization axis (*z* axis). In reality, however, spin can be allowed to point to different directions in space, also known as the noncollinear spin states. Systems whose descriptions are greatly improved by allowing this flexibility are sometimes found in metals,[12-14] metal alloys,[15] and bare metallic clusters.[16-20] Description of noncollinear spins require use of a more general version of spin orbitals, a spinor as a linear combination of the α and β components[18, 21-26]

$$\chi_i = \varphi_i^{\alpha}(\mathrm{r})\alpha + \varphi_i^{\beta}(\mathrm{r})\beta \qquad i = 1, 2, ..., 2N \tag{1.8}$$

Equation (1.8), like the other equations in this chapter, is written for the case of *2N* electrons, but the general idea is applicable to any number of electrons. Orbitals of this type are called generalized spin orbitals or noncollinear spin orbitals.

The accuracy of any electronic structure methods depend on the forms of both the reference wave function and the spin orbitals. Hence in this thesis we explore exploiting the extra degrees of freedom of noncollinear spin orbitals to improve descriptions of multi-reference systems while retaining the single-reference structure of KS-DFT.

1.4 Organization of the Thesis

Chapter 2 tests the performance of exchange-correlation functionals for isomerization reactions of large organic molecules. Weak interactions are found to be particularly challenging for DFT, and yet most studies focus on small to medium-sized systems, partially due to the simplicity to obtain accurate experimental data. In this study we used highly accurate electronic structure methods to obtain reference data for 24 reactions of large molecules, and compare the performances of a wide selection of xcFs for weak interactions in practical applications.

Chapter 3 studies a well-known conundrum of computational surface science – the adsorption energy/site preferences of CO on transition metals vs. surface formation energies of bare metals. GGAs are notoriously incapable of describing both accurately, as documented in previous studies, and we show that by adding the kinetic energy density to obtain a meta-GGA, M06-L, we achieve high accuracy for both challenges. Noteworthy is the fact that the training set of M06-L does not include any solid-state physics data, and so the triumph of M06-L in this test is a solid validation of its design philosophy.

Chapter 4 and 5 deal with d-block transition metals. They are of importance for many applications in materials and catalysis, but are difficult for DFT due to the existence of strong multi-reference character, with low-lying states, partial occupations, and s-d transitions. We studied the multiplicity-changing excitation energies of neutral

atoms and their cations with various exchange-correlations functionals, and combine the results with other important databases to make recommendations for top choices in real-world applications. We also categorized and characterized different groups of transition metals, providing inputs for designing better functionals for multi-reference systems.

Chapter 6 and 7 employ noncollinear DFT to study a wide spectrum of systems with multi-reference character. Chapter 6 shows that NC-DFT corrects the intrinsic incapability of collinear DFT to correctly dissociate NiO and MnO by allowing further symmetry breaking. Better results were also obtained by allowing noncollinear spin states in transition states of several well-known multi-reference transition states including O_3, BeH_2, and H_4. Chapter 7 showed that NC-DFT correctly predicts the spin-splitting of a biomimetic oxomanganese compound inspired by the oxygen evolving complex in Photosystem II (PS II).

References for Chapter 1

(1) Hohenberg, P.; Kohn, W. *Phys. Rev.* **1964**, *136*, B864-B871.

(2) Kohn, W.; Sham, L. J. *Phys. Rev.* **1965**, *140*, A1133-A1138.

(3) Slater, J. C. *Phys. Rev.* **1929**, *34*, 1293-1295.

(4) Barth, U.; Hedin, L. A. *J. Phys. C* **1972**, *5*, 1629-1642.

(5) Becke, A. D. *J. Chem. Phys.* **1998**, *109*, 2092-2098.

(6) Peverati, R.; Truhlar, D. G. *J. Chem. Theory Comput.* **2012**, *8*, 2310-2319.

(7) Truhlar, D. G. *J. Comput. Chem.* **2007**, *28*, 73-86.

(8) Löwdin, P.-O. *J. Math. Phys.* **1962**, *3*, 969-982.

(9) Hartree, D. R.; Black, M. M. *Proc. R. Soc. A* **1933**, *139*, 311-335.

(10) Nakano, H.; Nakajima, T.; Tsuneda, T.; Hirao, K. In *Theory and Applications of Computational Chemistry: The First Forty Years*. Dykstra, C. A.; Frenking, G.; Kim, K. S.; Scuseria, G. E. Eds., Elsevier: Amsterdam, 2005, p507.

(11) Roos, B. O. In *Theory and Applications of Computational Chemistry: The First Forty Years*. Dykstra, C. A.; Frenking, G.; Kim, K. S.; Scuseria, G. E. Eds., Elsevier: Amsterdam, 2005, p729.

(12) Sandratskii, L. M.; Guletskii, P. G. *J. Phys. F. Met. Phys*. **1986**, *16*, L43-L48.

(13) Gebauer, R.; Baroni, S. *Phys. Rev. B* **2000**, *61*, R6459-R6462.

(14) Sharma, S.; Dewhurst, J. K.; Ambrosch-Draxl, C.; Kurth, S.; Helbig, N.; Pittalis, S.; Shallcross, S.; Nordström, L.; Gross, E. K. U. *Phys. Rev. Lett.* **2007**, *98*, 196405/1-4.

(15) Sticht, J.; Höck, K.-H.; Kubler, J. *J. Phys. Condens. Matter* **1989**, *1*, 8155-8170.

(16) Oda, T.; Pasquarello, A.; Car, R.. *Phys. Rev. Lett*. **1998**, *80*, 3622-3625.

(17) Hobbs, D.; Kresse, G.; Hafner, J. *Phys. Rev. B* **2000**, *62*, 11556-11570.

(18) Anton, J.; Fricke, B.; Engel, E. *Phys. Rev. A* **2004**, *69*, 012505/1-10.

(19) Longo, R. C.; Alemany, M. M. G.; Ferrer, J.; Vega, A.; Gallego, L. J. *J. Chem. Phys*. **2008**, *121*, 114315/1-5.

(20) Soncini, A.; Chibotaru, L. F. *Phys. Rev. B* **2010**, *81*, 132403/1-4.

(21) Lunell, S. Chem. Phys. Lett. **1972**, *13*, 93-96.

(22) Hammes-Schiffer, S.; Andersen, H. C. *J. Chem. Phys.* **1993***, 99*, 523-532.

(23) Hammes-Schiffer, S.; Andersen, H. C. *J. Chem. Phys.* **1993***, 99*, 1901-1913.

(24) van Wüllen, C. *J. Comput. Chem*. **2002**, *23*, 779-785.

(25) Fukutome, H. *Int. J. Quantum Chem.* **1981***, 20*, 955-1065.

(26) Löwdin, P.-O.; Mayer, I. *Adv. Quantum Chem.* **1992***, 24*, 79-114.

Chapter 2

Density Functional Theory for Isomerization Reactions of Large Organic Molecules

2.1 Introduction

It is important to test electronic structure model chemistries[1] against a wide variety of data. Many validation studies have been based on small molecules where accurate data is most readily available. But some theoretical methods that work well for small molecules are not so successful for large ones. Further tests are necessary, but extracting accurate electronic structure test data from experiment is problematic for large molecules because electronic structure calculations directly predict Born-Oppenheimer energies (*E*), but experiment yields enthalpies (*H*) or free energies (*G*). Extracting *E* from *H* or *G* requires the removal of conformational-vibrational-rotational energy, which becomes progressively more complicated as molecular size increases.[2] Furthermore experimental *H* and *G* data becomes sparser as molecular size increases. In recent years though an alternative approach has become more affordable, namely the direct calculation of *E* by high-level wave function theory.[3] This also becomes harder as molecular size increases, but progress is being made in extending the capabilities to larger systems.

It has been pointed out[4] that "a good place to start is the energetics of isomerization reactions since this allows direct comparison on the performance for

differences in bonding, conjugation, and steric effects." Recently, Huenerbein et al.[5] very constructively pushed the limit of what can be done in this regard by using spin-component-scaled third-order Møller-Plesset perturbation theory (SCS-MP3) to calculate reference values of the isomerization energy (ΔE) of 24 large molecules containing 24–81 atoms. They estimated uncertainties to be typically smaller than 2 kcal/mol with maximum uncertainties of up to 4–5 kcal/mol. The reference values were used to test 22 density functional methods that were found to have mean unsigned deviations from the reference data of 2.5–14.8 kcal/mol. Their reference database is called ISOL24.[5] The ISOL24 reactions are shown in Fig. 2.1, which numbers each reaction (from 1 to 24) as in Ref. 5, for convenience.

The objective of the present work is twofold: (1) to improve the accuracy of the reference data and (2) to test 50 additional electronic structure methods (48 of which are single-component and doubly hybrid density functional theory methods) that are affordable for the entire benchmark suite. An electronic structure method is a short name for an electronic structure model chemistry,[1] which is a combination of a wave function level (e.g., MP3 or Hartree-Fock) or an approximate density functional with a one-electron basis set or a one-electron-basis-set extrapolation procedure. A method is denoted, as usual, as L/B where L denotes the wave function level or density functional, and B denotes the basis set or basis-set extrapolation procedure.

3.2 Methods

In the present work we directly use three basis sets: aDZ[6] (shorthand for aug-cc-pVDZ), MG3S,[7] and MG3SXP,[8] where aDZ is an augmented valence double zeta plus polarization set, MG3S is a minimally augmented valence triple zeta plus double

polarization set, and MG3SXP is MG3S plus extra polarization functions. We also consider some calculations extrapolated to a complete basis set (CBS), and we consider some multi-coefficient correlation methods[9–13] (MCCMs) involving different basis sets for different components, as defined in the original references, which are given below.

All geometries were optimized by Huenerbein et al.[5] with the B97/TZVP method. Since the same geometries are used for the reference calculations as for the tested methods, the comparisons are a direct test of the ability of the tested methods to predict relative energies (ΔE) at pre-specified geometries. But since the geometries predicted by B97/TZVP are expected to be reasonably close to the accurate equilibrium geometries, we interpret the results as Born-Oppenheimer isomerization energies.

In order to validate affordable methods for improving the reference results, we first carried out CCSD(T)-F12a/aDZ wave function calculations on the six smallest reactions (reactions 3, 9, 10, 13, 14, and 20); these reactions have 24-35 atoms. Here CCSD denotes coupled cluster theory with single and double excitations,[15] (T) denotes a quasiperturbative treatment of connected triple excitations,[16] and F12a denotes a simplified version[17] of the F12[18] method that includes functions of interelectronic distance (r_{12}) to accelerate convergence. The CCSD(T)-F12a/aDZ calculations are expected to be close to the CBS limit of CCSD(T).[17,19] We then compare these calculations to CCSD-F12a/aDZ, SCS-MP3/CBS, and seven MCCMs, which are explained next.

MCG3/3,[11] G3SX(MP3),[10] and BMC-CCSD[12] are MCCMs based entirely on wave function components. MCG3/3 and G3SX(MP3) each involve an expensive CCSD(T) step, but BMC-CCSD involves no step more expensive than CCSD and thus is more affordable for large systems.

MCG3-MPW[13] and MCG3-MPWB[13] are MCCMs that combine wave function and density functional components with the highest-order wave function component being CCSD(T). MCQCISD/MPW[13] and MCQCISD/MPWB[13] are similar but the highest-order wave function component is the less expensive quadratic configuration interaction with single and double excitations (QCISD). MC3MPW[13] and MC3MPWB[13] are even cheaper because the highest level of correlation included is based on the MP2 method. Since the Hartree-Fock orbitals on which CCSD(T), QCISD, and MP2 are built and the generalized Kohn-Sham orbitals on which some density functional components are built are both functionals of the electron density, these four methods are all doubly hybrid[14] density functional methods.

The other density functionals[8, 20-49] considered in this work are all applied to all 24 reactions. For comparison we also include three other doubly hybrid density functional methods, namely, B2-PLYP[39], mPW2-PLYP[40] and B2GP-PLYP[47], in which the MP2-like correlation is combined with DFT calculation. An empirical molecular-mechanics (MM) dispersion-like term can be added to these functionals in a post-SCF fashion (just as in the single-component functionals discussed below), and two of such combined doubly-hybrid-functional-plus-MM methods are also included in the test. All density functionals considered in this article are listed and explained in Table 2.1. The table contains 40 single-component density functional and nine doubly

hybrid functionals. The 40 single-component functional consist of 22 without MM terms and 18 with them. The nine multi-component functionals consist of seven without MM and two with MM.

3.3 Reference Values

Table 2.2 compares the isomerization energies calculated by 11 methods for the six smallest systems in the ISOL24 database. The last row of the table gives the "cost," which is defined as the sum of the computer times (in processor hours) for single-point energy calculations on reactions 10 and 20 (the two largest systems in Table 2.2) divided by the sum of the computer times for single-point MP2/6-31G calculations on the same two reactions, run with the same software on the same computer. We recognize that such timings depend on the software, the computer and its load, and the parallelization, but nevertheless they are usually meaningful when they differ by more than a factor of about 1.5–2. All costs are rounded to two significant figures. All coupled cluster and QCISD results were calculated with *Molpro*[50] and all density functional calculations were run with *Gaussian 09*.[51]

The second last line of Table 2.1 is the mean unsigned error (MUE) of each method as compared to the CCSD(T)-F12a/aDZ results. The BMC-CCSD, SCS-MP3/CBS, and CCSD-F12/aDZ methods have MUEs of 1.01, 0.90, and 0.74 kcal/mol respectively, and the four doubly hybrid methods have MUEs in the range 0.43–0.66 kcal/mol. The most accurate method that is affordable for the entire database of 24 reactions is MCQCISD-MPW. This method was applied to the other 18 reactions, and a new reference database was created containing CCSD(T)–

F12a/aDZ results for the six reactions of Table 2.2 and MCQCISD-MPW results for the other 18. This new set of reference data is called ISOL24/11 where the last two digits signify the update of 2011. The isomerization energies of the ISOL24/11 database are listed in Table 2.3.

3.4 Testing Density Functionals

All 40 single-component density functionals were tested against ISOL24/11 with the MG3SXP basis set. We also tested four of them with the MG3 basis set. As for the doubly hybrid functionals, B2-PLYP, B2GP-PLYP and mPW2-PLYP with and without dispersion corrections are also tested with the MG3SXP basis set, but MC3MPW and MC3MPWB have different basis sets for different level of calculations. Finally we tested MCQCISD-MPWB, BMC-CCSD, and SCS-MP3/CBS. In every case we computed the mean unsigned error (MUE). These MUEs are given in Tables 2.4–2.6.

Table 2.4 compares the results of M06, M06-2X and M06-HF with MG3S and MG3SXP basis sets. MG3SXP (where XP denotes “extra polarization”) differs from MG3S in that it adds an extra polarization function to MG3S basis. In particular, the 2df polarization functions of MG3S on Li-Ne are replaced by a 3df set, and the 3d2f polarization functions on Al-Ar are replaced by a 4d2f set. It has been shown in previous research that the extra polarization functions of MG3SXP is necessary for obtaining accurate results in certain systems containing fluorine atoms, and considering there are three reactions (reaction 12, 20 and 22) in the ISOL24/11 database involving fluorine, it is beneficial to clarify the necessity of extra

polarization. The MUEs of M06 and M06-2X decrease by 1.27 and 1.15 kcal/mol after adding the extra polarization, while the result of M06-HF with MG3SXP is unexpectedly worse than MG3S. In general we believe that MG3SXP provides validating results by properly treating the fluorine-containing systems with the extra polarization functions, and the quality of various density functionals can be appropriately compared by use of this basis set.

Table 2.5 compares the performance of various single-component and doubly hybrid density functionals against ISOL24/11 database. Empirical dispersion correction (D-correction) can also be added to the DFT calculations in a post-SCF fashion to improve accuracy for weak interactions, and here we include three versions of them. The label "D" refers to D-correction in Ref. 44 except for two cases: in ωB97X-D it refers to Ref. 42 and in B97-D, it refers to Ref. 35. On the other hand, "D3" refers to the D-correction in Refs. 45 and 46. Although Table 2.1 contains 49 density functionals, Table 2.5 contains only 48 because it omits MCQCISD-MPW, which is used for some of the benchmark values.

We first look at the "pure" density functionals without MM corrections. (These are the density functionals that do not have a suffix –D or –D3.) The popular B3LYP functional has an enormous MUE of 8.98 kcal/mol, while the best single-component functional without D-correction, namely, M08-SO, achieves a MUE of 2.19 kcal/mol. Several other Minnesota functionals, namely, M08-HX, M05-2X and M06-2X also perform quite well with MUEs of 2.27, 2.35 and 2.46 kcal/mol respectively. Furthermore, we observe no improvement when comparing PBE with its meta-GGA counterpart TPSS, but the hybrid PBE0 almost halves the error of PBE.

The range-separated functional ωB97X achieves an MUE of 2.77 kcal/mol, but the other two RS-hybrid functionals, namely, ωB97 and LC-ωB97, do not perform as well. This is well understood; the advantage of ωB97X is that it is not constrained to have zero Hartree-Fock exchange at small interelectronic distances.

On the other hand, the best MM-corrected functional, which is also the best single-component functional overall, is ωB97X-D with MUE of 1.90 kcal/mol. Also surprising is the good performance of PBE0-D3, which is almost equally good as ωB97X-D and also outperforms all the other single-component functionals in our test. Moreover, most of the Minnesota functionals do not significantly improve by adding the MM corrections, while other MM-corrected functionals in general significantly improve over their non-corrected counterparts. The only exception is that M06-L-D has a MUE of approximately 1 kcal/mol smaller than M06-L. We attribute the above observations to the fact that the whole family of Minnesota functionals has incorporated reasonably accurate medium-range correlation energy by virtue of their functional forms and their parameterization process and adding post-SCF dispersion-like corrections thus does not improve their performance significantly. If we restrict ourselves to functionals without Hartree-Fock exchange (which is an important consideration from the point of view of cost, especially for extended systems), the best functional without MM terms is M06-L and the best with MM terms is M06-L-D3.

We then proceed to consider the more expensive doubly hybrid functionals, in which an MP2-like or QCISD-like term is added as a post-SCF term to the DFT or weighted DFT result.

Because MP2 and QCISD are more expensive than DFT for a given basis set for large systems, these methods - when used with a single basis set - have the computational cost of MP2 or QCISD rather than that of DFT; however, this does not affect MCQCISD-type and MC3M-type methods because they involve two basis sets. It should be noticed that the cost of MP2 steps can be reduced by using RI-MP2 with appropriate auxiliary basis sets, but this is not adopted in this paper. For all the doubly hybrid functionals based on MP2 as the WFT component, which excludes those in Table 2.2, but includes B2-PLYP, B2GP-PLYP, mPW2-PLYP, MC3MPW, and MC3MPWB, the average cost is approximately one to two orders of magnitude higher than for single-component functionals. However, these methods are still quite affordable with presently available computational resources.

Although the MUE of MCQCISD-MPWB is only 0.46 kcal/mol, which is the smallest of all the tested methods, this is partly due to the fact that it is very similar to MCQCISD-MPW, which is the method we use to calculate 18 of the 24 reactions. On the other hand, the value is probably reasonable since it is close to the values in Table 2.2, which is based on comparison to the very accurate results. MC3MPWB and MC3MPW both achieve good performance without MM terms, achieving MUEs of 1.79 and 1.65 kcal/mol, which outperform all the single-component functionals. B2GP-PLYP also performs well, and its accuracy is further improved by adding the MM term.

Finally in Table 2.6 we compare the results for the methods whose costs scale as N^6, namely, SCS-MP3/CBS and BMC-CCSD. SCS-MP3/CBS is the method used in Ref. 5 to construct the original ISOL24 database, and we find its MUE against the updated

ISOL24/11 to be 1.68 kcal/mol. This result is consistent with the error estimation of 2 kcal/mol in Ref. 5, and also implies that the original ISOL24 is not accurate enough for evaluation of methods such as B2GP-PLYP-D3 or MC3MPW, for which the MUE is even smaller than SCS-MP3/CBS. Second, BMC-CCSD is found to have an MUE of 1.46 kcal/mol, which is only slightly worse than the best method in Table 2.5 if we exclude MCQCISD-MPW. In spite of the fact that it scales as N^6, its most expensive step only requires a CCSD calculation with a polarized valence double-zeta basis set, which should be affordable for a large number of applications.

3.5 Concluding Remarks

We have updated the ISOL24 database constructed in Ref. 5 by methods of higher accuracy, and the new ISOL24/11 database is composed of six reactions calculated by CCSD(T)/aDZ and 18 reactions by MCQCISD-MPW. This is validated by a careful investigation of a subset of the smallest six reactions by the very accurate CCSD(T)-F12a/aDZ method, which should be very close to the CCSD(T) results with a complete basis set, and MCQCISD-MPW is then found to be the most accurate method we can afford for the remaining 18 reactions. The new ISOL24/11 database is recommended for future tests and parameterization of methods aimed at treatment of chemical reactions of large size.

We have tested 48 single-component and doubly hybrid functionals with and without MM terms, together with 2 other methods, against the ISOL24/11 database, and we conclude this paper with recommendations as follows.

(a) ωB97X-D and PBE0-D3 are the most highly recommended single-component functionals with MM corrections, while Minnesota functionals with high HF exchange, namely, M08-SO, M08-HX, M05-2X and M06-2X perform the best even without D-correction.

(b) For the more expensive doubly hybrid functionals, whose most expensive component is an MP2 step, B2GP-PLYP-D3 and MC3MPWB are recommended.

The even more expensive MCG3-MPW, MCQCISD-MPW, and BMC-CCSD methods are also recommended for benchmark of large reactions involving weak-interactions, whenever they are affordable.

References for Chapter 2

(1). J. A. Pople, *Rev. Mod. Phys*., 1999, **71**, 1267.

(2). J. Zheng, T. Yu, E. Papajak, I. M. Alecu, S. L. Mielke and D. G. Truhlar, *Phys. Chem. Chem*. Phys., in press.

(3). See, e.g., A Karton, E. Rabinovich, J. M. L. Martin and B. Ruscic, *J. Chem. Phys*., 2006, **125**, 144108.

(4). K. W. Sattelmeyer, J. Tirado-Rives and W. L. Jorgensen, *J. Phys. Chem. A*, 2006, **110**, 13551.

(5). R. Huenerbein, B. Schirmer, J. Moellmann and S. Grimme, *Phys. Chem. Chem. Phys*., 2010, **12**, 6940.

(6). R. A. Kendall, T. H. Dunning, Jr. and R. J. Harrison, *J. Chem. Phys*., 1992, **96**, 6796.

(7). (a) R. Krishnan, J. S. Binkley, R. Seeger and J. A. Pople, *J. Chem. Phys*., 1980, **72**, 650. (b) T. Clark, J. Chandrasekhar, G. W. Spitznagel and P. v. R. Schleyer, *J. Comp. Chem*., 1983, **4**, 294. (c) L. A. Curtiss, K. Raghavachari, C. Redfern,

V. Rassolov and J. A. Pople, *J. Chem. Phys*., 1998, **109**, 7764. (d) P. L. Fast, M. L. Sanchez and D. G. Truhlar, *Chem. Phys. Lett*., 1999, **306**, 407. (e) B. J. Lynch, Y. Zhao and D. G. Truhlar, *J. Phys. Chem. A,* 2003, **107**, 1384.

(8). Y. Zhao and D. G. Truhlar, *J. Chem. Theory Comput*., 2008, **4**, 1849.

(9). P. L. Fast, J. C. Corchado, M. L. Sanchez and D. G. Truhlar, *J. Phys. Chem. A*, 1999, **103**, 5129.

(10). L. A. Curtiss, P. C. Redfern, K. Raghavachari and J. A. Pople, *J. Chem. Phys*., 2001, **114**, 108.

(11). B. J. Lynch and D. G. Truhlar, *J. Phys. Chem. A*, 2003, **107**, 3898.

(12). B. J. Lynch, Y. Zhao and D. G. Truhlar, *J. Phys. Chem.* A, 2005, **109**, 1643.

(13). Y. Zhao, B. J. Lynch and D. G. Truhlar, *Phys. Chem. Chem. Phys*., 2005, **7**, 43.

(14). Y. Zhao, B. J. Lynch and D. G. Truhlar, *J. Phys. Chem. A*, 2004, **108**, 4786.

(15). G. D. Purvis III and R. J. Bartlett, *J. Chem. Phys*., 1982, **76**, 1910.

(16). K. Raghavachari, G. W. Trucks, J. A. Pople and M. Head-Gordon, *Chem. Phys. Lett*., 1989, **157**, 479.

(17). G. Knizia, T. B. Adler and H.-J. Werner, *J. Chem. Phys*., 2009, **130**, 054104.

(18). J. Noga, S. Kedzuch, J. Simunek, and S. Ten-no, *J. Chem. Phys*., 2008, **128**, 174103.

(19). E. Papajak and D. G. Truhlar, *J. Chem. Theory Comput*., 2011, **7**, 10.

(20). J. P. Perdew, *Phys. Rev*., 1986, **33**, 8862.

(21). A. D. Becke, *Phys. Rev. A*, 1988, **38**, 3098.

(22). A. D. Becke, *J. Chem. Phys*., 1993, **98**, 5648.

(23). P. J. Stephens, F. J. Devlin, C. F. Chabalowski and M. J. Frisch, *J. Phys. Chem*., 1994, **98**, 11623.

(24). J. P. Perdew, K. Burke and M. Ernzerhof, *Phys. Rev. Lett*., 1996, **77**, 3865.

(25). J. P. Perdew, M. Ernzerhof and K. Burke, *J. Chem. Phys*., 1996, **105**, 9982.

(26). C. Adamo and V. Barone*, Chem. Phys. Lett*., 1998, **298**, 113.

(27). A. D. Boese and N. C. Handy, *J. Chem. Phys*., 2002, **116**, 9559.

(28). J. Tao, J. P. Perdew, V. N. Staroverov and G. E. Scuseria, *Phys. Rev. Lett*., 2003, **91**, 146401.

(29). V. N. Starverov, G. E. Scuseria, J. Tao and J. P. Perdew, *J. Chem. Phys*., 2003, **119**, 12129.

(30). A. D. Boese and J. M. L. Martin, *J. Chem. Phys*., 2004, **121**, 3405.

(31). Y. Zhao and D. G. Truhlar, *J. Phys. Chem. A*, 2004, **108**, 6908.

(32). N. Schultz, Y. Zhao and D. G. Truhlar, *J. Phys. Chem. A*, 2005, **109**, 11127.

(33). Y. Zhao, N. E. Schultz and D. G. Truhlar, *J. Chem. Phys*., 2005, **123**, 161103.

(34). O. A. Vydrov, J. Heyd, A. V. Krukau and G. E. Scuseria, *J. Chem. Phys*., 2006, **125**, 074106.

(35). S. Grimme, *J. Comp. Chem*., 2006, **27**, 1787.

(36). Y. Zhao, N. Schultz and D. G. Truhlar, *J. Chem. Theory Comput*., 2006, **2**, 364.

(37). Y. Zhao and D. G. Truhlar, *J. Chem. Phys*., 2006, **125**, 194101.

(38). Y. Zhao and D. G. Truhlar, *J. Phys. Chem. A*, 2006, **110**, 13126.

(39). S. Grimme, *J. Chem. Phys.*, 2006, **124**, 034108.

(40). T. Schwabe and S. Grimme, *Phys. Chem. Chem. Phys.*, 2006, **8**, 4398.

(41). Y. Zhao and D. G. Truhlar, *Theor. Chem. Acc*., 2008, **120**, 215.

(42). J.-D. Chai and M. Head-Gordon, *J. Chem. Phys*., 2008, **128**, 084106.

(43). J.-D. Chai and M. Head-Gordon, *Phys. Chem. Chem. Phys*., 2008, **10**, 6615.

(44). A. Karton, D. Gruzman and J. M. L. Martin, *J. Phys. Chem. A*, 2009, **113**, 8434.

(45). S. Grimme, J. Antony, S. Ehrlich, and H. Krieg, *J. Chem. Phys*., 2010, **132**, 154104.

(46). Y. Zhao and D. G. Truhlar, *J. Phys. Chem. A*, 2005, **109**, 5656.

(47). A. Karton, A. Tarnopolsky, J.-F. Lamère, G. C. Schatz, and J. M. L. Martin, *J. Phys. Chem. A,* 2008, **112**, 12868.

(48). L. Georigk and S. Grimme, *J. Chem. Theory. Comput.*, 2011, **7**, 291.

(49). L. Goerigk and S. Grimme, http://toc.uni-muenster.de/DFTD3/functionals.html (accessed Jan. 15, 2011).

(50). H.-J. Werner, P. J. Knowles, F. R. Manby, M. Schütz, P. Celani, G. Knizia, T. Korona, R. Lindh, A. Mitrushenkov, G. Rauhut, T. B. Adler, R. D. Amos, A. Bernhardsson, A. Berning, D. L. Cooper, M. J. O. Deegan, A. J. Dobbyn, F. Eckert, E. Goll, C. Hampel, A. Hesselmann, G. Hetzer, T. Hrenar, G. Jansen, C. Köppl, Y. Liu, A. W. Lloyd, R. A. Mata, A. J. May, S. J. McNicholas, W.

Meyer, M. E. Mura, A. Nicklaß, P. Palmieri, K. Pflüger, R. Pitzer, M. Reiher, T. Shiozaki, H. Stoll, A. J. Stone, R. Tarroni, T. Thorsteinsson, M. Wang, A. Wolf, *Molpro*, version 2010, University College Cardiff, Cardiff, 2010.

(51). M. J. Frisch, G. W. Trucks, H. B. Schlegel, G. E. Scuseria, M. A. Robb, J. R. Cheeseman, G.Scalmani, V. Barone, B. Mennucci, G. A. Petersson, H. Nakatsuji, M. Caricato, X. Li, H. P. Hratchian, A. F. Izmaylov, J. Bloino, G. Zheng, J. L. Sonnenberg, M. Hada, M. Ehara, K. Toyota, R. Fukuda, J. Hasegawa, M. Ishida, T. Nakajima, Y. Honda, O. Kitao, H. Nakai, T. Vreven, J. A. Montgomery, Jr., J. E. Peralta, F. Ogliaro, M. Bearpark, J. J. Heyd, E. Brothers, K. N. Kudin, V. N. Staroverov, R. Kobayashi, J. Normand, K. Raghavachari, A. Rendell, J. C. Burant, S. S. Iyengar, J. Tomasi, M. Cossi, N. Rega, J. M. Millam, M. Klene, J. E. Knox, J. B. Cross, V. Bakken, C. Adamo, J. Jaramillo, R. Gomperts, R. E. Stratmann, O. Yazyev, A. J. Austin, R. Cammi, C. Pomelli, J. W. Ochterski, R. L. Martin, K. Morokuma, V. G. Zakrzewski, G. A. Voth, P. Salvador, J. J. Dannenberg, S. Dapprich, A. D. Daniels, O. Farkas, J. B. Foresman, J. V. Ortiz, J. Cioslowski, and D. J. Fox, *Gaussian 09*, revision A.02, Gaussian, Inc., Wallingford CT, 2009.

Table 2.1. Density functional applied to all 24 reactions

Functional	Year	Ref.	type[a]
BP86	1986–8	20, 21	GGA
B3LYP	1993–4	22, 23	global-hybrid GGA
PBE	1996	24	GGA
PBE0	1996–8	25, 26	global-hybrid GGA
τHCTHhyb	2002	27	global-hybrid meta-GGA
TPSS	2003	28	meta-GGA
TPSSh	2003	29	global-hybrid meta-GGA
BMK	2004	30	global-hybrid meta-GGA
MPW3LYP	2004	31	global-hybrid GGA
MC3MPW	2005	13	doubly hybrid
MC3MPWB	2005	13	doubly hybrid
MCQCISD-MPW	2005	13	doubly hybrid
MCQCISD-MPWB	2005	13	doubly hybrid
MOHLYP	2005	32	global-hybrid GGA
PW6B95	2005	46	global-hybrid meta-GGA
M05	2005	33	global-hybrid meta-GGA
LC-ωPBE	2006	34	RS-hybrid GGA
B97-D	2006	35	GGA + MM
M05-2X	2006	36	global-hybrid meta-GGA
M06-L	2006	37	meta-GGA
M06-HF	2006	38	global-hybrid meta-GGA
B2-PLYP	2006	39	doubly hybrid
mPW2-PLYP	2006	40	doubly hybrid

M06	2008	41	global-hybrid meta-GGA
M06-2X	2008	41	global-hybrid meta-GGA
M08-HX	2008	8	global-hybrid meta-GGA
M08-SO	2008	8	global-hybrid meta-GGA
ωB97	2008	42	RS-hybrid GGA
ωB97X	2008	42	RS-hybrid GGA
ωB97X-D	2008	43	RS-hybrid GGA + MM
B2GP-PLYP	2008	47	doubly hybrid
M06-L-D	2009	37, 44	global-hybrid meta-GGA + MM
M06-D	2009	41, 44	global-hybrid meta-GGA + MM
BP86-D3	2010	20, 21, 45	GGA + MM
B3LYP-D3	2010	22, 23, 45	global-hybrid GGA + MM
PBE-D3	2010	24, 45	GGA + MM
PBE0-D3	2010	25, 26, 45	global-hybrid GGA + MM
TPSS-D3	2010	28, 45	meta-GGA + MM
B2P-PLYP-D3	2010	39, 45	doubly hybrid + MM
B97-D3	2010	45	GGA + MM
B2GP-PLYP	2011	47, 48	doubly hybrid + MM
TPSSh-D3	2011	29, 49	global-hybrid meta-GGA + MM
PW6B95-D3	2011	46, 49	global-hybrid meta-GGA + MM
M05-D3	2011	33, 49	global-hybrid meta-GGA + MM
M05-2X-D3	2011	36, 49	global-hybrid meta-GGA + MM
M06-L-D3	2011	37, 49	meta-GGA + MM
M06-HF-D3	2011	38, 49	global-hybrid meta-GGA + MM
M06-D3	2011	41, 49	global-hybrid meta-GGA + MM
M06-2X-D3	2011	41, 49	global-hybrid meta-GGA + MM

[a] "GGA" denotes generalized gradient approximation; "RS" denotes range-separated; "+ MM" denotes the addition of a post-SCF empirical molecular mechanics term.

Table 2.2. Isomerization energies (kcal/mol) for a 6-reaction subset of the ISOL24 database.

Reaction No.	CCSD(T)-F12a/aDZ	CCSD-F12/aDZ	MCG3-MPW	MCG3-MPWB	MG3/3	MCQCISD-MPW	MCQCISD-MPWB	SCS-MP3/CBS	BMC-CCSD	M06-L/MG3SXP-DF[a]	M06-L
3	9.77	10.98	11.05	10.67	10.57	11.30	11.02	11.70	11.16	4.58	4.58
9	21.76	21.34	21.21	20.93	22.44	20.90	20.33	22.30	20.20	19.05	19.03
10	6.82	5.93	6.34	6.25	6.92	6.30	6.10	7.90	8.57	2.72	2.70
13	33.52	32.75	33.52	33.48	34.57	33.47	33.30	35.10	34.75	32.44	32.42
14	5.30	4.19	5.22	5.04	5.19	5.43	5.18	5.20	5.33	3.46	3.45
20	4.66	4.70	4.86	4.76	4.69	4.63	4.47	4.50	4.75	3.14	3.15
MUE	0.00[b]	0.74	0.43	0.45	0.46	0.52	0.66	0.90	1.01	2.74	2.75
cost	3000	2600	1900	1900	1700	370	370	190	520	21	12

[a] same basis but with density fitting

[b] by definition

Table 2.3. The ISOL24/11 database (kcal/mol).

Reaction	ΔE	Reaction	ΔE
1	69.17	13	33.52
2	37.54	14	5.30
3	9.77	15	3.06
4	66.43	16	22.78
5	32.84	17	10.33
6	25.51	18	22.57
7	17.37	19	18.25
8	22.34	20	4.66
9	21.76	21	11.21
10	6.82	22	0.77
11	37.87	23	23.43
12	0.20	24	14.94

Table 2.4. Mean unsigned error (kcal/mol) for density functionals tested with both MG3S and MG3SXP basis sets.

	MUE	
Functionals	MG3S	MG3SXP
M06-2X	3.65	2.46
M06	4.29	3.06
M06-HF	3.56	4.47

Table 2.5. Mean unsigned errors (kcal/mol) for 48 density functionals. All calculations are performed with MG3SXP basis except for MCQCISD-MPWB, MC3MPW, and MC3MPWB, which have method-specific basis sets for each of their components.

Functional	MUE	Functional	MUE	Functional	MUE
MCQCISD-MPWB	0.47	PW6B95-D3	3.09	TPSS-D3	5.91
B2GP-PLYP-D3	1.36	ωB97	3.42	M06-L	5.94
MC3MPWB	1.65	PBE0	3.43	B3LYP-D3	6.02
MC3MPW	1.79	BMK	3.46	PBE	6.19
ωB97X-D	1.90	mPW2-PLYP	3.74	M05	6.49
PBE0-D3	1.91	BP86-D3	4.20	B97-D	6.71
M08-SO	2.19	B2-PLYP	4.39	TPSSh	6.78
M08-HX	2.27	PBE-D3	4.41	BP86	7.58
B2GP-PLYP	2.33	TPSSh-D3	4.41	TPSS	8.37
M06-2X-D3	2.34	PW6B95	4.44	MPW3LYP	8.48
M05-2X	2.35	M06-HF	4.47	B3LYP	8.98
M06-2X	2.46	LC-ωPBE	4.73	MOHLYP	13.49
M05–2X-D3	2.48	M06-HF-D3	4.77		
M06-D3	2.59	M06-L-D	4.82		
ωB97X	2.77	B97-D3	5.17		
M06-D	2.81	M05-D3	5.61		
B2-PLYP-D3	2.86	M06-L-D3	5.73		
M06	3.06	τHCTHhyb	5.87		

Table 2.6. Mean unsigned errors (kcal/mol) for other methods.

Method	MUE
BMC-CCSD	1.46
SCS-MP3/CBS	1.68

Table 2.7. Mean unsigned errors (kcal/mol) of the 6-reaction subset calculated by all the methods used in this paper with the results obtained by CCSD(T)-F12a/aDZ taken as reference data.

Functional	MUE	Functional	MUE	Functional	MUE
MCG3-MPW	0.43	B2PLYP	1.28	M05-D3	2.43
MCG3-MPWB	0.45	M06-D3	1.36	M06-HF-D3	2.43
MG3/3	0.46	ωB97	1.48	MPW3LYP	2.46
MCQCISD-MPW	0.52	PBE0	1.50	B97-D3	2.52
M08-HX	0.60	M06-2X-D3	1.53	B3LYP	2.63
B2GPLYP-D3	0.64	M06-2X	1.53	M06-L-D3	2.73
MCQCISD-MPWB	0.66	ωB97X	1.55	M06-L	2.74
B2GPLYP	0.67	M06-D	1.67	M05	2.75
CCSD-F12a/aDZ	0.74	B97D	1.75	TPSSh-D3	2.76
SCS-MP3/CBS	0.90	PW6B95-D3	1.75	TPSSh	3.12
B2PLYP-D3	1.00	BMK	1.81	TPSS-D3	3.34
BMC-CCSD	1.01	τHCTHhyb	1.82	TPSS	3.67
MC3MPW	1.03	PBE-D3	1.89	MOHLYP	4.32
mPW2PLYP	1.11	LC-ωPBE	1.91		
MC3MPWB	1.14	BP86-D3	1.99		
PBE0-D3	1.14	PW6B95	2.00		
ωB97X-D	1.14	PBE	2.02		
M08-SO	1.17	M06-L-D	2.09		
M05-2X	1.23	B3LYP-D3	2.14		
M06	1.26	BP86	2.30		
M05-2X-D3	1.27	M06-HF	2.42		

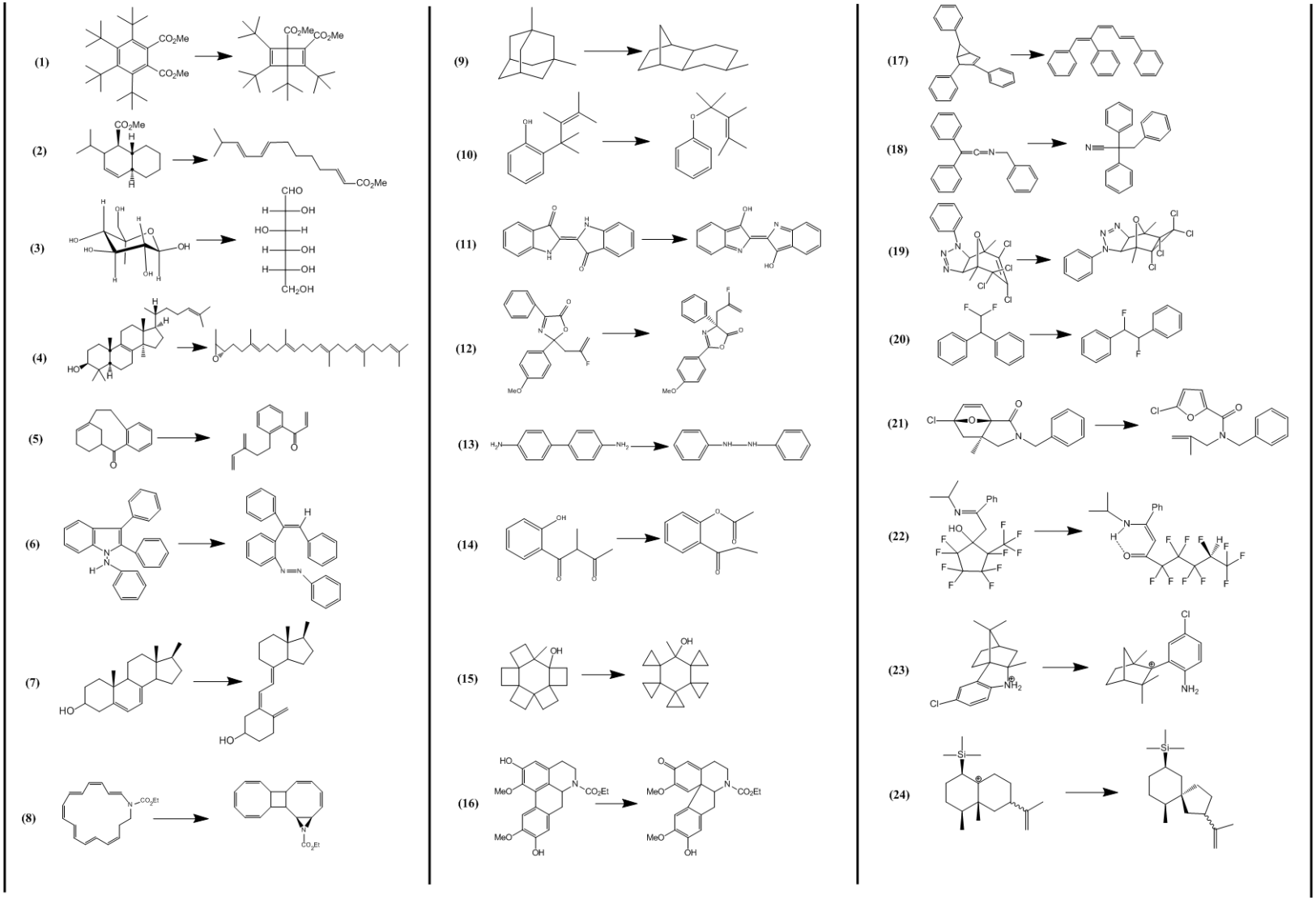

Figure 2.1 The 24 reactions of ISOL24 and ISOL24/11

Chapter 3

Density Functional Theory for Solid State Physics: CO Adsorption Energies, Site Preferences, and Surface Formation Energies of Transition Metals

3.1 Introduction

Kohn-Sham density functional theory (KS-DFT)[1] has become the preferred electronic structure method in surface science. The accuracy of KS-DFT is determined by the quality of the exchange-correlation functional, which is the only approximate aspect of KS-DFT. Key test cases for the application of KS-DFT to surfaces of transition metals have been identified as the energy of surface formation and the energy and site of carbon monoxide adsorption.[2-7] With regard to the latter, we note that one of the most important applications of DFT in surface science is CO adsorption on Pt, which is of critical importance for designing efficient fuel cells[8-11]. However, many local density functionals in the form of generalized gradient approximation (GGA) were previously shown to be incapable of describing both surface formation and CO adsorption in a consistent manner. There are two issues: (1) GGA functionals tend to underestimate surface formation energies and overestimate adsorption energies, resulting in a dilemma,[6] namely, changing the functional to improve surface formation energies leads to deterioration of its performance for adsorption, and vice versa. Therefore, it is challenging to develop a local density functional to predict accurately both the surface formation energies and the CO

adsorption energies. (2) Most the widely used GGA functionals are qualitatively wrong in predicting the on-top/hollow adsorption site preferences of many transition metals, For example, in a previous study by Feibelman *et al.,*[5] the popular GGA functionals predicted the CO molecule to be adsorbed at the fcc hollow site, rather than on-top site observed experimentally. To the knowledge of the authors, the only exception is BLYP, which correctly predicts the adsorption site preference for Rh, Pd, Ag, and Pt.[12]

Addition of nonlocal Hartree-Fock (HF) exchange (by which we mean evaluating the exchange from a single Slater determinant as in Hartree–Fock theory but with orbitals obtained from the KS or generalized KS equations) to local functionals (which are functionals—sometimes called semilocal in the physics literature—that depend on the local values of densities, density gradients, and kinetic energy densities) can only partly solve the above difficulties. For example, Stroppa et. al.[12] found that HSE predicted the correct site preference of Rh, Pd, Ag, and Pt, but greatly overestimated the adsorption energies. The same conclusions were also obtained for PBE0.[7] While B3LYP provided satisfactory accuracy for both adsorption energies and site preferences, it failed significantly in overall performance for metal properties, including lattice constants and surface energies.[12] More importantly, calculations with the resulting hybrid functionals are up to 10^3 times more expensive than local functionals (depending on specific software implementation and algorithm) and thus are computationally unfavorable for extended systems and sometimes even infeasible. Also noteworthy is the work by Stroppa et. al.[12] showing that the use of HF exchange with the random phase approximations (RPA) can solve the dilemma, but RPA is beyond the scope of our present discussion, which is concerned with KS DFT.

Adding kinetic energy density τ to a GGA yields a meta generalized gradient approximation (meta-GGA) local functional. Sun *et al.*[13] designed a meta-GGA, called revTPSS,[14] that overcomes the first difficulty discussed above in that it agrees reasonably well with experiments for lattice constants and surface formation energies and relatively well for adsorption energies. However, revTPSS still predicts wrong site preferences for most of the metals.

Therefore it is interesting to ask how well other meta-GGAs can predict surface formation energies, chemisorption energies, and chemisorption sites. We present here these results for an earlier meta-GGA functional, namely, M06-L,[15] for which we consider the energy to form a (111) surface from a face-centered cubic (fcc) bulk solid for five transition metals and the energy of adsorption and site of adsorption for CO on the these same surfaces; we compare the results to those for five GGAs as well as revTPSS. M06-L is shown below to provide the best overall performance, with improvements over revTPSS for both surface formation energies and adsorption energies, and equally importantly, with correct predictions of the site preference in four out of five tested metals.

An additional purpose of this paper is to test the performance of two GGA functionals, namely SOGGA[16] and SOGGA11,[17] that are correct through second order in an expansion in the reduced density. These functionals are of interest because the correct second order expansion was previously believed to be important in designing GGA functionals for solid-state physics.[18] SOGGA was tested together with M06-L in a previous study of lattice constants,[16] showing that it gave excellent lattice constants, but SOGGA11, which has a more flexible form, did not perform as well for lattice constants as might have been hoped.[19] Neither has been tested for surface formation energies or chemisorption. We

will show below that these two functionals produce the best surface formation energies among the GGAs, but they significantly overestimate the adsorption energies.

3.2 Computational Details

All the calculations presented in this paper were carried out with a locally modified version of *VASP 5.2*[20,21] using the projector augmented wave (PAW)[22] method with the improvements of Kresse and Joubert[23] with an energy cut-off of 500 eV (details of the PAW potentials are in supporting information). For all the metals, namely, Rh, Pt, Cu, Ag, and Pd, the fcc structure was considered, and lattice constants of each metal were optimized for the bulk metal; these were then used for all the rest of the calculations. For Brillouin-zone integration, symmetry-reduced Γ-centered $9\times9\times1$ grids were used in all calculations.

For the surface calculation, the unit cell was composed of periodic six-layer slabs with *c(2×4)* in-plane periodicity and a vacuum space of approximately 10 Å between each slab, containing totally 48 metal atoms in the supercell. Each slab has two surfaces, and the structure of the outmost two layers on each surface, namely, layers 1, 2, 5, and 6, were optimized during the calculations. The surface formation energy was calculated

$$\sigma_S = \frac{\frac{E(\text{slab})}{N(\text{slab})} - 6\frac{E(\text{bulk})}{N(\text{bulk})}}{2} \tag{3.1}$$

where E(slab) is the total energy of the slab structure, E(bulk) is the total energy of the bulk structure, and N(slab) and N(bulk) are the numbers of atoms in each of the calculations.

For the adsorption calculation, the unit cell was composed of the same six-layer slab, together with a CO molecule attached to the surface at either the on-top site or fcc hollow site on one side of the slab, so that the supercell has 50 atoms, and there is a vacuum space of approximately 10 Å. The CO is oriented with C toward the surface, and dipole

corrections were added in the calculations (see the supporting information for details). Only the structure of the CO molecule and the two layers closest to it were optimized during the calculations, and the adsorption energy was calculated as

$$E_{ads} = E(\text{slab+CO}) - E(\text{slab}) - E(\text{CO}) \quad (3.2)$$

where E(CO) is the energy of the isolated CO molecule, which was optimized using a unit cell of the same size as the system containing both slab and CO.

3.3 Results and Discussions

Table 3.1 presents the optimized lattice constants for each metal using various functionals and compares them to experimental[7] values. Our results for PBE[24], PBEsol[18], RPBE[25], and revTPSS are consistent with values reported in Ref. 13, and our results for BLYP are consistent with those reported in Ref. 12. The results for SOGGA are slightly different from those obtained in Ref. 16, possibly due to the differences in basis sets, while the results for M06-L show larger deviations from Ref. 16, probably due to the different treatments of core electrons, but these differences (at most a few hundredths of an Å) are still too small to effect our conclusions.

The GGA results in Table 3.1 are consistent with previous studies, showing that SOGGA and PBEsol are the two best GGAs for lattice constants. SOGGA11, although having a more flexible form than SOGGA, produces worse lattice constants, implying that a correct second order expansion alone does not guarantee a good GGA for solid-state lattice constants. At the meta-GGA level, we find revTPSS to perform better than M06-L, in agreement with previous finding that, although M06-L is generally good for geometrical quantities, TPSS and revTPSS perform better for transition metal lattice constants.[16]

Table 3.2 summarizes the calculated surface formation energies using the various functionals. Our results for PBE, PBEsol, RPBE, and revTPSS are consistent with those obtained in Ref. 13, and our results for BLYP are consistent with those in Ref. 12 (only results for Rh and Pt were reported). Clearly all GGAs underestimate the surface formation energies, while meta-GGAs greatly improve the results. Furthermore, M06-L improves over revTPSS for Rh, Pt, Ag, and Pd, yielding the best surface formation energies of all functionals tested. At the GGA level, SOGGA produces the best performance, and SOGGA11, with a performance here very similar to PBEsol, does not do as well as SOGGA.

It is interesting to consider that the revTPSS functional is a revision of the TPSS[26] functional, which is itself a revision of the PKZB[27] functional. The PZKB functional has a parameter fitted to give surface correlation energies in agreement with earlier values, and revTPSS was designed to improve lattice constant predictions while keeping good surface formation energy predictions. In contrast M06-L was entirely designed (on a different developmental footing) on the basis of atomic and molecular energies, and its very good performance for surface formation energies is a further confirmation of the reasonableness of the way that it incorporates the physics of both small and extended systems.

Finally we turn to CO adsorption energies, which are shown in Table 3.3 and Fig. 3.1. Again our results for the PBE, PBEsol, RPBE, and revTPSS functionals agree well with the values obtained in Ref. 12. First we look at the site preferences predicted by the various functionals (in comparing the site preferences to experiment, we note that we are neglecting changes in zero-point energies and thermal vibrational energies under the assumption the size and site dependence of vibrational energy changes upon adsorption are

too small to change the conclusions). M06-L correctly predicts the site preference for all metals except Cu, where the calculated hollow adsorption energy is only 0.05 eV lower than the one on-top site. This performance is unparalleled by most other functionals tested, which tend to favor the hollow site for almost all metals, with the only exception being BLYP, which also predicts the site preferences of four metals correctly, although with a very poor performance in lattice constants and surface energies. Next we study the values of the adsorption energies. All GGAs except for BLYP overestimate the adsorption energies, with SOGGA and SOGGA11 faring the most poorly. BLYP, on the contrary, greatly underestimate the adsorption energies, with an MUE of 0.33 eV. This is consistent with the well-established dilemma[6] that improvement of surface formation energies for GGAs leads to worse performance for adsorption energies (this problem may be overcome by nonseparable gradient approximations[28] or the RPA,[12] but examination of nonseparable approximations and the RPA is beyond our present scope). And since both SOGGA and SOGGA11 are designed to have a correct second order expansion, this seems to imply that the second order expansion, which is important only for nearly uniform densities, is not a crucial determinant of accuracy for practical applications.[3] The best GGA turns out to be RPBE, which was designed to be used for chemisorption, but, perhaps unsurprisingly in light of what we know now, it is the worst in surface formation energies. Both of the meta-GGAs improve over most GGA results (other than RPBE, which is the functional with smallest MUE in adsorption energies, although with wrong site preferences), implying that they have sidestepped the dilemma. Again we observe that M06-L presents a smaller error than revTPSS for Rh, Pt, Cu, and Pd, and it has an identical performance for Ag. Combined with the performance for surface formation energies, the structures of gold clusters,[29–31] a

database designed to test performance for types of energy calculations needed to model catalysis,[32] the equilibrium distances and the binding energies of aromatic molecules on metal surfaces,[33] and the attractive intermolecular interactions in self-assembled monolayers,[34] M06-L is validated to be the best current candidate for a functional with reliable and balanced performance for describing important properties of physical chemistry at molecule–solid interfaces.

The success of M06-L in several recent challenging applications[31,333,34,36,37] and the present study may be explained by considering the advantages of including dependence on τ. As discussed previously,[38–40] τ allows one to distinguish regions of space described by a single orbital (including one-electron regions) from many-orbital and many-electron regions, and also it allows us to distinguish regions of decaying density from bonding regions. The latter is particularly important for describing surfaces, since the density decays exponentially to zero at a surface but not in a bulk solid. By making the exchange energy density more realistic, large exchange interactions are modeled more realistically, and we have found in our development work that meta-GGA functionals can be designed to work well with a wider range of the percentage of HF exchange than can GGAs. In the presence of improved exchange, the smaller correlation energy can more readily be optimized in a physical way to improve medium-range and short-range correlation energy rather than restraining it unphysically it to compensate large systematic errors in the exchange. Again the presence of τ in correlation allows more flexibility than just employing the reduced density gradient. To take advantage of these features M06-L was developed by combining constraint satisfaction and semiempirical fitting to a diverse database to achieve a balanced description of main-

group thermochemistry, bond energies, barrier heights, transition metal chemistry, and noncovalent interactions. The parameters in M06-L have been regulated by the constraint enforcement and the diverse training data so that it can give broad accuracy for many challenging problems (even outside of the training data) for which GGAs and some other meta-GGAs fail.

References for Chapter 3

(1) Kohn, W.; Sham, L. J. *PhRv* **1965**, *140*, A1133.

(2) Abild-Pedersen, F.; Andersson, M. P. *Surf. Sci.* **2007**, *601*, 1747.

(3) Alaei, M.; Akbarzadeh, H.; Gholizadeh, H.; de Gironcoli, S. *Phys. Rev. B* **2008**, *77*.

(4) Doll, K. *Surf. Sci.* **2004**, *573*, 464.

(5) Feibelman, P. J.; Hammer, B.; Norskov, J. K.; Wagner, F.; Scheffler, M.; Stumpf, R.; Watwe, R.; Dumesic, J. *J. Phys. Chem. B* **2001**, *105*, 4018.

(6) Schimka, L.; Harl, J.; Stroppa, A.; Gruneis, A.; Marsman, M.; Mittendorfer, F.; Kresse, G. *Nat. Mater.* **2010**, *9*, 741.

(7) Stroppa, A.; Termentzidis, K.; Paier, J.; Kresse, G.; Hafner, J. *Phys. Rev. B* **2007**, *76*, 195440.

(8) Lee, S. J.; Mukerjee, S.; Ticianelli, E. A.; McBreen, J. *Electrochim. Acta* **1999**, *44*, 3283.

(9) Christoffersen, E.; Liu, P.; Ruban, A.; Skriver, H. L.; Norskov, J. K. *J. Catal.* **2001**, *199*, 123.

(10) Liu, P.; Logadottir, A.; Norskov, J. K. *Electrochim. Acta* **2003**, *48*, 3731.

(11) Modestov, A. D.; Tarasevich, M. R.; Filimonov, V. Y.; Davydova, E. S. *Electrochim. Acta* **2010**, *55*, 6073.

(12) Stroppa, A.; Kresse, G. *NJPh* **2008**, *10*.

(13) Sun, J. W.; Marsman, M.; Ruzsinszky, A.; Kresse, G.; Perdew, J. P. *Phys. Rev. B* **2011**, *83*, 121410.

(14) Perdew, J. P.; Ruzsinszky, A.; Csonka, G. I.; Constantin, L. A.; Sun, J. W. *Phys. Rev. Lett.* **2009**, *103*.

(15) Zhao, Y.; Truhlar, D. G. *J. Chem. Phys.* **2006**, *125*, 194101.

(16) Zhao, Y.; Truhlar, D. G. *J. Chem. Phys.* **2008**, *128*, 184109.

(17) Peverati, R.; Zhao, Y.; Truhlar, D. G. *J Phys Chem Lett* **2011**, *2*, 1991.

(18) Perdew, J. P.; Ruzsinszky, A.; Csonka, G. I.; Vydrov, O. A.; Scuseria, G. E.; Constantin, L. A.; Zhou, X. L.; Burke, K. *Phys. Rev. Lett.* **2008**, *100*, 136406.

(19) Peverati, R.; Truhlar, D. G. *J. Chem. Phys.* **2012**, *136*.

(20) Kresse, G.; Furthmuller, J. *Comput. Mater. Sci.* **1996**, *6*, 15.

(21) Kresse, G.; Furthmuller, J. *Phys. Rev. B* **1996**, *54*, 11169.

(22) Blochl, P. E. *Phys. Rev. B* **1994**, *50*, 17953.

(23) Kresse, G.; Joubert, D. *Phys. Rev. B* **1999**, *59*, 1758.

(24) Perdew, J. P.; Burke, K.; Ernzerhof, M. *Phys. Rev. Lett.* **1996**, *77*, 3865.

(25) Hammer, B.; Hansen, L. B.; Norskov, J. K. *Phys. Rev. B* **1999**, *59*, 7413.

(26) Tao, J. M.; Perdew, J. P.; Staroverov, V. N.; Scuseria, G. E. *Phys. Rev. Lett.* **2003**, *91*.

(27) Perdew, J. P.; Kurth, S.; Zupan, A.; Blaha, P. *Phys. Rev. Lett.* **1999**, *82*, 2544.

(28) Peverati, R.; Truhlar, D. G. *J. Chem. Theory Comput.* **2012**, *8*, 2310.

(29) Mantina, M.; Valero, R.; Truhlar, D. G. *J. Chem. Phys.* **2009**, *131*, 064706.

(30) Ferrighi, L.; Hammer, B.; Madsen, G. K. H. *J. Am. Chem. Soc.* **2009**, *131*, 10605.

(31) Vilhelmsen; L. B.; Hammer, B. *Phys. Rev. Lett.* **2012**, *108*, 126101.

(32) Yang, K.; Zheng, J.; Zhao, Y.; Truhlar, D. G. **2010**, *132*, 164117.

(33) Ferrighi, L.; Madsen, G. K. H.; Hammer, B. *J. Chem. Phys.* **2011**, *135*, 84704.

(34) Ferrighi, L.; Pan, Y.; Grönbeck, H.; Hammer, B. *J. Phys. Chem. C* **2012**, *116*, 7374.

(35) Vitos, L.; Ruban, A. V.; Skriver, H. L.; Kollar, J. *Surf. Sci.* **1998**, *411*, 186.

(36) Madsen, G. K. H.; Ferrighi, L.; Hammer, B. *J. Phys. Chem. Lett.* **2010**, *1*, 515.

(37) Andersen, M.; Hornekaer, L.; Hammer, B. *Phys. Rev. B* **2012**, *86*, 085405.

(38) A. D. Becke, *J. Chem. Phys.* **1996**, *104*, 1040.

(39) Y. Zhao and D. G. Truhlar, *J. Phys. Chem. A* **2005**, *109*, 5656.

(40) L. Ferrighi, B. Hammer and G. K. H. Madsen, *J. Am. Chem.Soc.* **2009**, *131*, 10605.

Table 3.1. Optimized equilibrium lattice constants (Å) of five transition metals by eight density functionals compared to experiment

	Exp. [a]	PBE	M06-L	RPBE	PBEsol	revTPSS	SOGGA	SOGGA11	BLYP
Rh	3.79	3.84	3.82	3.87	3.79	3.80	3.78	3.83	3.90
Pt	3.88	3.98	3.96	4.00	3.93	3.93	3.91	3.98	4.06
Cu	3.60	3.63	3.54	3.68	3.57	3.56	3.56	3.54	3.71
Ag	4.06	4.16	4.16	4.23	4.07	4.07	4.05	4.06	4.27
Pd	3.88	3.96	3.97	4.00	3.89	3.91	3.88	3.91	4.04
MUE [b]		0.07	0.07	0.11	0.02	0.03	0.02	0.05	0.15

[a] Experimental values taken from Ref. 7

[b] Mean unsigned error

Table 3.2. Surface formation energies (eV) for forming a (111) surface from fcc bulk metal for five transition metals, as calculated by eight density functionals and compared to experiment

	Exp.[a]	PBE	M06-L	RPBE	PBEsol	revTPSS	SOGGA	SOGGA11	BLYP
Rh	1.07	0.81	1.11	0.73	0.93	1.02	0.99	0.88	0.61
Pt	1.08	0.65	0.85	0.55	0.77	0.83	0.81	0.69	0.45
Cu	0.65	0.47	0.71	0.39	0.54	0.64	0.59	0.49	0.31
Ag	0.58	0.34	0.57	0.25	0.43	0.50	0.46	0.43	0.12
Pd	0.85	0.57	0.85	0.48	0.68	0.77	0.73	0.67	0.43
MUE[b]		0.28	0.07	0.37	0.18	0.09	0.13	0.21	0.46

[a] Converted from experimental results[35].

[b] Mean unsigned error

Table 3.3. CO adsorption energies (eV) and site preferences of five transition metals from eight density functionals compared to experiment.

Functional		Rh	Pt	Cu	Ag	Pd	MUE[d]
Exp.	E_{ads}[a]	-1.45	-1.37	-0.5	-0.28	-1.48	
	Site[b]	T	T	T	T	H	
PBE	E_{ads}(on-top)	-1.90	-1.63	-0.74	-0.17	-1.39	0.28
	E_{ads}(hollow)	-1.96	-1.77	-0.80	-0.13	-1.82	
	Site[c]	H	H	H	T	H	
M06-L	E_{ads}(on-top)	-1.78	-1.48	-0.65	-0.17	-1.3	0.17
	E_{ads}(hollow)	-1.41	-1.12	-0.70	-0.06	-1.64	
	Site	T	T	H	T	H	
RPBE	E_{ads}(on-top)	-1.59	-1.34	-0.45	0.05	-1.11	0.11
	E_{ads}(hollow)	-1.69	-1.43	-0.48	0.17	-1.47	
	Site	H	H	H	T	H	
PBEsol	E_{ads}(on-top)	-1.05	-1.96	-1.05	-0.45	-1.72	0.49
	E_{ads}(hollow)	-1.10	-2.18	-1.23	-0.49	-2.23	
	Site	H	H	H	H	H	
revTPSS	E_{ads}(on-top)	-1.87	-1.53	-0.74	-0.17	-1.36	0.24
	E_{ads}(hollow)	-1.93	-1.67	-0.80	-0.18	-1.75	
	Site	H	H	H	H	H	
SOGGA	E_{ads}(on-top)	-2.29	-2.02	-1.13	-0.51	-1.80	0.64
	E_{ads}(hollow)	-2.38	-2.29	-1.35	-0.59	-2.35	
	Site	H	H	H	H	H	
SOGGA11	E_{ads}(on-top)	-2.31	-2.03	-1.08	-0.53	-1.79	0.62
	E_{ads}(hollow)	-2.29	-2.16	-1.21	-0.55	-2.23	
	Site	T	H	H	H	H	
BLYP	E_{ads}(on-top)	-1.38	-0.90	-0.27	0.28	-0.74	0.33
	E_{ads}(hollow)	-1.21	-0.88	-0.34	0.48	-1.17	
	Site	T	T	H	T	H	

[a] Experimental values.[2] Experimental error bars are approximately 0.1 eV.

[b] Preferred adsorption site from experiment.[2] T denotes on-top site; H denotes hollow site.

[c] Preferred adsorption site predicted by calculations.

[d] The error is calculated as the difference between the calculated adsorption energies at the site preferred by experiment (hollow site for Pd, and on-top site for all the other metals) and the experimental values.

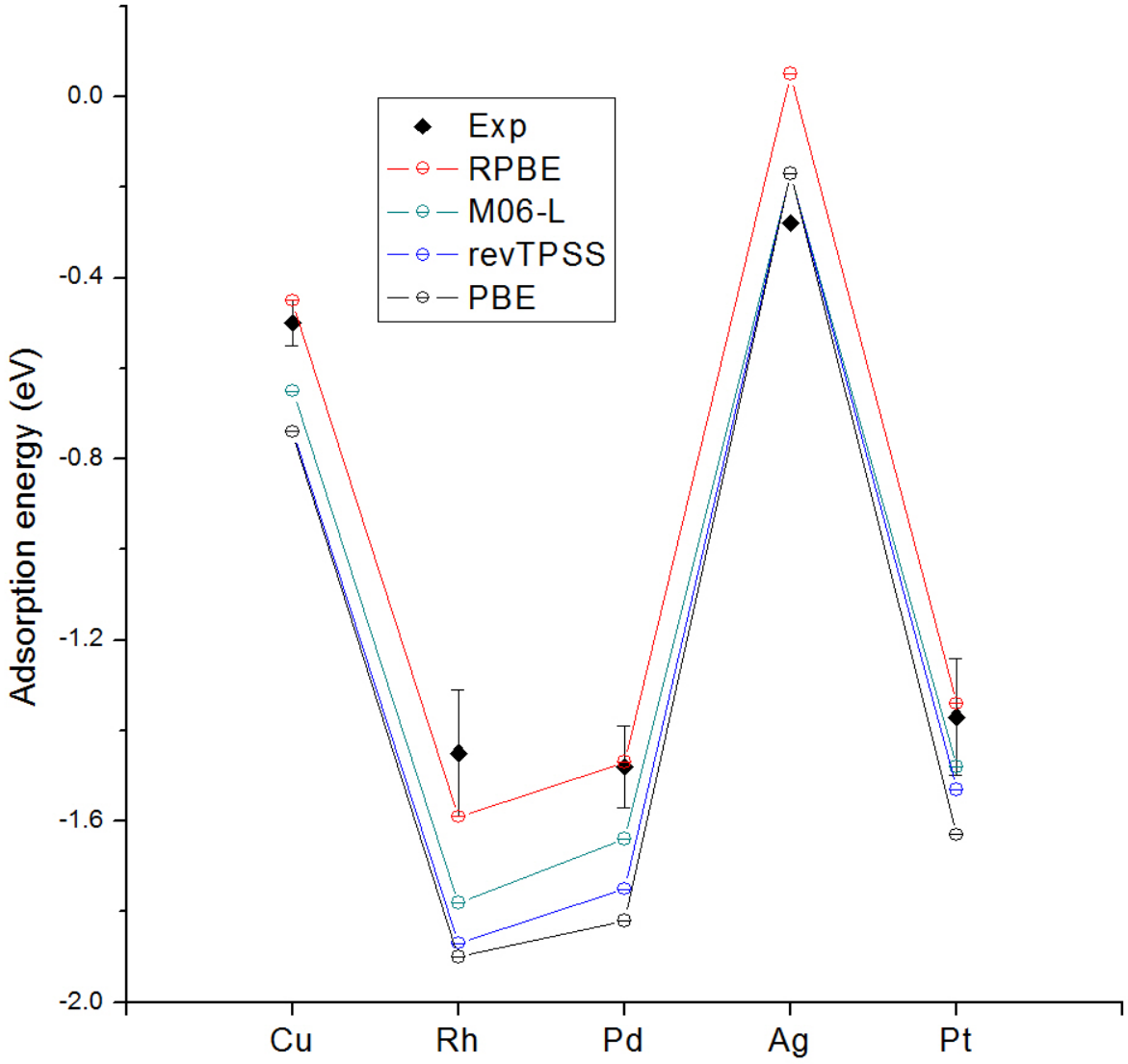

Figure 3.1. Adsorption energies compared to experiment. For each metal we show the adsorption energy at the site predicted to be more strongly bound by experiment.

Chapter 4

Density Functional Theory for Open-Shell Systems I: The 3d-Series Transition Metal Atoms and Their Cations

4.1 Introduction

Many systems involving transition metal atoms have open-shell electronic structures with several low-energy states differing in spin and/or in orbital occupancy. It is common practice to apply Kohn–Sham (KS) density functional theory (DFT)[1] to the lowest-energy state of each total electronic spin component (M_S),[2,3] to identify the ground state, and to model the properties, spectra, and reactivity of each spin state. However, when $2M_S$ is less than the number n_{SO} of singly occupied orbitals, the state is intrinsically multi-configurational, and one finds that KS-DFT, with its single-determinantal noninteracting reference state for computing the dominant portion of the kinetic energy, is often less accurate for the low-spin open-shell states than for the high-spin and closed-shell states ($M_S = n_{SO}/2$) for which a single Slater determinant is a good reference functions. This is mainly due to the fact that presently available exchange-correlation (xc) functionals, which are the only approximations in KS-DFT, usually cannot treat the multi-reference systems and single-reference ones equally well.[2-4] The difficulty is compounded when the different spin states differ in their *s* and *d* occupancies (e.g., $ns^N(n-1)d^{N'}$ in one spin state and $ns^{N-1}(n-1)d^{N'+1}$ in the other), since the

approximate xc functionals may have different accuracies for *ns* electrons than for (*n*–1)*d* electrons, which tend to be closer to the nucleus in a region of higher electron density. For the reasons above, it is worthwhile to test currently available xc functionals' performance in these difficult cases.

Testing the functionals requires care to be sure that the conclusions are not clouded by the following complications:

a. incomplete basis sets or inadequate effective core potentials;

b. incomplete treatment of relativistic effects, including spin-orbit coupling;

c. errors in reference data;

d. cancellation of errors in treating the transition metal with errors in treating ligands or the ligand field exerted on the transition metal site.

All of these possible complications are minimized or even eliminated by studying unligated monatomic atoms M and monatomic cations M^+ of the 3d-series. In particular, because these systems are small, one can afford to use nearly complete all-electron basis sets without effective core potentials. Also, the experimental excitation energies and ionization potentials are well established. Furthermore, the relativistic effects are small enough that Douglas–Kroll–Hess second-order calculations should account well for scalar relativistic effects, and spin-orbit effects can be largely removed from experiment by considering the weighted average of the configuration. Finally, by studying atoms and monatomic ions, the treatment of electronic structure is decoupled from geometry optimization, which can have a pronounced effect on such comparisons for molecules.

Thus in this article we present a systematic study of the ability of currently available xc functionals to predict the spin-transition excitation energies of all 3d-series

transition metal atoms (Sc through Zn) and their singly-charged cations (Sc^+ through Zn^+) as well as the ionization potentials connecting these two sets. The treatment of open-shell systems by KS-DFT or its generalizations is an important frontier area of practical work in DFT. The 3d transition metal series, because of it higher natural abundance than the other transition series, is very important for catalysis, including organometallic catalysts, heterogeneous catalysts, and biological catalysts.

In a certain sense, this paper is the third in a series, following up on closely related work on p-block atoms[5] and 4d-series atoms and ions.[6] Atoms and monatomic ions often have more near degeneracy character than catalytically important complexes with higher metal coordination numbers, and this can make them even more difficult to treat than the difficult transition metal compounds; in this sense, these tests on atoms are not only of fundamental interest, but also of interest in that they provides especially difficult challenges for DFT.

4.2 Computational Details and Experimental Data

All calculations were done with a locally modified version of *Gaussian 09*.[7] The integration grid for density functional calculations is a pruned grid obtained with 99 radial and 590 angular points, which is denoted as "ultrafine" in *Gaussian* 09. The all-electron relativistic cc-pVQZ-DK basis set was used,[8] and the scalar relativistic effect was included by using the Douglas-Kroll-Hess (DKH) second-order scalar relativistic Hamiltonian.[9-11] To calculate 4s and 3d subshell occupation numbers for interpretation purposes, natural bond orbital (NBO) analysis[12-19] was performed using the *NBO 3.1* package with *Gaussian 09.*

The experimental data were obtained from NBS tables.[20] For each experimental multiplet, the energy was averaged over the total angular momentum quantum number *J*; the (2*J*+1) degeneracy of each term was taken into account with the degeneracy-weighted average formula

$$\overline{E}(^{2S+1}\mathrm{L}) = \frac{\sum_{J=|L-S|}^{L+S}(2J+1)E(^{2S+1}L_J)}{\sum_{J=|L-S|}^{L+S}(2J+1)} \tag{4.1}$$

Note that experimental *S* and *L* values are only nominal because *S* and *L* are not good quantum numbers. Since the spin-orbit operator is traceless, spin-orbit coupling does not change $\overline{E}$ to first order, and therefore $\overline{E}$ may be interpreted as an atomic energy in the absence of spin–orbit coupling (i.e., an atomic energy from which spin-orbit coupling has been removed). Although eq 1 is written in the Russell-Saunders coupling scheme, a degeneracy-weighted average also removes spin-orbit effects to first order when the coupling scheme is better described as *j-j* coupling. For our comparisons of theory to experiment, we compare calculations without spin-orbit coupling to experimental values obtained using degeneracy-weighted averages.

We label $\overline{E}$ of the ground state as $E(\mathrm{GS})$. The excited state of interest in this paper is the lowest-energy excited state (ES) that has an *S* value different from the ground state (GS). The $\overline{E}$ of this state is called $E(\mathrm{ES})$. Table 4.1 lists the excitation energies defined as

$$\Delta E = E(\mathrm{ES}) - E(\mathrm{GS}) \tag{4.2}$$

The energies and excitation energies for singly charged cations are labeled $E(\mathrm{GS}^+)$, $E(\mathrm{ES}^+)$, and ΔE^+. The ionization potential (IP) is

$$IP = E(\mathrm{GS}^+) - E(\mathrm{GS}) \tag{4.3}$$

Table 4.1 also lists 2*S*+1, *L*, and the electron configuration of the GS and ES of each neutral atom and cation as well as ΔE^+ and IP.

4.3 Density Functionals Tested

We tested 75 xc functionals as well as the Hartree-Fock[21-23] method. In a general way, xc functionals may be divided into two groups: hybrid, in which some local exchange is replaced by a percentage *X* of nonlocal Hartree-Fock exchange, and local, in which the xc functional depends only on local variables, in particular on the local values of spin-labeled electron density, ρ_σ , where σ is α or β, on optionally also on the local values of the square of the reduced density gradient[5], s_σ^2 , which is defined as $\left|\nabla\rho_\sigma\right|^2 \Big/ \rho_\sigma^{8/3}$, and on the local values of the spin-labeled kinetic energy densities τ_α and τ_β .

None of the xc functionals tested here has nonlocal correlation; therefore they may be divided into two general categories: local and hybrid, where the latter refers to a nonlocal functional in which the nonlocality is limited to including some Hartree–Fock nonlocal exchange. The xc functionals are listed in Table 4.2, where they are divided into the two categories and into 14 subtypes as follows:

Local exchange-correlation functionals

- LSDA: a functional that depends only on ρ_σ (for closed shells, this is sometimes called LDA)
- GGA: a functional that also depends on s_σ^2, with the separability requirement that the exchange functional for each spin component σ is expressed as a product of a function of ρ_σ time a function of s_σ^2 (the correlation functional also depends only on ρ_σ and s_σ^2)
- NGA: a functional that depends on the same variables as a GGA, but without the separability requirement[6]
- meta-GGA: a functional like a GGA, but that also depends on spin-labeled kinetic energy densities τ_α and τ_β
- range-separated meta-GGA: a functional like a meta-GGA, but the parameters of the functional depend on interelectronic separation
- meta-NGA: a functional like an NGA, but that also depends on τ_α and τ_β

Hybrid exchange-correlation functionals

- global-hybrid GGA: a hybrid GGA where the percentage *X* of local exchange that is replaced by Hartree-Fock exchange is a global constant, that is, it is independent of point in space, ρ_σ, $\nabla\rho_\sigma$, τ_σ, or interelectronic separation
- global-hybrid meta-GGA: a hybrid meta-GGA where the percentage *X* of local exchange that is replaced by Hartree-Fock exchange is a global constant

- long-range-corrected GGA: a hybrid GGA in which *X* increases as a function of interelectronic separation
- long-range-corrected meta-GGA: a hybrid meta-GGA in which *X* increases as a function of interelectronic separation
- screened exchange GGA: a hybrid GGA in which *X* decreases to zero as interelectronic separation increase
- screened exchange NGA: a hybrid NGA in which *X* decreases to zero as interelectronic separation increases
- screened exchange meta-NGA: like a screened-exchange NGA except the local part also depends on τ_α and τ_β (same as a long-range-corrected hybrid meta-GGA but using a meta-NGA rather than a meta-GGA and *X* decreases rather than increases with interelectronic separation)

Table 4.1 also shows the percentage of Hartree-Fock exchange *X* and gives the references[25-86] for each functional. Further details of the functional forms of the subtypes and the individual functionals may be found in these references. Many of the functionals are also discussed in more detail in refs. 5 and 6; we simply note here that the functionals chosen for study in the present article are selected for various reasons, including their popularity, their good performance for one or another property in previous work, and their interest from a fundamental point of view.

We note one important point about the tests in the present article and most of the other tests and validation studies carried out in our group. Unlike most such tests, the list of xc functionals studied is not limited to those found in any single program. No single available software package has all the functionals studied in this paper. As just one

example, the relatively recent OreLYP is not found in any software package that we know of, but we have coded this and other xc functionals for a local version of *Gaussian 09* to make our study more comprehensive.

Finally we comment on the motivation a group of eight new functionals tested here. Recently there has been extensive interest in designing better xc functionals for van der Waals interactions, and some studies have pointed to PW86[106], a GGA exchange functional developed in the pioneering days of functional development, and C09[107], a very recent GGA exchange functional, for their performance in conjunction with nonlocal correlation functionals.[108-110] These functionals apparently benefit from a reduced dependence on the density gradient for small values of the magnitude of the density gradient—thus either restoring the density gradient expansion through second order, as is done in the SOGGA[43] and SOGGA11[45] functionals, or nearly restoring it. With these functionals garnering attention, it is worthwhile to test their ability for application in general chemistry applications. In this study we combine them with four correlation functionals for comprehensive evaluation, in particular with the PBE[31] and LYP[29] correlation functions, which are among the most popular GGA correlation functionals, with the reLYP correlation functional,[38] which is a new re-optimized version of LYP designed for treating atoms with atomic number greater than 19 (the atoms in the 3d transition series have atomic numbers in the range 21 to 30), and with the SOGGA11 correlation functional, which is of special interest in this context because it has been shown to be accurate for a wide range of applications in chemistry and physics when combined with the SOGGA11 exchange functional, which shares with C09 an adherence to the correct gradient expansion through second order.

4.4 Theory and Methods

4.4.1 Stability Optimization

One important aspect of treating open-shell systems is the symmetry problem. Atoms (and many diatomic molecules) often have higher symmetry than catalytically important complexes with higher metal coordination numbers. However, the goal of this paper is to test the potential abilities of various xc functionals for treating real-world molecules containing transition metal atoms, and most molecules of interest have low symmetry. Furthermore, it is not theoretically justified to force specific symmetries on the KS Slater determinant because the KS Hamiltonian need not have the same symmetry as the real electronic Hamiltonian.[3,87,88] As a consequence one needs to consider broken-symmetry solutions, which are solutions to the self-consistent-field (SCF) equations that, even in the absence of spin-orbit coupling, do not belong to one of the irreducible representations of the atomic or molecular point group or are not eigenfunctions of $\hat{S}^2$ where $\hat{S}$ is the total electron spin operator.[89,90] For closed-shell systems, which are always singlets, we generally do not find broken-symmetry solutions. However, for systems with a partially filled subshell, such as most cases in this work, the lowest-energy solutions to the KS equations are often found to be broken-symmetry solutions. For these reasons, in all calcuations, we did not require the orbitals or reference Slater determinants to satisfy any symmetry other than having collinear spin-orbitals and having fixed values of M_S. Rather, we chose to obtain the lowest energy state for each case under consideration by full minimization subject only to the constraint of integer occupation numbers of collinear spin-orbitals with a given M_S.

In order to describe the methods that we used, it is convenient to first define and review some terminology. In all the calculations presented in this article, the spin parts of the spin orbitals are either α or β, i.e., the calculations are collinear. Therefore, M_S, which is the component of total electron spin along the arbitrary spin quantization axis, is a good quantum number and is equal to the half the difference between number of α electrons and the number of β electrons. The eigenvalues of $\hat{S}^2$ are $S(S+1)$, where S is the total electron spin quantum number; however, the KS Slater determinant need not be an eigenfunction of $\hat{S}^2$. We let n_{SO} be the number of nominally single occupied orbitals (we say "nominally" because [as usual for an unrestricted calculation] the α and β orbitals of a "doubly occupied" pair are not identical.) In all 20 cases (ten atoms, ten cations) studied in this paper, the ground state has $S = n_{SO}/2$, where n_{SO} is the number of singly occupied orbitals, if any; that is that the electrons in singly occupied orbitals all have the same spin, which we take as α. In 11 of the cases, the excited state also has $S = n_{SO}/2$. The other nine cases have $S < n_{SO}/2$, which makes them intrinsically multiconfigurational and leads to broken-symmetry solutions because Kohn–Sham theory always represents the density by a single Slater determinant. We are interested, for each atom and cation considered, in the lowest excitation that changes the value of S, as enumerated in Table 4.1.

The self-consistent field (SCF) optimization of Slater determinants for transition elements is a challenging procedure because the SCF method may not converge to the lowest-energy solution, but to some local minimum or just a higher-order extremum (typically a saddle point). This difficulty is exacerbated by the presence of nearly degenerate s and d

orbitals in transition metals. In all of our variational calculations we performed a stability analysis[91,92] on the SCF wave functions (by using the "stable=opt" keyword in *Gaussian 09*), followed by reoptimization of the reference wave function if an internal instability was found, and this stabilization procedure was repeated until the lowest-energy solution was obtained with no internal instabilities. In this process all the symmetry constraints were relaxed, as explained above. To verify that we have achieved the global minimum, we recalculated each state of each atom or cation with several different initial guesses and made sure they would converge to an identical solution. The need for stabilization is one of the major complications of using DFT to study open-shell systems, and it will be discussed further in the next subsection.

4.4.2 Treatment of Open-Shell States

First we classify possible electronic states of a system into one of two categories: nominally single-determinant (NSD) states and intrinsically multi-determinant (IMD) states. The NSD states are those with $S = n_{SO}/2$, and the IMD states are those with $S < n_{SO}/2$.

In all cases the energy of NSD states are equated to the stabilized SCF energy of the state with M_S = S. It is well known that the best way to calculate the energy of an IMD state is problematic, and we will calculate energies in three ways for all IMD states.

The *first* method is called the *variational method*. In this method,

$$E_{\mathrm{IMD}}^{\mathrm{var}}\left(n_{\mathrm{SO}}, S, M_S\right) = E_{\mathrm{IMD}}^{\mathrm{SCF}}\left(n_{\mathrm{SO}}, S, M_S = S\right) \tag{4.4}$$

where the right-hand side is the energy of the stably optimized SCF calculation of the state with M_S = S.

However, when one optimizes a state with $M_S = S < n_{SO}/2$, it is always possible to form, from the same orbitals as those in the optimized state, another $M_S = S$ state that has $S = n_{SO}/2$. Because our xc functionals are not exact, the optimized state can be considered to be a mixture of these two states; this situation is often signaled by the $<S^2>$ value of the SCF solution.[93] For example, in the simplest case of an open-shell singlet which has two unpaired electrons, one of α spin and one of β spin, one sometimes finds $<S^2> = 1.0$. If the spatial parts of the spin orbitals were the same in the singlet and the triplet, such a broken-symmetry solution could be considered to be a 50:50 mixture of the corresponding singlet ($<S^2>=0$) and triplet ($<S^2>=2$) states, and, the energy difference between the real singlet and the triplet would be twice as much as the energy difference between the calculated broken-symmetry $M_S = 0$ state and the triplet $M_S = 1$ state. The generalization of this situation to other multiplicities has been called the weighted-average broken symmetry (WABS) method, and it is our *second* method. The result is encapsulated in the formula given by Yamaguchi,[94] which yields

$$\begin{aligned} E_{IMD}^{WABS}\left(n_{SO},S,M_S\right) &= E_{NSD}^{SCF}\left(n_{SO},S=n_{SO}/2,M_S=n_{SO}/2\right) \\ &- k[E_{NSD}^{SCF}\left(n_{SO},S=n_{SO}/2,M_S=n_{SO}/2\right) \\ &- E_{IMD}^{SCF}\left(n_{SO},S,M_S=S\right) \end{aligned} \tag{4.5}$$

where

$$\begin{aligned} k &= n_{SO}/[<S^2>_{NSD}^{SCF}\left(n_{SO},S=n_{SO}/2,M_S=n_{SO}/2\right) \\ &\quad -<S^2>_{IMD}^{SCF}\left(n_{SO},S,M_S=S\right)] \\ &= \frac{2S_{HS}}{<S^2>_{HS}-<S^2>_{BS}} \end{aligned} \tag{4.6}$$

This method has become popular in practical applications and has been discussed in detail elsewhere.[4,87]

A theoretical objection to this second approach is that eqs 5 and 6 are derived under the assumption that the IMD and NSD states have the same spatial orbitals such that the only difference between these states is that in the NSD state all singly occupied orbitals are α orbitals, while in the IMD state one or more of these orbitals become occupied by a β electron. Nevertheless the Yamaguchi formula is popularly applied even if one is uncertain regarding the validity of these assumptions, merely with knowledge of their energies and $< \hat{S}^2 >$ values. Hence it is important to test this formula, and in our second method we utilized Yamaguchi formula for all IMD cases, even when orbitals that are occupied in the NSD state do not correspond to those that are occupied in the IMD state.

In our *third* method, for each IMD state, we calculated the SCF energy of an artificial $S = n_{SO}/2$ state with the same orbitals as in the IMD state (we obtain this state by flipping the spin of one or more singly occupied orbital), and this post-SCF state (labeled PSCF in equations) was used for the $S = n_{SO}/2$ state in eq 5, with the true NSD state still used in eqs 2 and 3. We call this the *reinterpreted broken symmetry* (RBS) approach. This yields

$$\begin{aligned} E_{IMD}^{RBS}\left(n_{SO},S,M_S\right) &= E^{PSCF}\left(n_{SO},S=n_{SO}/2,M_S=n_{SO}/2\right) \\ &- k[E^{PSCF}\left(n_{SO},S=n_{SO}/2,M_S=n_{SO}/2\right) \\ &- E_{IMD}^{SCF}\left(n_{SO},S,M_S=S\right) \end{aligned} \tag{4.7}$$

where

$$k = n_{SO} / [< S^2 >^{PSCF} \left(n_{SO}, S = n_{SO}/2, M_S = n_{SO}/2\right) - < S^2 >^{SCF}_{IMD} \left(n_{SO}, S, M_S = S\right)] = \frac{2S_{HS}}{< S^2 >_{HS} - < S^2 >_{BS}} \quad (4.8)$$

For example, consider the state Fe(^{3}F, 4s^{1}3d^7). In the variational method, the energy difference between ^{3}F and ^{5}D SCF states was calculated from the two stabilized SCF calculations. In the WABS method, the triplet state was calculated by the Yamaguchi formula where the NSD state is the stabilized quintet state, which is the Fe(^{5}D, 4s^{2}3d^6) state. For the RBS method, we need to consider the nature of the triplet state; it turns out that, for all the xc functionals under test in the present article, the triplet state has three dα electrons and one sβ electron. We therefore calculate a post-SCF artificial quintet state by flipping the spin of the s electron, and we obtain the energy of the triplet using eqs 7 and 8 with this artificial post-SCF quintet state, which is a nominally a state with 4s^{1}3d^7. If the triplet had been a state with two dα electrons, one dβ electron, and one sα electron, we would have had to flip the dβ electron.

The most appropriate way to flip the 4s β electron would take exactly the same β orbital and occupy it with an α electron. Since the spatial part of α and β orbitals are generally not orthogonal to each other, this step would require additional orthogonalization. To alleviate the computational complications, we flip the electron by identifying the α virtual orbital that is most similar to the β orbital we intend to flip, and calculate the post-SCF NSD state energy by occupying this particular α orbital. This works well when the orbitals of both spins are similar to each other, which is usually true. However, for some atoms, some of the density functionals produce states where the highest-energy nominally doubly occupied orbitals are very different for the alpha and beta electrons.

The RBS method is inappropriate for these cases, and it can produce very large errors. We recommend that when the flipped-state post-SCF energy is higher than the unflipped-state energy by more than 100 kcal/mol, one should apply neither the WABS method nor the RBS method. The cases where one of more functional raises the energy of the flipped state by more than 100 kcal/mol are the singlet state of Ni and doublet state of Co. If we delete excitation energies and ionization potentials that involve these states, there are only 28 of the 30 data available, and – among other statistical measures – we will give mean unsigned errors for these 28 cases to provide a more useful estimate of which functionals prove most accurate if a user restricts using the WABS and RBS method to cases where these methods are recommended.

4.4.3 Orbital Analysis

According to experimental data, there are nine cases of species with IMD electronic configurations, namely $Sc^+(^1D, 4s^13d^1)$, $Ti^+(^2F, 4s^13d^2)$, $V^+(^3F, 4s^13d^3)$, $Cr(^5S, 4s^13d^5)$, $Cr^+(^4D, 4s^13d^4)$, $Mn^+(^5S, 4s^13d^5)$, $Fe(^3F, 4s^13d^7)$, $Co(^2F, 4s^13d^8)$, and $Ni(^1D, 4s^13d^9)$. In four of these cases, $Sc^+(^1D, 4s^13d^1)$, $Ti^+(^2F, 4s^13d^2)$, $Cr(^5S, 4s^13d^5)$, and $Mn^+(^5S, 4s^13d^5)$, the correct corresponding NSD state is the ground state, and the only difference between the NSD and post-SCF states is that for the post-SCF ones, the orbitals are not optimized but rather are taken to be the same as in the IMD state. In the other five cases, $V^+(^3F, 4s^13d^3)$, $Cr^+(^4D, 4s^13d^4)$, $Fe(^3F, 4s^13d^7)$, $Co(^2F, 4s^13d^8)$, and $Ni(^1D, 4s^13d^9)$, the post-SCF state used for eqs 7 and 8 has different orbitals occupied than the ground states. This is clear for atoms where the orbitals have distinct

symmetries, but it would not always be obvious for low-symmetry molecules, for example, in C_1 symmetry where all the orbitals have the same symmetry.

The analysis is complicated by the fact that the calculated electronic states do not always correspond to the experimental ones. In many cases the calculated orbitals are described as spatial-symmetry-broken combinations of s and d orbitals, and the electronic configuration consequently has fractional atomic-orbital occupancy. The discrepancy between the experimental and calculated number of s electrons (s-occupancy-error) is given in Tables 4.3 and 4.4 (note that p orbitals do not participate in this mixing because they have different symmetry with regards to the inversion center).

We analyzed the correlation between s-orbital-occupancy error and spin contamination of the Slater determinant, and we found two kinds of cases.

In the first kind of case $< \hat{S}^2 >$ depends on s-orbital-occupancy error linearly. Cases of this type are Sc(^{2}D, 4s^{2}3d^1), Ti(^{3}F, 4s^{2}3d^2), V(^{4}F, 4s^{2}3d^3), Cr(^{5}S, 4s^{1}3d^5), Mn^+(^{5}S, 4s^{1}3d^5), Fe^+(^{4}F, 3d^7), Co^+(^{3}F, 3d^8), and Ni^+(^{2}D, 3d^9). For electronic states of this type, the shift of electron density from an s orbital to d orbitals results in a state that is a mixture of two states – multi-determinant and single-determinant. For example, for Sc(^{2}D, 4s^{2}3d^1) some functionals give a state where a beta s-electron is partially moved to a d-orbital, which means that the resulting state is a mixture of the experimentally observed nominally single-determinant state Sc(^{2}D, 4s^{2}3d^1) and a multi-determinant state Sc(4s^{1}3d^2) with electrons with opposite spins occupying two different d orbitals. The interesting opposite situation is observed for Cr(^{5}S, 4s^{1}3d^5). The initial state is multi-

determinantal, while a shift of the beta s-electron to any of five singly occupied d-orbitals results in mixture of the experimental state and a single-determinant Cr($3d^6$) state.

The second type of case includes Sc^+(^1D, $4s^13d^1$), Ti^+(^2F, $4s^13d^2$), V^+(^3F, $4s^13d^3$), Cr^+(^4D, $4s^13d^4$), Mn(^6S, $4s^23d^5$), Fe(^3F, $4s^13d^7$), Co(^2F, $4s^13d^8$), and Ni(^1D, $4s^13d^9$), where $<S^2>$ doesn't depend on s-orbital-occupancy error. Here both GS and ES states are multi-determinantal, except for the single-determinant Mn(^6S, $4s^23d^5$). For Fe(^3F, $4s^13d^7$), Co(^2F, $4s^13d^8$), and Ni(^1D, $4s^13d^9$) the situation is much simpler because in all these three cases the electron configuration has either exactly integer occupations, or one that is very close to an integer (see Table 4.3). In all these three cases the stably optimized ground states do not have the same orbitals occupied as the excited states, so the post-SCF states Fe(quintet $4s^13d^7$), Co(quartet $4s^13d^8$), and Ni(triplet $4s^13d^9$), are quite different from the stably optimized states.

Figures 4.1 and 4.2 illustrate the above observations by presenting plots of $<S^2>$ vs. s-occupancy error.

4.5 Results

4.5.1 Orbital Bias: s and d Orbitals

Let's first consider the s-orbital-occupancy error of various xc functionals because this is one possible criterion for assessing each functional's ability to describe the s and d orbitals in a balanced manner. Table 4.3 shows that DFT functionals with a small percentage *X* of Hartree-Fock exchange tend to have negative s-orbital-occupancy error, while functionals with high Hartree-Fock exchange tend to have less negative or even slightly positive s-orbital-occupancy error, and the predicted electronic configuration is

closer to the experimental dominant configuration, as can be seen also from the mean unsigned errors in Table 4.4. This is consistent with other studies.[6,95]

An obvious implication from this observation is that a judicious percentage of Hartree-Fock exchange is necessary for obtaining a balanced treatment of s and d electrons, which is further verified by considering excitation energies with s – d transitions. According to the experimental data, in the 20 multiplicity-changing transitions under consideration, 12 cases involve electron excitations between s and d orbitals. These cases are Sc, Ti, V, V^+, Cr^+, Fe, Fe^+, Co, Co^+, Ni, Ni^+, and Cu^+. The average difference (over 68 methods) between number of s electrons for IMD and NSD states are 0.9, 0.9, 0.8, 0.3, 0.3, 0.7, 0.9, 0.7, 1.0, 0.4, 1.0, and 1.0 for each case respectively. Due to s-orbital-occupancy error, in the cases of V^+, Cr^+, and Ni, many functionals incorrectly predict the electronic state, resulting in both states presenting about the same number of s and d electrons, so they are excluded from further discussions of this aspect, and we only considered the nine remaining cases. Tables 4.5-4.7 show the performance of various functionals for prediction of s→d excitation of the nine species above. It is interesting to compare data from Tables 4.3 and 4.7, because they both are related to the calculated energy gaps between s and d orbitals. The scattergram obtained this way is presented in Figure 4.3, which clearly shows that methods with negative s-orbital-occupancy error tend to underestimate energy of s→d excitation, and vice versa. This makes perfect sense since a negative s-orbital-occupancy error implies a bias of the corresponding functional towards the d orbitals, which leads to a smaller s→ d transition energy, and vice versa.

Table 4.6 allows us to put the over stabilization of s orbitals relative to d orbitals by Hartree-Fock exchange on a quantitative basis. For example, HFLYP has an MSE for s→d excitation energies of 24.4 kcal/mol, whereas MPWLYP, BLYP, and OLYP, which have precisely the same correlation functional but local exchange, have MSEs of -6.0, -6.2, and -9.7 kcal/mol, respectively. B1LYP, which is 20:80 mixture of HFLYP and BLYP, has an MSE of 0.7 kcal/mol, much closer to the value for BLYP than to that for HFLYP. Correlation favors d orbitals, as seen by comparing the MSEs for HF (31.2 kcal/mol) and HFLYP (24.4 kcal/mol) or B88 (-1.3 kcal/mol) and BLYP (-6.2 kcal/mol); the differences are remarkably similar (6.8 and 7.5 kcal/mol). Similarly Table 4.6 shows that PW91 correlation over favors d orbitals by a larger amount than LYP, in particular comparing HFPW91 to HF shows a difference of 12.1 kcal/mol (which may fairly be compared to the 6.8 kcal/mol difference mentioned in the previous sentence). This is very relevant because PW91 correlation is almost the same as the widely used PBE correlation.

Some functionals have MSEs of absolute magnitude less than 2 kcal/mol in Table 4.6, namely B97-3, B97-1, M08-HX, M06, CAM-B3LYP, MPW3LYP, B1LYP, M06-L, B3V5LYP, M08-SO, OreLYP, MPWKCIS1K, and BB, with X values of 26.93, 21, 56.79, 27, 19–65, 21.8, 20, 0, 20, 52.23, 0, 41, and 0, respectively. Many other functionals with X in this range do less well or even much less well, so clearly the systematic errors depends on much more than the just the value of X.

In Table 4.7, SOGGA11-X and M06 have MSEs with magnitudes larger than 2.0 kcal/mol, but – along with M06-L and B97-3 – are among the four leading MUEs in Table 4.7.

4.5.2 Spin States and Ionization Potentials

Next we turn to the errors for energies of excitation from ground states to excited states, calculated by the variational method, by the WABS method, and by the RBS method, as given in Tables 4.8, 4.9, and 4.10, respectively. In all three tables the methods are sorted according their mean unsigned error, MUE(20), for the 20 cases. We find the accuracy of RBS to be almost equal to that of the WABS, and thus it is potentially another choice for treating the broken-symmetry problem; we prefer RBS because it uses only the orbitals optimized for the IMD state to calculate its energy, which seems more consistent with the assumptions of the Yamaguchi formula. It is also clear that the variational method is the worst among the three methods, implying that either RBS or WABS should be used as long as the system does not conflict the general criteria for application of them. According to the RBS results in Table 4.10, one concludes that the six best functionals for excitation energies are SOGGA11-X, ωB97X-D, MPW1B95, MPW1K, B97-3, and CAM-B3LYP.

Table 4.10 shows that the MUE of B3LYP*, which is a functional specifically reparametrized for spin states of 3d-series transition metal compounds, is 5.8 kcal/mol, somewhat worse than that of the older B3LYP method (5.3 kcal/mol).

The errors for ionization potentials for the variational method, the WABS method, and the RBS method are given in Tables 4.11-4.13. Although most of the ground states of both atoms and cations are NSD states, the spin contamination from an unbalanced treatment of s and d orbitals in many states still leads to a slightly different corrected energy with WABS or RBS method. Thus for more than half of the xc functionals under examination, we find changes in MSE as well as MUE values across Table 4.11-4.13,

further resulting in variations in performance rankings. An immediate observation is the good performance of the B97-*X* (*X* = 1, 2, 3) series of functionals, all with an MUE(10) of less than 4.0 kcal/mol in all three tables. Other best methods in Table 4.12 are B98, ωB97X-D, PW6B95, ωB97X, B1LYP, M08-SO, MPW1B95, and CAM-B3LYP – all of which have an MUE(10) < 4.0 kcal/mol. Most of them perform well also for excitation energies using the RBS correction. However, SOGGA11-X, which is one of the best methods for excitation energies, has a larger error of 6.7 kcal/mol.

The overall performance for excitation energies and ionization potentials, calculated as the MUE(30), is given in Table 4.14, where the methods are sorted according to their performance for IP and excitation energies with RBS corrections. Although the RBS method attempts to account for variation in orbital character better than the WABS method, this orbital variation can still be a source of problems, as already discussed briefly in Section 4.2. When a low-spin state has an orbital flipped, we remove one electron from a minority-spin orbital (i.e., a β orbital) and place in the majority-spin (i.e., α) manifold. Sometimes the orbital one wants to flip is not the highest-energy β orbital, and we were careful to find the right orbital in every case by a manual search. However, there is another problem that is harder to handle, namely that some combinations of functional and atomic state produce very different α and β orbitals. For example, singlet Ni is an open-shell singlet with one alpha electron in 3d and one β electron in 4s, and the eight other valence electrons paired in the remaining four 3d orbitals. However, some functionals, such as M06-HF and MN12-SX, produce very different orbitals for α and β electrons; in these cases the β-HOMO is not a pure 4s orbital, but has a strong mixing of 3d orbitals, while the α-LUMO is a very "pure" 4s

orbital. When the β-HOMO is moved to the α manifold, the resulting post-SCF high-spin state is very high in energy. This produces excitation energies with errors like 50 or 100 kcal/mol. This problem is observed most often for M06-HF and MN12-L, for three or four cases each. Other functionals do not lead to this problem in such a serious way; nevertheless we recommend basing final conclusions on Table 4.15 (which excludes these two cases as discussed at the end of section 4.2) rather than Table 4.14 to exclude the inappropriate cases for the RBS method.

As discussed at the end of section 3, the present study also features tests of the performance of eight new GGAs formed from the PW86 and C09 exchange functionals. By combining them with PBE, LYP, reLYP, and SOGGA11, we create eight new GGAs for testing. Table 4.15 shows the disappointing performance of the resulting functionals, with the smallest error coming from C09reLYP, at 6.6 kcal/mol. By comparing results from C09LYP, C09reLYP, and C09PBE with OLYP, OreLYP, and OPBE, we conclude that C09 has comparable performance to OptX for 3d transition metals. For PW86, one also finds PW86PBE to be very similar errors to to OPBE, but the best performance for PW86 comes from combining it with the SOGGA11 correlation functional.

The seven highest-ranking functionals in Table 4.15, which in some sense is the culmination of the present study of the 3d-series of transition metals, are ωB97X-D, B97-3, M08-SO, MPW1B95, and B98, followed closely by PW6B95, CAM-B3LYP, MPWB1K, SOGGA11-X, and B97-1. These higher-performing functionals include four global-hybrid GGAs, four global-hybrid meta-GGAs, one long-range-corrected GGA, one long-range-corrected GGA-plus- molecular-mechanics, and no local functionals of

any kind (the highest local functional in Table 4.15 is M06-L). In the next section we examine these functionals plus the eight new functionals from a broader perspective.

4.5.3 Broader Comparisons

To achieve a broader conclusion about the overall performance of various functionals, in Table 4.16 we compare the results in this study of the 3d-series with the results for five previously considered databases. The functionals listed in Table 4.16 are limited to those in the top 15 for either the 3d-series database or the 4d-series database plus the eight new functionals, plus SOGGA11 because it is of special interest to compare it to the eight new functionals and plus M06 because of its generally good performance across a broad spectrum of problems. The first six numerical columns give the MUE for each of the six considered databases, namely – in order – the MUE(28) of the RBS column of Table 4.15, the MUE(22) for spin-state excitation energies and ionization potentials of 4d-series atoms and monatomic cations from Ref. 6, MUE(VR17) for p-block spin-state excitation energies from Table 7 of Ref. 5, and AE6/11, PPS5/05, and ABDE12 from a recent review[96] of respectively main-group atomization energies, alkyl bond dissociation energies, and noncovalent π-π interaction energies. In some cases those earlier compilations did not include all the functionals in Table 4.16, and so the missing results were calculated as part of the present work, specifically for this comparison.

The next four columns of Table 4.16 show the average MUE of the first two, three, four, or five databases in Table 4.16, and the final column shows the average over all six. These results are labeled AMUE*x*(*y*), where *x* is the number of MUEs averaged, and *y* is the total number of data in the *x* databases. Note that these are averages over

MUEs, not averages over the collected data; averages over MUEs have the effect of weighting the six databases more evenly than would be the case if we averaged over data because the various databases have greatly different numbers of data. The functionals in Table 4.16 are listed in order of increasing values in this last column. Of course a complete assessment would require that even more databases be considered,[4,6,,96-99] but that is the job for a review article. Here we simply consider six databases to show which of the functionals that do well in Table 4.15 or in the closely related study of the 4d-series also do well across a broader spectrum of data and to provide a comparison of the new functionals to other functionals across a broader spectrum than just the 3d transition series atoms.

Consider first AMUE2(39), which merges the assessments for the 3d-series with those for the 4d-series. This provides the most comprehensive available assessment of spin excitation energies and ionization potentials for d-block atoms and cations. We find that SOGGA11-X, a functional with the same ingredients as the popular and historically important B3LYP functional, does the best. This is a fairly recent functional, and it is encouraging that a recently parametrized functional does so well. This is even more encouraging when we note that the data in the 3d-series, 4d-series, and p-block databases are quite different than the data used for parametrization in any of the parametrized functionals. The second- and third-best functionals for the AMUE2(39) figure of merit are CAM-B3LYP and B1LYP, followed closely by PW6B95 and B3V5LYP.

Next consider AMUE3(67), which adds in the p-block results for spin-state excitation energies. The p-block database includes both valence and Rydberg excitations of atoms in the 2p, 3p, and 4p blocks. Over this broader data base, which now includes a

wide expanse of the periodic table, the best performing functional becomes PW6B95 (whose design involved the optimization of only six parameters), followed by MPW1B95 (which was created by optimizing only one parameter) and CAM-B3LYP.

PW6B95 remains the best functional for AMUE4(73) and AMUE5(85). The good performance of PW6B95 when averaged over the three, four, or five databases culminating in AMUE5(85) is very interesting because Grimme, in several studies, has noted the especially good performance of this functional (sometimes augmented by molecular mechanics terms) on broad data sets of thermochemical data,[98-102] which although broad and diverse—are quite different from the p-block and d-block atomic data considered here.

The last column of Table 4.16 provides the broadest assessment considered in the present paper. Although one might have recommended functionals such as B3V5LYP, B1LYP, and B97-1 due to their good performances in spin state and ionization potential tests, we actually find they fail to deliver consistently best accuracy when broader data are considered. M08-SO and PW6B95 do best, followed closely by MPW1B95, MPWB1K, SOGGA11-X, and CAM-B3LYP, but a key point is that eleven of the functionals that made their way into Table 4.16 by good performance on the 3d-series or 4d-series databases of atomic spin state excitation energies and ionization potentials have average mean unsigned errors larger than those of the best functionals in Table 4.16 by a factor of 1.5 or more when assessed broadly. So a prospective user of these functionals should consider more than one kind of database when choosing a functional for a series of applications.

Table 4.16 also clearly shows the disappointing performance of the PW86 and C09 exchange functionals in treating the wider range of systems in that the eight new functionals occupy the eight lowest positions in the table. A somewhat surprising observation is their poor performance on PPS/5 since they are meant to be more accurate for weak interactions. Overall one finds the error of even the best of the four, namely, PW86PBE, to be 7.0 kcal/mol, more than twice as large as the errors of the top 5 functionals in the table. It is also interesting to note that none of these functionals does as well as SOGGA11, whose exchange functional shares the major characteristic of the PW86 and C09 exchange functionals, that is, good agreement with the exact gradient expansion at small values of the reduced gradient. To the knowledge of the authors, the present study is the broadest available test of the PW86 and C09 functionals, and it seems safe to exclude both from the list of exchange functionals recommended for use in GGAs for general applications in chemistry.

Note that, excluding the eight new functionals, only three local functionals are included in Table 4.16, namely, revTPSS and M06-L, which are both meta-GGA functionals, and SOGGA11, which is a GGA. Among these, revTPSS has the best overall accuracy (4.4 kcal/mol). The older M06-L functional does better than revTPSS on four of the six databases but is ranked lower in Table 4.16 primarily because of poor performance for open-shell p-block states, in particular for the Rydberg state component of that database. SOGGA11, with one less ingredient than M06-L or revTPSS, does better than former on two of the six databases and does better than the latter on two of the six databases (not the same two).

4.6 Summary and Conclusions

To achieve a broader conclusion about the overall performance of various functionals, in Table 4.16 we compare the results in this study of the 3d-series with the results for five previously considered databases. The functionals listed in Table 4.16 are limited to those in the top 15 for either the 3d-series database or the 4d-series database plus the eight new functionals, plus SOGGA11 because it is of special interest to compare it to the eight new functionals and plus M06 because of its generally good performance across a broad spectrum of problems. The first six numerical columns give the MUE for each of the six considered databases, namely – in order – the MUE(28) of the RBS column of Table 4.15, the MUE(22) for spin-state excitation energies and ionization potentials of 4d-series atoms and monatomic cations from Ref. 6, MUE(VR17) for p-block spin-state excitation energies from Table 7 of Ref. 5, and AE6/11, PPS5/05, and ABDE12 from a recent review[96] of respectively main-group atomization energies, alkyl bond dissociation energies, and noncovalent π-π interaction energies. In some cases those earlier compilations did not include all the functionals in Table 4.16, and so the missing results were calculated as part of the present work, specifically for this comparison.

The next four columns of Table 4.16 show the average MUE of the first two, three, four, or five databases in Table 4.16, and the final column shows the average over all six. These results are labeled AMUE*x*(*y*), where *x* is the number of MUEs averaged, and *y* is the total number of data in the *x* databases. Note that these are averages over MUEs, not averages over the collected data; averages over MUEs have the effect of weighting the six databases more evenly than would be the case if we averaged over data

because the various databases have greatly different numbers of data. The functionals in Table 4.16 are listed in order of increasing values in this last column. Of course a complete assessment would require that even more databases be considered,[4,6,,96-99] but that is the job for a review article. Here we simply consider six databases to show which of the functionals that do well in Table 4.15 or in the closely related study of the 4d-series also do well across a broader spectrum of data and to provide a comparison of the new functionals to other functionals across a broader spectrum than just the 3d transition series atoms.

Consider first AMUE2(39), which merges the assessments for the 3d-series with those for the 4d-series. This provides the most comprehensive available assessment of spin excitation energies and ionization potentials for d-block atoms and cations. We find that SOGGA11-X, a functional with the same ingredients as the popular and historically important B3LYP functional, does the best. This is a fairly recent functional, and it is encouraging that a recently parametrized functional does so well. This is even more encouraging when we note that the data in the 3d-series, 4d-series, and p-block databases are quite different than the data used for parametrization in any of the parametrized functionals. The second- and third-best functionals for the AMUE2(39) figure of merit are CAM-B3LYP and B1LYP, followed closely by PW6B95 and B3V5LYP.

Next consider AMUE3(67), which adds in the p-block results for spin-state excitation energies. The p-block database includes both valence and Rydberg excitations of atoms in the 2p, 3p, and 4p blocks. Over this broader data base, which now includes a wide expanse of the periodic table, the best performing functional becomes PW6B95

(whose design involved the optimization of only six parameters), followed by MPW1B95 (which was created by optimizing only one parameter) and CAM-B3LYP.

PW6B95 remains the best functional for AMUE4(73) and AMUE5(85). The good performance of PW6B95 when averaged over the three, four, or five databases culminating in AMUE5(85) is very interesting because Grimme, in several studies, has noted the especially good performance of this functional (sometimes augmented by molecular mechanics terms) on broad data sets of thermochemical data,[98-102] which although broad and diverse—are quite different from the p-block and d-block atomic data considered here.

The last column of Table 4.16 provides the broadest assessment considered in the present paper. Although one might have recommended functionals such as B3V5LYP, B1LYP, and B97-1 due to their good performances in spin state and ionization potential tests, we actually find they fail to deliver consistently best accuracy when broader data are considered. M08-SO and PW6B95 do best, followed closely by MPW1B95, MPWB1K, SOGGA11-X, and CAM-B3LYP, but a key point is that eleven of the functionals that made their way into Table 4.16 by good performance on the 3d-series or 4d-series databases of atomic spin state excitation energies and ionization potentials have average mean unsigned errors larger than those of the best functionals in Table 4.16 by a factor of 1.5 or more when assessed broadly. So a prospective user of these functionals should consider more than one kind of database when choosing a functional for a series of applications.

Table 4.16 also clearly shows the disappointing performance of the PW86 and C09 exchange functionals in treating the wider range of systems in that the eight new

functionals occupy the eight lowest positions in the table. A somewhat surprising observation is their poor performance on PPS/5 since they are meant to be more accurate for weak interactions. Overall one finds the error of even the best of the four, namely, PW86PBE, to be 7.0 kcal/mol, more than twice as large as the errors of the top 5 functionals in the table. It is also interesting to note that none of these functionals does as well as SOGGA11, whose exchange functional shares the major characteristic of the PW86 and C09 exchange functionals, that is, good agreement with the exact gradient expansion at small values of the reduced gradient. To the knowledge of the authors, the present study is the broadest available test of the PW86 and C09 functionals, and it seems safe to exclude both from the list of exchange functionals recommended for use in GGAs for general applications in chemistry.

Note that, excluding the eight new functionals, only three local functionals are included in Table 4.16, namely, revTPSS and M06-L, which are both meta-GGA functionals, and SOGGA11, which is a GGA. Among these, revTPSS has the best overall accuracy (4.4 kcal/mol). The older M06-L functional does better than revTPSS on four of the six databases but is ranked lower in Table 4.16 primarily because of poor performance for open-shell p-block states, in particular for the Rydberg state component of that database. SOGGA11, with one less ingredient than M06-L or revTPSS, does better than former on two of the six databases and does better than the latter on two of the six databases (not the same two).

References for Chapter 4

(1) Kohn, W.; Sham, L. J. *Phys. Rev*. **1965**, *140*, A1133.
(2) Reiher, M. *Faraday Discuss.* **2007**, *135*, 97.

(3) Jacob, C. R.; Reiher, M. *Int. J. Quantum Chem.* **2012**, *112*, 3661.

(4) Cramer, C.J.; Truhlar, D. G. *Phys. Chem. Chem. Phys.* **2009**, 11, 10757.

(5) Yang, K.; Peverati, R.; Truhlar, D. G.; Valero, R. *J. Chem. Phys.* **2011**, *135*, 044118.

(6) Luo, S.; Truhlar, D. G. *J. Chem. Theory Comput.* **2012**, 8, 4112.

(7) Frisch, M. J.; Trucks, G. W.; Schlegel, H. B. Scuseria, G. E.; Robb, M. A.; Cheeseman, J. R.; Scalmani, G.; Barone, V.; Mennucci, B.; Petersson, G. A.; Nakatsuji, H.; Caricato, M.; Li, X.; Hratchian, H. P.; Izmaylov, A. F.; Bloino, J.; Zheng, G.; Sonnenberg, J. L.; Hada, M.; Ehara, M.; Toyota, K.; Fukuda, R.; Hasegawa, J.; Ishida, M.; Nakajima, T.; Honda, Y.; Kitao, O.; Nakai, H.; Vreven, T.; Montgomery, Jr., J. A.; Peralta, J. E.; Ogliaro, F.; Bearpark, M.; Heyd, J. J.; Brothers, E.; Kudin, K. N.; Staroverov, V. N.; Kobayashi, R.; Normand, J.; Raghavachari, K.; Rendell, A.; Burant, J. C.; Iyengar, S. S.; Tomasi, J.; Cossi, M.; Rega, N.; Millam, J. M.; Klene, M.; Knox, J. E.; Cross, J. B.; Bakken, V.; Adamo, C.; Jaramillo, J.; Gomperts, R.; Stratmann, R. E.; Yazyev, O.; Austin, A. J.; Cammi, R.; Pomelli, C.; Ochterski, J. W.; Martin, R. L.; Morokuma, K.; Zakrzewski, V. G.; Voth, G. A.; Salvador, P.; Dannenberg, J. J.; Dapprich, S.; Daniels, A. D.; Farkas, Ö.; Foresman, J. B.; Ortiz, J. V.; Cioslowski, J.; Fox, D. J. *Gaussian 09*, Revision C.1, Gaussian, Inc., Wallingford, CT, 2009.

(8) Balabanov, N.B.; Peterson, K.A. *J. Chem. Phys.* **2005**, 123, 064107.

(9) Douglas, M.; Kroll, N. M. *Ann. Phys.* **1974,** 82, 89.

(10) Hess, B. A. *Phys. Rev. A* **1986**, 33, 3742.

(11) Jansen, G.; Hess, B. A. *Phys. Rev. A* **1989**, 39, 6016.

(12) Foster, J. P.; Weinhold, F. *J. Am. Chem. Soc.* **1980**, 102, 7211.

(13) Reed, A. E.; Weinhold, F. *J. Chem. Phys.* **1983**, 78, 4066.

(14) Reed, A. E.; Weinstock, R. B.; Weinhold, F. *J. Chem. Phys.* **1985**, 83, 735.

(15) Reed, A. E.; Weinhold, F. *J. Chem. Phys.* **1985**, 83, 1736.

(16) Carpenter, J. E. Ph. D. thesis, University of Wisconsin, Madison, WI, 1987.

(17) Carpenter, J. E.; Weinhold, F. *J. Mol. Struct. (Theochem)* **1988**, 46, 41.

(18) Reed, A. E.; Curtiss, L. A.; Weinhold, F. *Chem. Rev.* **1988**, 88, 899.

(19) Weinhold, F; Carpenter, J. E. In *The Structure of Small Molecules and Ions*; Ed. R. Naaman and Z. Vager, Plenum: New York, 1988, pp 227-36.

(20) Moore, C. E. *Atomic Energy Levels*; National Bureau of Standards: Washington, DC, 1949–1958, Vols. 1–3.

(21) Roothaan, C. C. J. *Rev. Mod. Phys.* **1951**, 23, 69.

(22) Pople, J.A.; Nesbet, R. K. *J. Chem. Phys.* **1954**, 22, 571.

(23) McWeeny, R.; Diercksen, G. *J. Chem. Phys.* **1968**, 49, 4852.

(24) Becke, A. D. *J. Chem. Phys.* **1998**, *107*, 8554.

(25) Gáspár, R. *Acta Phys. Hung*. **1974**, *35*, 213.

(26) Vosko, S. H.; Wilk, L.; Nusair, M. *Can. J. Phys.* **1980**, *58*, 1200.

(27) Becke, A. D. *Phys. Rev. A* **1988**, *38*, 3098.

(28) Perdew, J. P. *Phys. Rev. B* **1986**, *33*, 8822.

(29) Lee, C.; Yang, W.; Parr, R. G. *Phys. Rev. B* **1988**, *37*, 785.

(30) Perdew, J. P. In *Electronic Structure of Solids '91*; edited by Ziesche P.; Eschrig, H. Akademie Verlag: Berlin, 1991, pp 11–20.

(31) Perdew, J. P.; Burke, K.; Ernzerhof, M. *Phys. Rev. Lett.* **1996**, *77*, 3865.

(32) Adamo, C.; Barone, V. *J. Chem. Phys.* **1998**, *108*, 664.

(33) Hamprecht, F. A.; Cohen, A.; Tozer, D. J.; Handy, N. C. *J. Chem. Phys.* **1998**, *109*, 6264.

(34) Boese, A. D.; Handy, N.C. *J. Chem. Phys.* **2001**, *114*, 5497.

(35) Hammer, B.; Hansen, L. B.; Norskov, J. K. *Phys. Rev. B* **1999**, *59*, 7413.

(36) Handy, N. C.; Cohen, A.J. *Mol. Phys.* **2001**, *99*, 403.

(37) Schultz, N. E.; Zhao, Y.; Truhlar, D. G. *J. Phys. Chem. A* **2005**, *109*, 11127.

(38) Thakkar, A. J.; McCarthy, S. P. *J. Chem. Phys.* **2009**, *131*, 134109.

(39) Peverati, R.; Truhlar, D. G. *J. Chem. Theory. Comput.* **2012**, *8*, 2310.

(40) Van Voorhis, T.; Scuseria, G. E. *J. Chem. Phys.* **1998**, *109*, 400.

(41) Tao, J.; Perdew, J. P.; Staroverov, V. N.; Scuseria, G. E. *Phys. Rev. Lett.* **2003**, *91*, 146401.

(42) Zhao, Y.; Truhlar, D. G. *J. Chem. Phys.* **2006**, *125*, 194101.

(43) Zhao, Y.; Truhlar, D. G. *J. Chem. Phys.* **2008**, *128*, 184109.

(44) Perdew, J. P.; Ruzsinszky, A.; Csonka, G. I.; Constantin, L. A.; Sun, J. *Phys. Rev. Lett.* **2009**, *103*, 026403.

(45) Peverati, R.; Zhao, Y.; Truhlar, D. G. *J. Phys. Chem. Lett.* **2011**, *2*, 1911.

(46) Peverati, R.; Truhlar, D. G. *J. Phys. Chem. Lett.* **2011**, *2*, 2810.

(47) Peverati, R.; Truhlar, D. G. *Phys. Chem. Chem. Phys.* **2012**, *14*, 13171.

(48) Hoe, M. W.; Cohen, A. J.; Handy, N. C. *Chem. Phys. Lett.* **2001**, *341*, 319.

(49) Reiher, M.; Salomon, O.; Hess, B. A. *Theor. Chem. Acc.* **2001**, *107*, 48.

(50) Becke, A.D. *J. Chem. Phys.*, **1993**, *98*, 1372.

(51) Stephens, P. J.; Devlin,; Chabalowski, C. F.; Frisch, M. J. *J. Phys. Chem.* **1994**, *98*, 11623.

(52) Hartwig, R. H.; Koch, W. *Chem. Phys. Lett.* **1997**, *268*, 345.

(53) Zhao, Y.; Truhlar, D. G. *J. Phys. Chem. A* **2004**, *108*, 6908.

(54) Schmider, H. L.; Becke, A. D. *J. Chem. Phys.* **1998**, *108*, 9624.

(55) Adamo C.; Barone, V. *J. Chem. Phys.* **1999**, 110, 6158.

(56) Adamo, C.; Barone, V. *Chem. Phys. Lett.* **1997**, *274*, 242.

(57) Hamprecht, F. A.; Cohen, A.; Tozer, D. J.; Handy, N. C. *J. Chem. Phys.* **1998**, *109*, 6264.

(58) Wilson, P. J.; Bradley, T. J.; Tozer, D. J. *J. Chem. Phys.* **2001**, *115*, 9233.

(59) Keal, T.W.; Tozer, D.J. *J. Chem. Phys.* **2005**, *123*, 121103.

(60) Peverati, R.; Truhlar, D. G. *J. Chem. Phys.* **2011**, *135*, 191102.

(61) Lynch, B. J.; Fast, P. L.; Harris, M.; Truhlar, D. G. *J. Phys. Chem. A* **2000**, *104*, 4811.

(62) Zhao, Y.; Truhlar, D. G. *J. Phys. Chem. A* **2004**, *108*, 6908.

(63) Becke, A.D. *J. Chem. Phys.* **1993**, *98*, 1372.

(64) Staroverov, V. N.; Scuseria, G. E.; Tao, J.; Perdew, J. P. *J. Chem. Phys.* **2003**, *119*, 12129.

(65) Tao, J.; Perdew, J. P.; Staroverov, V. N.; Scuseria, G. E. *Phys. Rev. Lett.* **2003**, *91*, 146401.

(66) Krieger, J. B.; Chen, J.; Iafrate, G. J.; Savin, A. in *Electron Correlations and Materials Properties*; edited by A. Gonis, and N. Kioussis, Plenum: New York, 1999, pp 463.

(67) Zhao, Y.; Lynch, B. J.; Truhlar, D. G. *Phys. Chem. Chem. Phys.* **2005**, *7*, 43.

(68) Boese, A. D.; Handy, N. C. *J. Chem. Phys.* **2002**, *116*, 9559.

(69) Zhao, Y.; Truhlar, D. G. *Theor. Chem. Acc.* **2008**, *120*, 215.

(70) Zhao, Y.; Truhlar, D. G. *Acc. Chem. Res.* **2008**, *41*, 157

(71) Zhao, Y.; Schultz, N. E.; Truhlar, D. G. *J. Chem. Phys.* **2005**, *123*, 161103.

(72) Zhao Y.; Truhlar, D. G. *J. Phys. Chem. A* **2005**, *109*, 5656.

(73) Zhao, Y.; González-García, N.; Truhlar, D. G. *J. Phys. Chem. A* **2005**, *109*, 2012.

(74) Boese, A. D.; Martin, J. M. L. *J. Chem. Phys.* **2004**, *121*, 3405.

(75) Zhao, Y.; Truhlar, D. G. *J. Chem. Theory Comput.* **2008**, *4*, 1849.

(76) Zhao, Y.; Schultz, N. E.; Truhlar, D. G. *J. Chem. Theory Comput.* **2006**, *2*, 364.

(77) Zhao, Y.; Truhlar, D. G. *J. Phys. Chem. A* **2006**, *110*, 13126.

(78) Heyd, J.; G. E. Scuseria, G. E.; Ernzerhof, M. *J. Chem. Phys.* **2003**, *118*, 8207.

(79) Henderson, T. M.; Izmaylov, A. F.; Scalmani, S.; Scuseria, G. E. *J. Chem. Phys.* **2009**, *131*, 044108.

(80) Yanai, T.; Tew, D.P.; Handy, N.C. *Chem. Phys. Lett.* **2004**, *393*, 51.

(81) Iikura, H.; Tsuneda, T.; Yanai, T.; Hirao, K. *J. Chem. Phys.* **2001**, *115*, 3540.

(82) Vydrov, O. V.; Scuseria, G. E. *J. Chem. Phys.* **2006**, *125*, 234109.

(83) Chai, J.; Head-Gordon, M. *J. Chem. Phys.* **2008**, *128*, 084106.

(84) Chai, J.; Head-Gordon, M. *Phys. Chem. Chem. Phys.* **2008**, *10*, 6615.

(85) Peverati, R; Truhlar, D. G. *Phys Chem Chem Phys.* **2012**, *14*, 16187.

(86) Peverati, R.; Truhlar, D. G. *J. Phys. Chem. Lett.* **2011**, *2*, 2810.

(87) Noodleman, L.; Han, W. G. *J. Biol. Inorg. Chem*. **2006**, *11*, 674.

(88) Görling, A. *Phys. Rev. A* **1993**, *47*, 2783.

(89) Philipsen, P. H. T.; Baerends, E. J. *Phys. Rev. B* **1996***, 54*, 5326.

(90) Johnson, E. R.; Becke, A. D. *Can J. Chem*. **2009**, *87*, 1369.

(91) Seeger, R.; Pople, J. A. *J. Chem. Phys.* **1977**, *66*, 3045.

(92) Bauernschmitt, R.; Ahlrichs, R. *J. Chem. Phys.* **1996**, *104***,** 9047.

(93) Gräfenstein, J.; Hjerpe, A. M.; Kraka, E.; Cremer, D. *J. Phys. Chem. A* **2000**, *104*, 1748.

(94) Nishino, M.; Yamanaka, S.; Yoshioka, Y.; Yamaguchi, K. *J. Phys. Chem. A* **1997**, *101*, 705.

(95) Yanagisawa, S.; Tsuneda, T.; Hirao, K. *J. Chem. Phys.* **2000**, *112*, 545.

(96) Peverati, R.; Truhlar, D. G. *Philos. T. Roy. Soc. A* online as of April 23, 2013, http://arxiv.org/abs/1212.0944.

(97) Yang, K.; Zheng, J.; Zhao, Y.; Truhlar, D. G. *J. Chem. Phys.* **2010**, *132*, 164117.

(98) Korth, M.; Grimme, S. *J. Chem. Theory Comput.* **2009**, *5*, 993.

(99) Goerigk, L.; Grimme, S. *Phys. Chem. Chem. Phys.* **2011**, *13*, 6670.

(100) Grimme, S. *WIREs Comput. Mol. Sci.* **2011**, *1*, 211.

(101) Goerigk, L.; Kruse, H.; Grimme, S. *ChemPhysChem* **2011**, *12*, 3421.

(102) Grimme, S.; Mu̎ck-Lichtenfeld, C. *Israel J. Chem.* **2012**, *52*, 180.

(103) Zhao, Y.; Truhlar, D. G. *J. Chem. Phys. Lett.* **2011***, 502*, 1.

(104) Li, R.; Peverati, R.; Isegawa, M.; Truhlar, D. G. *J. Phys. Chem. A* **2013***, 117,* 169, and references therein.

(105) Harvey, J. N. *Structure and Bonding* **2004**, *112*, 151.

(106) Perdew, J. P.; Wang, Y. *Phys. Rev. B* **1986**, 33, 8800.

(107) Cooper, V. R. *Phys. Rev. B* **2010**, 81, 161104.

(108) Kanneman, F. O.; Becke, A. D. *J. Chem. Theory Comput.* **2009**, 5, 719.

(109) Murray, É. D. ; Lee, K. ; Langreth, D. C. *J. Chem. Theory Comput.* **2009**, 5, 2754.

(110) Lee, K.; Murray, E. D.; Kong, L.; Lundqvist, B. I.; Langreth, D. C. *Phys. Rev. B* **2010**, 82, 081101.

Table 4.1. Experimental Data[a]

	GS	ES	ΔE		GS^+	ES^+	ΔE^+	IP
Sc	$^2D, 4s^23d^1$	$^4F, 4s^13d^2$	32.9	Sc^+	$^3D, 4s^13d^1$	$^1D, 4s^13d^1$	7.0	151.3
Ti	$^3F, 4s^23d^2$	$^5F, 4s^13d^3$	18.6	Ti^+	$^4F, 4s^13d^2$	$^2F, 4s^13d^2$	13.0	157.6
V	$^4F, 4s^23d^3$	$^6D, 4s^13d^4$	5.6	V^+	$^5D, 3d^4$	$^3F, 4s^13d^3$	24.9	155.1
Cr	$^7S, 4s^13d^5$	$^5S, 4s^13d^5$	21.7	Cr^+	$^6S, 3d^5$	$^4D, 4s^13d^4$	56.7	156.0
Mn	$^6S, 4s^23d^5$	$^8P, 4s^13d^54p^1$	53.1	Mn^+	$^7S, 4s^13d^5$	$^5S, 4s^13d^5$	27.1	171.4
Fe	$^5D, 4s^23d^6$	$^3F, 4s^13d^7$	34.3	Fe^+	$^6D, 4s^13d^6$	$^4F, 3d^7$	5.7	182.2
Co	$^4F, 4s^23d^7$	$^2F, 4s^13d^8$	20.3	Co^+	$^3F, 3d^8$	$^5F, 4s^13d^7$	9.9	181.1
Ni	$^3F, 4s^23d^8$	$^1D, 4s^13d^9$	7.0	Ni^+	$^2D, 3d^9$	$^4F, 4s^13d^8$	25.0	175.0
Cu	$^2S, 4s^13d^{10}$	$^4P, 4s^13d^94p^1$	113.5	Cu^+	$^1S, 3d^{10}$	$^3D, 4s^13d^9$	64.8	178.2
Zn	$^1S, 4s^23d^{10}$	$^3P, 4s^13d^{10}4p^1$	93.5	Zn^+	$^2S, 4s^13d^{10}$	$^4P, 4s^13d^94p^1$	299.4	216.6

[a] GS – electronic state of neutral ground state; ES – electronic state of neutral excited state; ΔE – excitation energy of neutral, kcal/mol; GS^+ – electronic state of cation ground state; ES^+ – electronic state of cation excited state; ΔE^+ – excitation energy of cation, kcal/mol; IP – ionization potential, kcal/mol

Table 4.2 Various xc Functionals Tested in this Work.

Type	xcF	X^a	ref
LSDA	GVWN3[b]	0	25,26
GGA	B88	0	27
	BP86	0	27,28
	BLYP	0	27,29
	PW91	0	30
	BPW91	0	27,30
	PBE	0	31
	mPWLYP	0	29,32
	HCTH	0	33,34
	RPBE	0	35
	OLYP	0	29,36
	OPBE	0	31,36
	MOHLYP	0	37
	OreLYP	0	38
	SOGGA	0	43
	SOGGA11	0	45
	PW86LYP	0	29,106
	PW86PBE	0	31,106
	PW86reLYP	0	38,106
	C09LYP	0	29,107
	C09PBE	0	31,107
	C09reLYP	0	38,107
	PW86SOGGA11	0	45,106
	C09SOGGA11	0	45,107
NGA	N12	0	39
Meta-GGA	VS98	0	40
	TPSS	0	41
	τHCTH	0	68
	M06-L	0	42
	revTPSS	0	44
Range-separated meta-GGA	M11-L	0	46
Meta-NGA	MN12-L	0	47
Global-hybrid GGA	MPWLYP1M	5	37
	O3LYP	11.61	48
	B3LYP*	15	49
	B3PW91	20	50
	B3LYP	20	51
	B3V5LYP	20	52
	MPW3LYP	21.8	53
	B98	21.98	54
	PBE0	25	55
	B1LYP	25	56
	B97-1	21	57

	B97-2	21	58
	B97-3	26.93	59
	SOGGA11-X	40.15	60
	MPW1K	42.8	61
	MPW1B95	31	62
	MPWB1K	44	62
	BHandH	50	63
	BHandHLYP	50	29,63
	HFLYP	100	29
	HFPW91	100	30
Global-hybrid meta-GGA	TPSSh	10	64
	TPSS1KCIS	13	65-67
	τHCTHhyb	15	68
	M06	27	67, 69
	M05	28	66
	PW6B95	28	72
	MPWKCIS1K	41	32, 66, 73
	BMK	42	74
	M08-SO	52.23	75
	M06-2X	54	69, 70
	M05-2X	56	70, 75
	M08-HX	56.79	75
	M06-HF	100	77
Screened-exchange GGA	HSE	0-25	78,79
Long-range-corrected GGA	CAM-B3LYP	19-65	80
	LC-MPWLYP	0-100	81
	LC-ωPBE	0-100	82
	ωB97X	15.77-100	83
Screened-exchange NGA	N12-SX	0-25	85
Long-range-corrected meta-GGA	M11	42.8-100	86
Screened-exchange meta-NGA	MN12-SX	0-25	85
Long-range-corrected GGA + MM	ωB97X-D	22.2-100	84

[a] For hybrid functionals that are not global hybrids, the first number is *X* at short range, and the second is *X* at long range.

[b] GVWN3 denotes the combination of the Gáspár exchange functional (also used by Kohn and Sham and sometimes called GKS) with the third approximation of Vosko, Wilk, and Nusair for the correlation functional. The GVWN3 functional has the keyword SVWN in *Gaussian 09* and it is one of many (fairly similar) approximations in the generic class of LSDA functionals. We note that the Gáspár exchange functional is the same as Slater's Xα functional if the parameter α is set equal to 2/3.

Table 4.3 Mean Signed Deviation of 4s Subshell Occupations from that of the Dominant Experimental Configuration in the Stably Optimized SCF Solutions

N12	-0.20	MPWLYP1M	-0.10
OPBE	-0.18	MPWKCIS1K	-0.10
M11-L	-0.17	PBE0	-0.10
LC-ωPBE	-0.17	M06-L	-0.10
M11	-0.17	C09PBE	-0.10
N12-SX	-0.16	B3LYP*	-0.09
BPW91	-0.16	PW86LYP	-0.09
OLYP	-0.16	PW86SOGGA11	-0.09
GVWN3	-0.15	B88	-0.09
OreLYP	-0.15	PW6B95	-0.08
SOGGA	-0.15	ωB97X-D	-0.08
PW91	-0.15	MPW1K	-0.08
HCTH	-0.15	B98	-0.08
BP86	-0.14	M06	-0.08
TPSS	-0.14	B97-2	-0.07
O3LYP	-0.14	CAM-B3LYP	-0.07
PBE	-0.14	ωB97X	-0.07
PW86PBE	-0.14	M05	-0.07
RPBE	-0.14	M08-SO	-0.07
C09LYP	-0.13	B3LYP	-0.07
revTPSS	-0.13	B3V5LYP	-0.07
MOHLYP	-0.13	MPW3LYP	-0.06
SOGGA11	-0.13	M08-HX	-0.05
HSE	-0.12	B97-3	-0.05
τHCTH	-0.12	MPW1B95	-0.05
B3PW91	-0.12	SOGGA11-X	-0.05
TPSS1KCIS	-0.12	B1LYP	-0.04
TPSSh	-0.12	B97-1	-0.04
BLYP	-0.12	MPWB1K	-0.04
C09reLYP	-0.11	BHandHLYP	-0.03
LC-MPWLYP	-0.11	M05-2X	-0.01
MPWLYP	-0.11	M06-HF	-0.01
MN12-L	-0.11	BHandH	0.00
PW86reLYP	-0.11	HFPW91	0.00
MN12-SX	-0.11	M06-2X	0.00
C09SOGGA11	-0.11	BMK	0.04
VS98	-0.10	HFLYP	0.05
τHCTHhyb	-0.10	HF	0.10

Table 4.4 Mean Unsigned Deviation of 4s Subshell Occupation of the Stably Optimized Solution from that of the Dominant Experimental Configuration

HFPW91	0.00	TPSS1KCIS	0.14
M06-2X	0.00	B3PW91	0.14
BHandH	0.00	HSE	0.14
M05-2X	0.02	VS98	0.14
BHandHLYP	0.03	M06-L	0.15
MPWB1K	0.04	MPWLYP1M	0.15
SOGGA11-X	0.05	PW86LYP	0.16
M08-HX	0.05	SOGGA11	0.16
HFLYP	0.05	O3LYP	0.16
M06-HF	0.06	τHCTH	0.16
B97-3	0.07	MPWLYP	0.16
B1LYP	0.07	M11	0.17
MPW1B95	0.07	PW86PBE	0.17
B97-1	0.08	BLYP	0.17
MPW1K	0.08	LC-ωPBE	0.17
MPW3LYP	0.08	MOHLYP	0.17
BMK	0.09	C09SOGGA11	0.18
ωB97X	0.09	B88	0.18
PW6B95	0.09	GVWN3	0.18
CAM-B3LYP	0.09	TPSSh	0.18
M05	0.09	PW86reLYP	0.18
M08-SO	0.09	revTPSS	0.18
B3V5LYP	0.10	C09LYP	0.18
B98	0.10	OLYP	0.18
B3LYP	0.10	OreLYP	0.18
ωB97X-D	0.10	HCTH	0.18
M06	0.10	PBE	0.19
MPWKCIS1K	0.10	RPBE	0.19
HF	0.10	SOGGA	0.19
B97-2	0.11	N12-SX	0.19
LC-MPWLYP	0.11	PW91	0.19
PBE0	0.11	BP86	0.19
B3LYP*	0.12	TPSS	0.19
τHCTHhyb	0.12	BPW91	0.20
PW86SOGGA11	0.12	OPBE	0.21
C09reLYP	0.12	MN12-L	0.22
MN12-SX	0.12	M11-L	0.22
C09PBE	0.13	N12	0.22

Table 4.5. MSE(9) and MUE(9) of ΔE(s → d excitation) for the Variational Method

Functional	MSE	MUE	Functional	MSE	MUE
SOGGA11-X	-2.0	2.7	OreLYP	1.9	9.5
M08-HX	0.1	3.2	RPBE	-3.2	9.9
M08-SO	-0.1	4.4	SOGGA11	-1.7	9.9
M06	2.8	4.5	BP86	-3.0	9.9
B97-3	0.2	4.5	MPWKCIS1K	-6.1	10.0
B97-1	2.2	5.3	PW86PBE	-4.2	10.2
M06-2X	0.0	5.3	PBE0	-6.6	10.2
B98	1.8	5.4	PBE	-3.8	10.2
ωB97X-D	0.6	5.4	MPW1K	-9.2	10.3
M06-L	-1.0	5.5	HCTH	7.3	10.5
ωB97X	5.4	5.7	PW91	-3.7	10.5
PW86reLYP	-0.6	6.1	SOGGA	-4.6	10.6
CAM-B3LYP	-1.6	6.6	B3PW91	-5.8	10.7
PW86LYP	-1.1	6.7	revTPSS	-4.7	10.7
MPWB1K	-6.0	6.9	TPSS	-4.0	10.8
B97-2	4.3	7.2	TPSS1KCIS	-4.0	10.9
PW6B95	-3.3	7.3	TPSSh	-4.7	11.0
C09reLYP	-0.8	7.3	BPW91	-5.0	11.0
B1LYP	-3.9	7.3	C09PBE	-5.8	11.1
MPW3LYP	-2.8	7.3	LC-ωPBE	-0.5	11.2
MPW1B95	-4.2	7.3	HSE	-6.7	11.2
BHandH	-7.7	7.7	OLYP	1.1	11.3
BMK	-5.2	7.7	C09SOGGA11	-7.3	11.8
B3V5LYP	-3.1	7.9	M11	0.6	11.8
M05-2X	1.9	7.9	PW86SOGGA11	-2.6	12.3
B3LYP	-2.9	7.9	N12-SX	9.3	12.6
VS98	-0.5	8.0	M06-HF	0.4	12.9
τHCTHhyb	5.3	8.2	SVWN	-0.5	13.0
B3LYP*	-2.2	8.2	MN12-L	11.1	13.4
BHandHLYP	-7.3	8.3	OPBE	-2.3	13.5
LC-MPWLYP	3.4	8.3	B88	-13.3	15.8
M05	8.1	8.4	τHCTH	15.9	16.6
MPWLYP1M	-0.8	8.5	HFPW91	-16.4	17.0
MOHLYP	0.0	8.6	M11-L	4.8	17.3
MPWLYP	-0.4	8.8	MN12-SX	18.2	18.2
BLYP	-1.0	9.2	HFLYP	-14.0	20.1
C09LYP	-1.8	9.2	N12	3.5	20.8
O3LYP	-0.4	9.3	HF	-27.2	28.0

Table 4.6. MSE(9) and MUE(9) of ΔE(s → d excitation) for WABS Method

Functional	MSE	MUE	Functional	MSE	MUE
B97-3	-1.6	3.2	PBE0	-8.3	8.5
B97-1	0.6	3.7	M05	6.6	8.6
B98	0.1	3.7	PW86PBE	-5.6	8.8
ωB97X-D	-1.1	3.8	PBE	-5.2	8.8
ωB97X	3.7	4.0	revTPSS	-6.0	9.0
M08-HX	-2.2	4.7	PW91	-5.1	9.1
M06	0.9	5.0	TPSS	-5.3	9.2
CAM-B3LYP	-3.1	5.1	SOGGA	-6.3	9.2
SOGGA11-X	-4.7	5.4	B3PW91	-7.1	9.3
PW6B95	-4.9	5.6	BMK	-7.8	9.4
B97-2	2.8	5.6	TPSSh	-6.0	9.5
MPW3LYP	-4.4	5.7	TPSS1KCIS	-5.2	9.5
C09reLYP	-2.3	5.7	MPWKCIS1K	-7.6	9.6
B1LYP	-5.6	6.0	C09PBE	-7.6	9.6
MPW1B95	-6.0	6.0	BPW91	-6.5	9.6
M06-L	-2.4	6.0	OLYP	0.0	9.7
B3V5LYP	-4.6	6.3	HSE	-8.1	9.8
B3LYP	-4.3	6.4	LC-ωPBE	-1.6	10.2
M08-SO	-2.7	6.5	BHandH	-10.4	10.4
VS98	-2.2	6.7	BHandHLYP	-10.0	10.8
τHCTHhyb	4.0	6.7	M11	-0.4	10.8
B3LYP*	-3.5	6.8	M05-2X	-1.4	11.2
PW86reLYP	-2.8	7.0	MPW1K	-11.4	11.4
MOHLYP	-1.0	7.0	PW86SOGGA11	-3.3	11.6
PW86LYP	-2.8	7.0	SVWN	-1.9	11.8
MPWLYP1M	-2.0	7.1	N12-SX	8.9	12.1
M06-2X	-2.4	7.3	OPBE	-4.0	12.2
LC-MPWLYP	2.4	7.3	C09SOGGA11	-9.7	12.7
MPWLYP	-1.4	7.4	M06-HF	-0.8	14.0
BLYP	-2.1	7.8	MN12-L	9.7	14.5
C09LYP	-3.1	7.8	B88	-15.4	15.4
OreLYP	0.7	7.8	τHCTH	15.5	15.6
O3LYP	-1.5	7.9	M11L	4.4	16.0
MPWB1K	-8.2	8.2	MN12SX	16.6	17.6
HCTH	6.6	8.3	N12	2.6	20.2
RPBE	-4.5	8.4	HFPW91	-20.5	21.0
SOGGA11	-3.0	8.4	HFLYP	-18.3	24.4
BP86	-4.4	8.5	HF	-32.1	32.9

Table 4.7. MSE(9) and MUE(9) of ΔE(s → d excitation) for RBS Method

Functional	MSE	MUE	Functional	MSE	MUE
SOGGA11-X	-2.1	2.8	PBE	-3.0	8.2
M06-L	0.8	4.2	PW91	-2.9	8.3
M06	3.1	4.3	BHandHLYP	-7.5	8.3
B97-3	0.1	4.3	SOGGA	-3.7	8.4
M08-SO	1.6	4.6	TPSS	-3.5	8.4
M08-HX	1.9	5.0	revTPSS	-4.4	8.6
B98	1.6	5.0	BPW91	-4.0	8.7
ωB97X-D	0.2	5.1	OLYP	3.1	8.8
B971	2.0	5.1	PW86PBE	-5.6	8.8
C09reLYP	-2.3	5.7	LC-MPWLYP	4.3	9.0
ωB97X	5.5	5.8	M05	8.8	9.1
CAM-B3LYP	-1.8	6.3	PBE0	-7.3	9.2
M06-2X	1.4	6.5	TPSS1KCIS	-4.2	9.4
PW6B95	-3.8	6.6	TPSSh	-5.0	9.4
MPWB1K	-6.4	6.7	B3PW91	-6.4	9.5
MPW1B95	-4.8	6.7	C09PBE	-7.6	9.6
B1LYP	-4.4	6.7	MPW1K	-9.8	9.9
MPW3LYP	-3.3	6.7	HSE	-7.4	10.2
MOHLYP	2.1	6.7	OPBE	-0.1	10.2
B97-2	4.4	6.9	MPWKCIS1K	-9.4	10.2
PW86reLYP	-2.8	7.0	SOGGA11	2.1	10.2
PW86LYP	-2.8	7.0	HCTH	10.2	10.5
B3V5LYP	-3.5	7.1	LC-ωPBE	-0.1	10.9
B3LYP	-3.3	7.2	SVWN	0.0	11.1
M05-2X	2.5	7.3	B88	-11.1	11.5
OreLYP	2.9	7.4	PW86SOGGA11	-3.3	11.6
B3LYP*	-2.5	7.4	N12-SX	9.3	12.6
MPWLYP1M	-0.6	7.5	C09SOGGA11	-9.7	12.7
MPWLYP	0.4	7.5	MN12-L	11.2	14.2
BMK	-5.9	7.6	M06-HF	4.1	15.4
RPBE	-1.9	7.6	M11-L	5.4	15.8
BLYP	-0.3	7.7	M11	4.7	15.8
BP86	-2.1	7.8	HFPW91	-15.9	16.4
C09LYP	-3.1	7.8	τHCTH	18.9	18.9
VS98	0.3	7.9	HFLYP	-13.0	19.1
BHandH	-7.9	7.9	HF	-26.1	26.9
O3LYP	0.1	8.0	N12	11.2	27.2
τHCTHhyb	5.5	8.1	MN12-SX	29.0	29.0

Table 4.8. MSE(20) and MUE(20) of ΔE (kcal/mol) for the Variational Method

Functional	MSE	MUE	Functional	MSE	MUE
SOGGA11-X	0.7	3.8	C09reLYP	4.3	8.0
M08-SO	2.0	4.4	PW91	0.5	8.0
MPW1B95	-0.8	4.6	B97-2	6.7	8.1
MPWB1K	-2.4	5.1	VS98	3.3	8.1
M08-HX	2.3	5.1	MPW1K	-6.3	8.1
PW6B95	0.4	5.1	BPW91	-0.8	8.2
wB97X-D	3.1	5.3	SOGGA	-1.0	8.3
B97-3	3.8	5.8	BHandHLYP	-2.2	8.5
CAM-B3LYP	2.1	5.9	MPWLYP1M	4.3	8.5
B1LYP	1.1	6.1	SOGGA11	2.1	8.6
B3V5LYP	1.6	6.5	C09PBE	-2.4	8.7
MPW3LYP	2.0	6.5	M11	0.3	8.7
B98	4.9	6.5	BLYP	4.3	8.9
B3LYP	1.8	6.6	C09SOGGA11	-3.2	9.0
MPWKCIS1K	-2.9	6.7	PW86LYP	5.6	9.0
PBE0	-3.3	6.7	PW86SOGGA11	1.2	9.1
BHandH	-2.5	6.8	MPWLYP	5.0	9.1
B97-1	5.4	6.8	τHCTHhyb	7.8	9.2
M06-L	2.9	6.8	OLYP	4.7	9.3
B3PW91	-2.5	6.9	OreLYP	6.0	9.4
TPSSh	-1.5	7.0	PW86reLYP	6.7	10.0
B3LYP*	2.4	7.0	OPBE	-0.4	10.1
revTPSS	-0.9	7.1	M06-2X	6.8	10.2
TPSS1KCIS	-0.9	7.1	M05-2X	7.2	10.5
LC-MPWLYP	5.0	7.2	SVWN	3.3	10.6
HSE	-3.3	7.3	M05	10.8	11.3
RPBE	0.7	7.3	B88	-9.0	11.7
O3LYP	3.0	7.4	N12-SX	10.0	11.7
TPSS	-0.2	7.5	HCTH	10.4	11.9
ωB97X	7.4	7.5	MN12-L	10.9	12.0
LC-ωPBE	-0.2	7.6	M11-L	4.2	14.1
BMK	0.1	7.6	N12	6.7	15.9
M06	6.3	7.7	HFPW91	-13.0	16.5
PBE	0.3	7.7	τHCTH	16.6	16.9
MOHLYP	3.9	7.8	MN12-SX	18.6	18.7
PW86PBE	0.5	7.8	HFLYP	-7.8	19.4
BP86	1.5	7.9	M06-HF	9.8	21.4
C09LYP	2.9	7.9	HF	-20.4	24.0

Table 4.9. MSE(20) and MUE(20) of ΔE (kcal/mol) for WABS Method

Functional	MSE	MUE	Functional	MSE	MUE
B97-3	1.3	4.0	M11	-1.9	7.7
ωB97X-D	0.3	4.2	LC-ωPBE	-2.9	7.7
PW6B95	-2.4	4.2	PBE	-2.5	7.8
CAM-B3LYP	-0.5	4.3	PW86PBE	-2.1	7.8
MPW1B95	-3.7	4.3	PW91	-2.3	7.9
B1LYP	-1.5	4.4	τHCTHhyb	5.4	8.2
MPW3LYP	-0.5	4.7	M06	3.3	8.2
M08-HX	-0.3	4.7	PW86SOGGA11	-0.8	8.2
B3V5LYP	-0.9	4.8	OLYP	2.4	8.2
M08-SO	-1.0	4.9	OreLYP	3.6	8.2
B3LYP	-0.7	4.9	BMK	-3.3	8.2
B98	2.4	5.0	BPW91	-3.7	8.4
B97-1	2.9	5.2	PW86LYP	3.1	8.5
B3LYP*	-0.1	5.6	SOGGA	-4.1	8.6
MPWB1K	-5.7	5.7	SOGGA11	-0.7	8.8
SOGGA11-X	-3.2	5.9	VS98	-0.1	8.8
LC-MPWLYP	2.8	5.9	C09PBE	-5.6	9.0
ωB97X	4.9	6.0	BHandHLYP	-5.6	9.1
O3LYP	0.6	6.2	PW86reLYP	4.1	9.6
MOHLYP	1.7	6.5	C09SOGGA11	-6.4	9.9
RPBE	-1.9	6.8	MPW1K	-10.1	10.1
PBE0	-6.4	6.8	OPBE	-3.5	10.2
revTPSS	-3.5	6.8	SVWN	0.4	10.6
TPSSh	-4.1	6.9	M06-2X	5.2	10.9
MPWKCIS1K	-5.8	6.9	N12-SX	8.7	11.0
TPSS1KCIS	-3.5	6.9	HCTH	8.6	11.0
C09reLYP	1.8	6.9	M05	8.4	11.4
TPSS	-2.8	7.0	MN12-L	9.1	11.8
MPWLYP1M	2.1	7.0	M05-2X	4.3	11.8
B97-2	4.1	7.1	B88	-12.6	13.0
B3PW91	-5.4	7.1	M11-L	2.1	14.2
C09LYP	0.5	7.2	N12	4.2	16.2
BHandH	-6.0	7.2	τHCTH	15.0	16.5
M06-L	0.0	7.2	MN12-SX	17.3	18.7
BP86	-1.0	7.3	HFPW91	-18.2	18.9
HSE	-6.3	7.4	HFLYP	-12.5	22.4
BLYP	2.1	7.5	M06-HF	10.6	23.3
MPWLYP	2.8	7.7	HF	-25.6	27.4

Table 4.10. MSE(20) and MUE(20) of ΔE (kcal/mol) for RBS Method

Functional	MSE	MUE	Functional	MSE	MUE
SOGGA11-X	0.1	3.6	HSE	-4.5	7.7
ωB97X-D	1.9	4.3	M08-HX	5.0	7.8
MPW1B95	-2.6	4.5	PW86PBE	-2.1	7.8
MPWB1K	-3.8	4.5	SOGGA	-1.8	7.9
B97-3	3.0	4.9	OLYP	5.1	8.0
CAM-B3LYP	1.3	5.1	VS98	2.6	8.0
B3V5LYP	0.3	5.2	MPWLYP	4.7	8.1
B3LYP	0.4	5.3	PW86SOGGA11	-0.8	8.2
B98	3.9	5.5	MPW1K	-7.8	8.4
PW6B95	-0.1	5.5	τHCTHhyb	7.2	8.5
M08-SO	3.9	5.6	BHandHLYP	-2.1	8.5
MPW3LYP	1.0	5.6	PW86LYP	3.1	8.5
B97-1	4.4	5.8	MPWKCIS1K	-7.7	8.5
BHandH	-3.5	5.8	OPBE	-0.4	8.7
B3LYP*	1.1	5.8	OreLYP	6.5	8.7
B1LYP	0.7	5.9	LC-ωPBE	0.3	8.8
revTPSS	-1.5	6.0	SOGGA11	3.4	8.8
RPBE	0.5	6.0	C09PBE	-5.6	9.0
M06-L	3.3	6.0	PW86reLYP	4.1	9.6
TPSSh	-2.3	6.2	C09SOGGA11	-6.4	9.9
TPSS	-0.6	6.2	SVWN	1.8	10.0
MOHLYP	4.1	6.2	M05-2X	8.1	10.3
O3LYP	2.8	6.4	B88	-9.4	10.6
TPSS1KCIS	-2.0	6.4	M05	10.3	11.4
B3PW91	-3.9	6.4	N12-SX	9.9	11.6
PBE0	-5.1	6.5	M06-2X	8.9	12.2
PW91	0.0	6.8	HCTH	11.9	12.6
PBE	-0.6	6.8	MN12-L	11.6	12.9
BP86	0.9	6.8	M11-L	5.4	13.7
BMK	-1.2	6.9	LC-MPWLYP	12.6	14.7
C09reLYP	1.8	6.9	HFPW91	-12.7	15.1
ωB97X	6.9	7.0	M11	7.6	15.9
M06	5.4	7.1	HFLYP	-6.4	18.6
B97-2	6.0	7.2	τHCTH	18.9	19.3
C09LYP	0.5	7.2	HF	-20.4	23.3
BPW91	-1.6	7.3	N12	13.2	24.0
MPWLYP1M	3.6	7.4	MN12-SX	25.5	26.1
BLYP	3.7	7.5	M06-HF	15.9	27.0

Table 4.11. MSE(10) and MUE(10) for the Ionization Potentials (kcal/mol) for the Variational Method

Functional	MSE	MUE	Functional	MSE	MUE
B97-3	1.8	2.0	C09reLYP	4.2	6.3
B97-1	1.6	2.3	TPSSh	-1.9	6.3
B98	1.8	2.6	N12-SX	-4.3	6.3
ωB97X-D	-0.5	2.7	revTPSS	0.6	6.4
PW6B95	0.9	2.9	M06-HF	0.2	6.4
ωB97X	0.5	3.0	MN12-L	-3.7	6.4
B1LYP	1.6	3.4	TPSS	0.4	6.6
M08-SO	1.2	3.6	M11-L	-3.3	6.7
MPW1B95	-2.0	3.6	SOGGA11	3.0	6.8
B97-2	-1.7	3.6	SOGGA11-X	6.8	6.8
CAM-B3LYP	2.5	3.9	RPBE	2.9	6.9
B3V5LYP	3.0	4.3	M06	5.1	7.1
BHandHLYP	-0.6	4.3	MPWLYP1M	6.1	7.2
MPWB1K	-3.7	4.3	SOGGA	1.6	7.3
OreLYP	0.9	4.4	OPBE	-4.9	7.5
M08-HX	-3.5	4.5	LC-ωPBE	-7.0	7.7
τHCTHhyb	4.0	4.6	BLYP	6.0	7.8
LC-MPWLYP	-2.0	4.7	C09PBE	-2.1	7.9
O3LYP	-2.4	4.9	PW86SOGGA11	-3.6	8.0
MOHLYP	-1.3	5.0	HCTH	8.0	8.1
PBE0	-1.5	5.1	PBE	4.9	8.2
MPWKCIS1K	-4.6	5.1	MPWLYP	7.3	8.3
MPW3LYP	4.8	5.1	BPW91	3.9	8.5
BHandH	-3.1	5.3	N12	-5.7	8.5
B3LYP	4.9	5.4	PW91	6.2	8.9
τHCTH	3.9	5.5	M05-2X	7.1	9.1
BMK	4.5	5.5	HFLYP	-6.5	9.1
OLYP	-2.4	5.5	BP86	8.5	9.8
HSE	-0.8	5.6	PW86PBE	8.3	10.0
VS98	1.1	5.7	MN12-SX	-0.6	10.0
MPW1K	-3.9	5.7	PW86LYP	12.0	12.0
C09LYP	0.6	5.8	B88	-8.1	12.3
M06-L	1.0	5.8	HFPW91	-12.0	13.2
B3PW91	-0.1	5.9	C09SOGGA11	-13.6	14.9
M05	-0.5	5.9	M11	-16.3	16.3
M06-2X	5.2	5.9	PW86reLYP	16.4	16.4
TPSS1KCIS	-1.7	6.0	SVWN	20.6	20.6
B3LYP*	5.5	6.2	HF	-25.7	25.7

Table 4.12. MSE(10) and MUE(10) for the Ionization Potentials (kcal/mol) for the WABS Method

Functional	MSE	MUE	Functional	MSE	MUE
B97-3	1.8	2.1	TPSSh	-1.7	6.2
B97-1	1.7	2.3	B3LYP*	5.6	6.2
B98	1.8	2.6	C09reLYP	4.2	6.2
ωB97X-D	-0.5	2.7	MN12-L	-3.8	6.2
PW6B95	0.9	2.9	N12-SX	-4.3	6.3
ωB97X	0.5	3.1	TPSS	0.5	6.4
B1LYP	1.7	3.4	RPBE	3.1	6.6
M08-SO	1.2	3.6	SOGGA11	3.2	6.7
MPW1B95	-2.0	3.6	SOGGA11-X	6.8	6.8
B97-2	-1.7	3.6	M06	5.2	7.0
CAM-B3LYP	2.5	3.9	M11-L	-2.8	7.1
OreLYP	1.1	4.2	MPWLYP1M	6.2	7.1
B3V5LYP	3.1	4.3	SOGGA	1.8	7.2
BHandHLYP	-0.5	4.3	OPBE	-4.6	7.3
MPWB1K	-3.7	4.3	BLYP	6.1	7.6
M08-HX	-3.5	4.5	LC-ωPBE	-6.9	7.7
LC-MPWLYP	-2.0	4.7	C09PBE	-2.0	7.8
τHCTHhyb	4.1	4.7	PW86SOGGA11	-3.5	8.0
O3LYP	-2.2	4.7	PBE	5.0	8.0
MOHLYP	-1.1	4.7	MPWLYP	7.4	8.2
PBE0	-1.4	5.0	M06-HF	-1.3	8.2
MPWKCIS1K	-4.6	5.1	BPW91	4.0	8.3
MPW3LYP	4.8	5.1	HCTH	8.5	8.5
M06-L	1.5	5.2	N12	-5.7	8.6
OLYP	-2.1	5.3	PW91	6.3	8.7
BHandH	-3.1	5.3	M05-2X	7.1	8.9
B3LYP	4.9	5.4	HFLYP	-6.5	9.1
BMK	4.5	5.5	BP86	8.6	9.7
HSE	-0.8	5.5	MN12-SX	-0.4	9.8
VS98	1.1	5.6	PW86PBE	8.4	9.9
C09LYP	0.7	5.6	B88	-8.1	12.1
MPW1K	-3.9	5.7	PW86LYP	12.1	12.1
M06-2X	5.1	5.8	HFPW91	-12.0	13.2
τHCTH	4.7	5.8	C09SOGGA11	-13.5	14.8
B3PW91	0.0	5.8	M11	-16.3	16.3
M05	-0.5	5.8	PW86reLYP	16.4	16.4
TPSS1KCIS	-1.6	5.9	SVWN	20.6	20.6
revTPSS	0.7	6.1	HF	-25.6	25.6

Table 4.13. MSE(10) and MUE(10) for the Ionization Potentials (kcal/mol) for the RBS Method

Functional	MSE	MUE	Functional	MSE	MUE
B97-3	1.8	2.1	MN12-L	-3.7	6.2
B97-1	1.7	2.3	B3LYP*	5.6	6.2
B98	1.9	2.5	C09reLYP	4.2	6.2
ωB97X-D	-0.5	2.7	M06-2X	5.3	6.4
ωB97X	0.5	3.1	N12-SX	-4.3	6.4
B97-2	-1.5	3.5	SOGGA11-X	6.7	6.7
MPW1B95	-2.0	3.6	M06	5.4	6.8
OreLYP	2.2	3.7	OPBE	-4.2	6.8
CAM-B3LYP	2.6	3.9	SOGGA	2.1	6.9
MOHLYP	-0.6	4.0	MPWLYP1M	6.3	6.9
M08-SO	2.5	4.1	BLYP	6.2	6.9
B3V5LYP	3.1	4.3	SOGGA11	3.6	7.1
MPWB1K	-3.6	4.3	M11-L	-2.2	7.2
O3LYP	-1.9	4.4	τHCTH	6.4	7.4
M06-L	1.8	4.4	PBE	5.4	7.4
OLYP	-1.3	4.6	BPW91	4.2	7.7
PW6B95	2.7	4.6	C09PBE	-2.0	7.8
B1LYP	3.1	4.8	MPWLYP	7.5	7.9
τHCTHhyb	4.2	4.8	PW86SOGGA11	-3.5	8.0
PBE0	-1.4	5.0	LC-ωPBE	-6.6	8.2
MPWKCIS1K	-4.6	5.1	PW91	6.7	8.3
MPW3LYP	4.8	5.2	M05-2X	6.8	8.4
BHandH	-3.1	5.3	HCTH	9.1	9.1
VS98	1.0	5.3	MN12-SX	2.2	9.3
BHandHLYP	-1.6	5.4	BP86	9.1	9.3
B3LYP	5.0	5.4	HFLYP	-6.8	9.3
HSE	-0.7	5.5	PW86PBE	8.4	9.9
BMK	4.5	5.5	B88	-8.4	11.1
M05	-0.6	5.5	PW86LYP	12.1	12.1
revTPSS	0.8	5.6	HFPW91	-12.0	13.2
C09LYP	0.7	5.6	C09SOGGA11	-13.5	14.8
MPW1K	-3.9	5.6	PW86reLYP	16.4	16.4
RPBE	3.6	5.6	LC-MPWLYP	11.9	18.6
TPSS1KCIS	-1.3	5.6	M11	-12.7	19.8
M08-HX	-3.3	5.7	SVWN	20.6	20.6
TPSS	0.9	5.7	N12	4.1	22.2
B3PW91	0.1	5.7	HF	-25.5	25.5
TPSSh	-1.4	5.9	M06-HF	-6.8	31.1

Table 4.14. MUE(30) in kcal/mol[a]

Functional	Var.	WABS	RBS	Functional	Var.	WABS	RBS
SOGGA11-X	6.2	4.8	3.6	ωB97X	5.0	6.0	7.1
ωB97X-D	3.7	4.4	4.3	B97-2	5.9	6.6	7.2
MPW1B95	4.1	4.3	4.5	M06	7.8	7.5	7.2
MPWB1K	5.3	4.8	4.6	M08-HX	4.6	4.9	7.4
C09reLYP	6.7	7.4	4.6	BPW91	8.4	8.2	7.4
C09LYP	6.7	7.1	4.8	MPWLYP1M	7.1	8.1	7.5
B97-3	3.3	4.5	4.9	BLYP	7.6	8.5	7.7
CAM-B3LYP	4.2	5.2	5.1	HSE	6.8	6.7	7.8
M08-SO	4.4	4.1	5.2	OLYP	7.3	7.9	8.0
PW86PBE	8.5	8.5	5.2	SOGGA	8.2	7.9	8.1
PW6B95	3.8	4.4	5.2	VS98	7.8	7.3	8.2
B3V5LYP	4.7	5.8	5.3	MPWLYP	7.9	8.8	8.2
B3LYP	5.1	6.2	5.4	MPWKCIS1K	6.3	6.1	8.4
PW86SOGGA11	8.1	8.7	5.5	τHCTHhyb	7.0	7.7	8.5
B98	4.2	5.2	5.5	BHandHLYP	7.5	7.1	8.6
B1LYP	4.1	5.2	5.6	MPW1K	8.6	7.3	8.7
MPW3LYP	4.8	6.1	5.7	LC-ωPBE	7.7	7.6	8.7
PW86LYP	9.7	10.1	5.7	SOGGA11	8.1	7.9	8.7
B97-1	4.2	5.3	5.8	OreLYP	7.0	7.6	8.8
BHandH	6.6	6.3	5.8	OPBE	9.3	9.2	8.9
B3LYP*	5.8	6.8	5.9	SVWN	13.9	13.9	10.2
C09PBE	8.6	8.4	6.0	M05-2X	10.9	9.9	10.5
RPBE	6.8	7.1	6.1	B88	12.8	11.8	11.0
revTPSS	6.7	6.8	6.1	M05	9.6	9.5	11.4
M06-L	6.8	6.3	6.1	N12-SX	9.4	9.9	11.7
TPSSh	6.7	6.7	6.3	LC-MPWLYP	5.5	6.3	12.2
TPSS	6.9	7.1	6.3	M06-2X	9.3	8.7	12.2
MOHLYP	6.0	6.8	6.4	HCTH	10.1	10.7	12.6
O3LYP	5.7	6.5	6.4	MN12-L	10.0	10.1	13.1
PW86reLYP	11.9	12.1	6.4	M11-L	11.7	11.8	13.9
TPSS1KCIS	6.6	6.7	6.5	M11	10.6	11.3	14.8
B3PW91	6.7	6.5	6.5	HFPW91	17.0	15.4	15.2
C09SOGGA11	11.6	10.9	6.6	HFLYP	17.9	15.9	18.6
PBE0	6.2	6.2	6.7	τHCTH	12.8	13.2	19.4
BMK	7.3	6.9	6.9	N12	13.6	13.4	22.1
PW91	8.2	8.2	6.9	HF	26.8	24.5	23.3
PBE	7.9	7.8	6.9	M06-HF	17.7	17.0	25.7
BP86	8.1	8.5	6.9	MN12-SX	15.8	15.7	25.8

[a] The functionals are arranged in order of increasing MUE for the RBS method. When the MUE for RBS is the same (rounded to the nearest tenth of a kcal/mol), the order is the sum of the MUs for the variational, WABS, and RBS methods.

Table 4.15. MUE(28) in kcal/mol[a]

Functional	Var.	WABS	RBS	Functional	Var.	WABS	RBS
ωB97X-D	4.4	3.9	3.8	τHCTHhyb	7.7	7.3	7.3
B97-3	4.6	3.4	3.9	VS98	7.5	8.0	7.3
M08-SO	4.2	4.4	4.2	MPWLYP1M	8.2	7.2	7.4
MPW1B95	4.2	4.3	4.3	BHandHLYP	7.1	6.5	7.5
B98	5.2	4.4	4.5	PW91	8.5	8.5	7.6
PW6B95	4.3	4.0	4.6	BLYP	8.7	7.7	7.6
CAM-B3LYP	5.2	4.4	4.6	BPW91	8.5	8.7	7.7
B97-1	5.3	4.5	4.7	MPW1K	7.7	8.5	7.9
MPWB1K	5.1	5.0	4.7	SOGGA	8.1	8.5	7.9
SOGGA11X	4.8	5.4	4.7	BP86	8.8	8.4	8.0
B1LYP	5.3	4.1	5.0	SOGGA11	8.2	8.2	8.0
B3V5LYP	5.8	4.9	5.0	PW86SOGGA11	8.6	7.9	8.1
B3LYP	6.3	5.3	5.5	MPWLYP	9.1	8.0	8.3
MPW3LYP	6.1	5.1	5.6	LC-ωPBE	7.7	8.0	8.4
M06-L	6.6	6.2	5.6	OPBE	9.5	9.7	8.4
MOHLYP	7.0	6.1	5.6	PW86PBE	8.8	8.8	8.5
ωB97X	6.1	5.3	5.7	C09PBE	8.7	9.0	8.6
O3LYP	6.5	5.8	5.7	M05	9.5	9.8	9.4
BHandH	6.4	5.8	5.7	PW86LYP	10.7	9.8	9.8
B97-2	6.6	6.2	5.9	N12-SX	9.9	9.6	9.9
B3LYP*	6.8	5.9	6.0	M05-2X	10.1	9.9	10.0
RPBE	7.3	7.0	6.1	M06-2X	9.3	9.3	10.3
revTPSS	7.1	6.8	6.1	MN12-L	10.7	10.0	10.8
TPSS	7.4	7.0	6.2	LC-MPWLYP	6.1	5.4	11.3
PBE0	6.3	6.6	6.3	HCTH	11.0	10.8	11.3
BMK	6.9	6.3	6.3	B88	12.5	13.2	11.5
TPSSh	6.9	6.8	6.3	C09SOGGA11	11.5	11.7	11.7
TPSS1KCIS	6.8	6.7	6.3	M11-L	11.7	11.3	11.8
M08-HX	5.1	4.6	6.3	PW86reLYP	12.6	11.6	12.1
B3PW91	6.6	6.9	6.4	SVWN	14.5	14.7	14.3
C09reLYP	7.3	6.9	6.6	HFPW91	14.9	14.7	14.5
C09LYP	7.6	6.9	6.7	M11	11.4	10.9	15.2
OLYP	8.2	7.5	6.8	τHCTH	13.4	13.4	15.2
OreLYP	7.9	7.1	7.1	HFLYP	15.1	15.1	15.3
MPWKCIS1K	6.0	6.4	7.1	MN12-SX	16.7	16.3	19.5
HSE	6.7	7.0	7.1	N12	13.7	14.2	19.8
M06	7.6	8.2	7.2	HF	24.4	24.8	24.0
PBE	8.0	8.2	7.3	M06-HF	17.1	18.8	25.9

[a] The functionals are arranged in order of increasing MUE for the RBS method. When the MUE for RBS is the same (rounded to the nearest tenth of a kcal/mol), the order is the sum of the MUs for the variational, WABS, and RBS methods.

Table 4.16. Summary of Overall MUE (kcal/mol) of 19 Functionals for Six Databases.

	3d	4d	p	AE6/11	ABDE12	PPS5/05	AMUE2(39)[a]	AMUE3(67)[b]	AMUE4(73)[c]	AMUE5(85)[d]	AMUE6(90)[e]
M08-SO	4.2	5.4	4.2	0.4	3.4	0.3	4.8	4.6	3.5	3.5	3.0
PW6B95	4.6	3.7	3.2	0.4	5.4	0.8	4.2	3.8	3.0	3.5	3.0
MPW1B95	4.3	4.3	3.4	0.8	4.6	1.1	4.3	4.0	3.2	3.5	3.1
MPWB1K	4.7	5.2	3.5	1.1	4.8	0.7	5.0	4.5	3.6	3.8	3.3
SOGGA11-X	4.7	3.1	5.5	0.7	5.0	2.1	3.9	4.4	3.5	3.8	3.5
CAM-B3LYP	4.6	3.6	3.9	0.4	7.4	1.9	4.1	4.0	3.1	4.0	3.6
BMK	6.3	3.7	6.5	0.5	3.8	2.4	5.0	5.5	4.2	4.1	3.9
ωB97X-D	3.8	5.9	8.1	0.4	4.5	0.7	4.9	5.9	4.5	4.5	3.9
B97-3	3.9	5.2	4.9	0.6	6.7	2.3	4.6	4.7	3.7	4.3	3.9
B98	4.5	5.1	4.6	0.7	6.8	2.0	4.8	4.7	3.7	4.3	3.9
MPW3LYP	5.6	3.5	4.7	0.3	8.5	2.0	4.6	4.6	3.5	4.5	4.1
revTPSS	6.1	4.5	3.5	1.2	8.6	2.5	5.3	4.7	3.8	4.8	4.4
B3LYP	5.5	3.6	4.1	0.8	9.8	2.9	4.6	4.4	3.5	4.8	4.4
B3LYP*	5.5	3.6	3.4	3.1	8.3	2.8	4.6	4.2	3.9	4.8	4.5
TPSS1KCIS	6.3	4.1	3.8	0.6	9.7	2.3	5.2	4.7	3.7	4.9	4.5
MPWKCIS1K	7.1	4.3	4.0	1.6	8.0	1.8	5.7	5.1	4.3	5.0	4.5
B97-1	4.7	5.9	5.0	4.6	5.8	1.7	5.3	5.2	5.0	5.2	4.6
TPSSh	6.3	4.2	3.2	1.2	10.5	2.5	5.3	4.6	3.7	5.1	4.6
SOGGA11	8.0	6.8	4.8	1.8	6.9	0.4	7.4	6.5	5.3	5.7	4.8
M06	7.2	8.8	8.4	0.5	4.1	0.2	8.0	8.1	6.2	5.8	4.9
M06-L	5.6	6.3	9.3	0.6	7.8	0.2	6.0	7.1	5.5	5.9	5.0
B1LYP	5.0	3.1	4.6	2.7	11.6	2.9	4.1	4.2	3.8	5.4	5.0
B3V5LYP	5.0	3.3	4.2	4.9	10.2	2.9	4.2	4.2	4.4	5.5	5.1
MOHLYP	5.6	4.0	5.0	2.3	14.9	6.1	4.8	4.9	4.2	6.4	6.3
BHandH	5.7	3.9	3.7	21.9	5.0	1.0	4.8	4.4	8.8	8.0	6.9
PW86PBE	8.5	6.2	6.9	7.6	10.2	2.5	7.4	7.2	7.3	7.9	7.0
C09LYP	6.7	4.9	5.1	22.7	3.9	3.2	5.8	5.5	9.8	8.6	7.7
PW86LYP	9.8	6.1	11.4	6.7	12.0	2.3	8.0	9.1	8.5	9.2	8.1
C09reLYP	6.6	4.3	6.1	26.5	3.9	3.6	5.5	5.7	10.9	9.5	8.5
PW86reLYP	12.1	7.6	12.8	5.5	11.8	2.7	9.8	10.8	9.5	9.9	8.7
C09PBE	8.6	7.3	6.1	29.4	3.9	3.5	7.9	7.3	12.8	11.1	9.8
C09SOGGA11	11.7	11.0	4.2	30.1	22.6	9.3	11.4	9.0	14.2	15.9	14.8
PW86SOGGA11	8.1	8.1	5.6	56.8	32.4	8.6	8.1	7.3	19.6	22.2	19.9

[a] Averaged over columns 3d and 4d [b] Averaged over column 3d, 4d, and p [c] Averaged over column 3d, 4d, p, and AE6/11 [d] Averaged over column 3d, 4d, p, AE6/11, and ABDE12 [e] Averaged over columns 3d, 4d, p, AE6/11, ABDE12, and PPS5/05

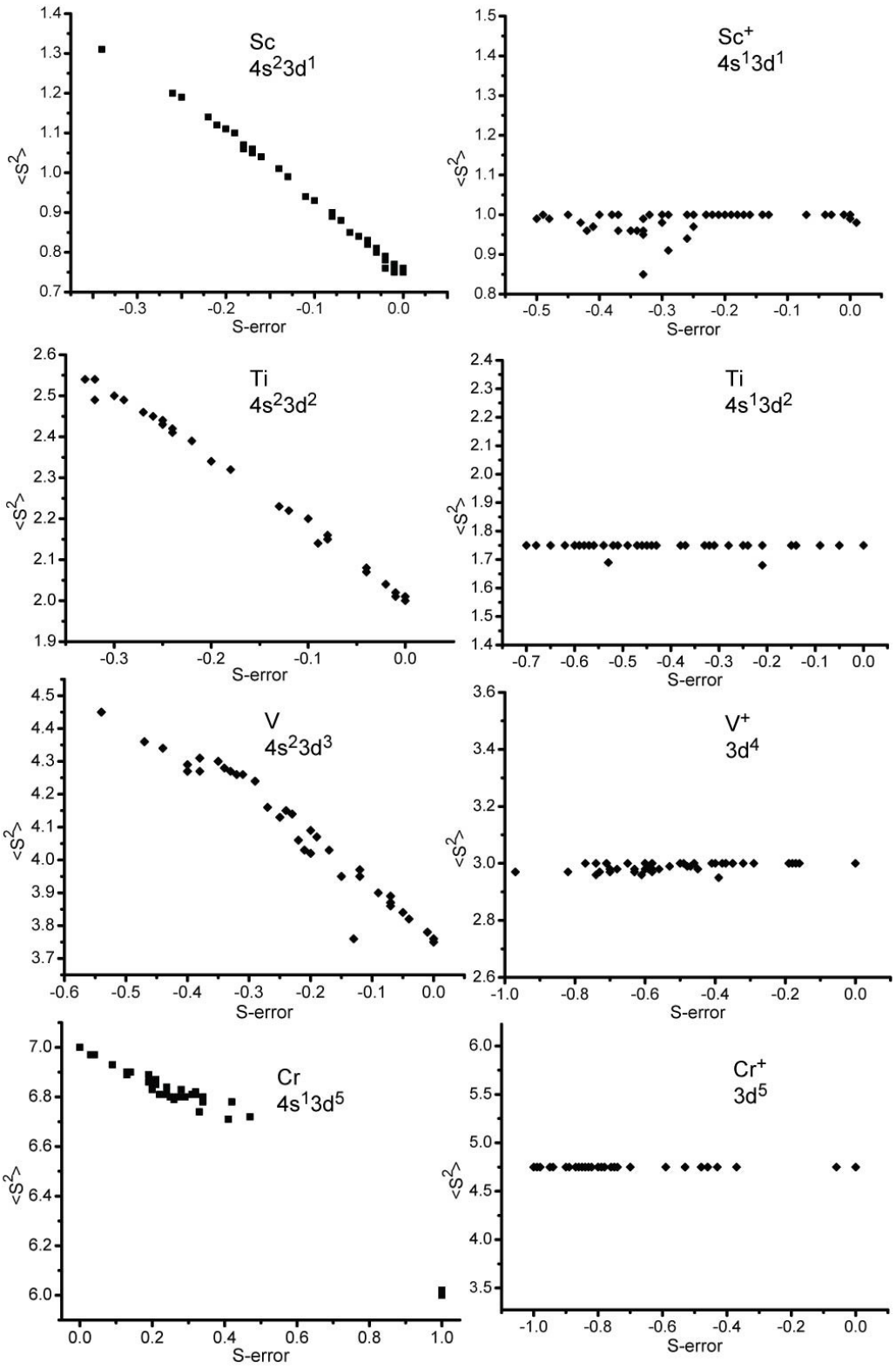

Figure 4.1. Plots of $\langle S^2 \rangle$ values versus s-orbital-occupancy error for M and M^+ (M = Sc, Ti, V, Cr).

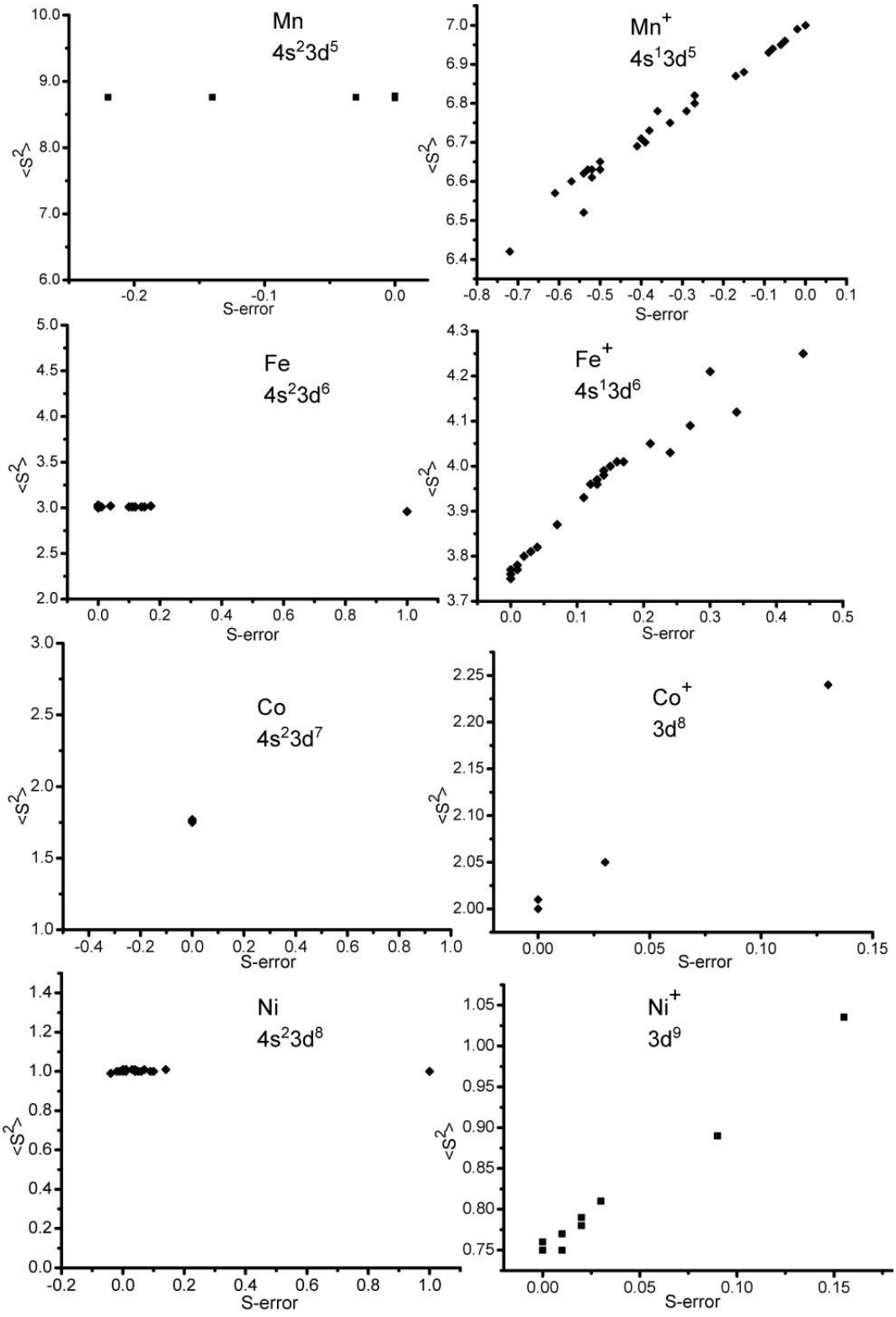

Figure 4.2. Plots of $\langle S^2 \rangle$ values versus s-orbital-occupancy error for M and M^+ (M = Mn, Fe, Co, Ni).

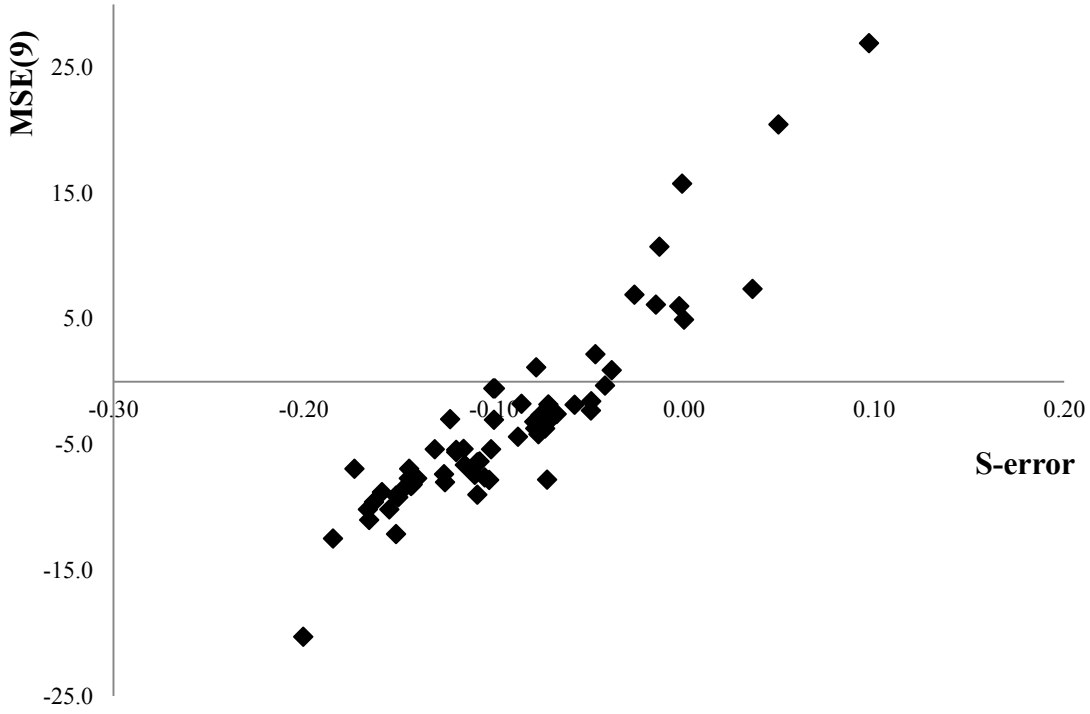

Figure 4.3. Correlation between s-orbital-occupancy error (Table 4.3) and MSU(9) (Table 4.12).

Chapter 5

Density Functional Theory for Open-Shell Systems II: The 4d-Series Transition Metal Atoms and Their Cations

5.1 Introduction

Kohn-Sham density functional theory[1] and its generalizations to open-shell systems[2] and to orbital-dependent functionals[3] have been widely applied to transition metal chemistry, and they have been very successful and useful.[4] Nevertheless, if one were to generalize, one would have to say that the theory is not as accurate for typical transition metal systems as for main-group applications, so there is room for improvement. Since the theory is formally exact if one uses the unknown exact exchange–correlation (xc) functional, we seek improvement at the level of the xc functional, which is always approximate.

There are three specific issues that need to be considered in assessing the reliability of an xc functional for a transition metal complex: (i) Does it treat s and d subshells with comparable accuracy, or is it biased toward certain subshell occupancies? (ii) Does it treat high-spin and low-spin states with the same accuracy, or is it biased toward one or another? (iii) Does it accurately balance localization on a single center (often leading to higher ionic character, higher spin state, or both) and delocalization across centers? Considerable information about these questions can be gleaned from molecular calculations, but there are advantages in studying them in atoms too. The main advantages of atoms are: (a) Data on atomic energy levels is

very complete and very accurate,[5] whereas molecular data is often missing for key compounds that would allow for systematic studies and when available often has large uncertainties. (b) Studying atoms allows us to study questions (i) and (ii) without the complication of question (iii) or the possible complication of systematic errors in molecular geometry, thereby disentangling some of the physics.

Motivated by these considerations, the present article reports a systematic study of the ability of approximate xc functionals to calculate energy levels in transition metal atoms, with a special emphasis on transitions involving a change in spin multiplicity or s and d occupancies or both. In particular, for each of the 4d transition metals in groups 3-10 of the periodic table, we study the lowest-energy multiplicity-changing transition in the neutral atom and its singly positive cation, as well as the adiabatic ionization potential. In ten of the 16 cases (eight neutral atoms and eight cations), the lowest-energy multiplicity-changing transition involves a shift of electrons from an s orbital to a d orbital or vice versa (in four of these states the low-spin state has more s electrons than the high-spin state).

Our study will also consider the role of broken-symmetry solutions to the Kohn–Sham equations. It is well known that the wave functions of systems with $n/2 > M_S$, where n is the number of unpaired electrons and M_S is the component of total electron spin (S) along the quantization axis, cannot be described properly by a single Slater determinant, and yet Kohn–Sham theory uses a single Slater determinant to represent the density. Therefore $M_S \leq S$, levels with $n > 2S$ cannot be treated in a natural way by Kohn–Sham theory. With the unknown exact xc functional, one would nevertheless get the correct energy and the correct density for the ground state, but

the Kohn–Sham orbitals would not necessarily be spatial symmetry orbitals. Actually they need not be symmetry orbitals even when $n/2$ is not greater than M_S, and presently available approximate density functionals often lead to a broken-spin-symmetry determinant. When $n/2 > M_S$, that broken-symmetry solution often seems to correspond to a mixture of two (or more) states with differing values of S (i.e., differing multiplicity). Interpreting the Kohn-Sham determinant as such a mixture of states allows one to approximate the correct spin state by performing two (or more) calculations with different M_S and combining the results linearly with weights based on wave function theory,[6] and we call this the weighted-average broken symmetry (WABS) method. The WABS method has ben very successful for transition metal complexes containing weakly coupled centers.[7] Extensions to strongly coupled cases (such as the states here where all orbitals are on the same center) have also been proposed.[8] Here we will explore the question of whether this method[8] provides general improvement over the straight variational approach.

We emphasize here that all the SCF calculations presented in this paper were converged to a stable solution, meaning that the symmetry of spatial orbitals is allowed to be completely broken in search for the lowest possible energy solution. Although useful insights might be obtained by careful analysis of the spatial orbitals of each spin state by restoring the spatial symmetry from the broken-symmetry solutions, this lies beyond the scope of the present work, which is intended to assess the qualities of various density functionals in describing 4d transition metal spin states in practical applications, where high spatial symmetry is usually not present.

We note that studies with some similarity to the present one have previously been carried out for p block elements[9] and for the 3d transition metals.[10] The former study included 56 density functionals for SCF calculations of multiplicity-changing excitations, and the latter included five density functionals.

Section 5.2 present the experimental data to which we will compare. Section 5.3 specifies the xc functionals to be tested. Section 5.4 discusses the theory, computational methods, and basis sets. Section 5.5 contains the results and section 5.6 the discussion.

5.2 Experimental Data

Although the total electron spin quantum number S is not a good quantum number we follow the usual Russell-Saunders labeling scheme in which atomic levels are labeled ^{2S+1}L where L is total electronic angular momentum. For each element the two levels that we consider are the ground level and the lowest-energy level that has a different S.

The database for the present study is composed of all eight 4d transition metals in groups 3-10 of the periodic table, namely Y, Zr, Nb, Mo, Tc, Ru, Rh, and Pd. For each element the database contains the ionization potential (IP) and the lowest-energy multiplicity-changing excitation energy (ΔE) of both the neutral atom and its singly positive cation. Thus there are 24 data.

Scalar relativistic effects are included in the present calculations, but vector relativistic effects are not. Thus each level has degeneracy equal to $(2S + 1)$ or $(2L + 1)$, which ever is smaller. To obtain reference data for comparison with such calculations we removed spin-orbit coupling (which is a vector relativistic effect)

from the experimental data published in Ref. 5. We do this by taking advantage of the fact that the spin-orbit operator is traceless. Therefore it can be removed to first order by a degeneracy-weighted average:

$$\overline{E}(^{2S+1}\mathrm{L}) = \frac{\sum_{J=|L-S|}^{L+S}(2J+1)E(^{2S+1}L_J)}{\sum_{J=|L-S|}^{L+S}(2J+1)} \tag{5.1}$$

where $^{2S+1}L_J$ denotes the state with total angular momentum J, and the left-hand side is the spin–orbit-free energy of the level. The energies resulting from applying eq. 1 to the experimental data are shown as reference data in Table 5.1. Table 5.1 contains 16 ΔEs (eight for neutral atoms and eight for cations) and eight IPs. Since all 16 excitations considered here involve a change in S, we call one state the low-spin (LS) state and the other the high-spin (HS) state. All the ΔEs are calculated with the following sign convention:

$$\Delta E = E_{HS} - E_{LS} \tag{5.2}$$

5.3 Density Functionals

The exchange-correlation functional (xcF) is the quantity that must be approximated in the Kohn–Sham formalism.[1] Approximate xcFs can be categorized by considering the ingredients that they include. In their simplest form the xcFs only depend on the spin densities, ρ_σ, where σ is α or β, and such xcFs are known as local spin density approximations (LSDAs). When the reduced gradients, s_σ, of the spin densities are also used in the functionals, the functionals will be called gradient approximations. In most gradient approximations, called generalized gradient approximations (GGAs), the exchange part of the xcF has a separable form; if

exchange is treated with a nonseparable form that also includes some correlation energy, the resulting functional is called a nonseparable gradient approximation (NGA). If the spin-labeled kinetic energy densities τ_σ (or the Laplacians of spin densities) are further introduced, the resulting xcFs are called meta-GGAs or NGAs.

The energy densities of LSDAs, GGAs, NGAs, meta-GGAs, and meta-NGAs at a given spatial coordinate depend on functions (ρ_σ, s_σ, τ_σ) evaluated at that coordinate, and such functions are called local functionals. On the other hand the Hartree–Fock (HF) exchange energy density at a point in space depends on the integral of Kohn-Sham orbitals over the whole space, and by replacing a portion of local exchange with nonlocal Hartree–Fock exchange, one obtains a nonlocal functional. If the portion replaced is a constant percentage (i.e., a percentage independent of coordinates, ρ_σ, s_σ, τ_σ, or interelectronic separation), the resulting functional is called a global hybrid. Another way to include Hartree–Fock exchange is to partition the Coulomb operator into a short-range part and a long-range part, and treat one of them by local exchange and the other by Hartree–Fock exchange; xcFs constructed in this manner are called range-separated hybrid functionals. In some functionals, an empirical molecular mechanics term is added to the DFT energy to account for damped dispersion-like interactions. This kind of functional is called a DFT-D functional; if the MM term is added to a GGA, it may be labeled GGA-D.

The Hartree–Fock approximation, although not an actual density functional method (and thus not shown in Table 5.2) is also included in this paper since it can be viewed as an approximate xcF, that is, as a pure-exchange density functional with no correlation and 100 percent of Hartree–Fock exchange. The comparison of the

Hartree–Fock method with functionals such as HFLYP (LYP correlation with 100% Hartree–Fock exchange) and HFPW91 (PW91 correlation with 100% Hartree–Fock exchange) allows for studying the effects of the correlation functional on the calculated EEs and IPs in a particularly transparent way.

We have in total tested 58 density functionals plus the Hartree–Fock method; the tested xcFs are listed in Table 5.2, each with one or more references.[11–66] There are one LSDA, 13 GGAs, one NGA, 19 global-hybrid GGAs, five range-separated hybrid GGAs, one range-separated hybrid GGA plus molecular mechanics dispersion (GGA-D), five meta-GGAs, one meta-NGA, 13 global-hybrid meta-GGAs, and one range-separated hybrid meta-GGA. The LSDA, the GGAs, the NAG, the meta-GGAs, and the meta-NGA are local; the hybrid functionals are nonlocal.

The specific considerations for choosing these density functionals were given a thorough discussion in a previous study of p block elements,[9] and we only point out here that several new functionals were added in the present work, most notably the new second order GGA family (SOGGA11[24] and SOGGA11-X[40]), the Minnesota 11 family (M11-L[49] and M11[66]), the recently proposed nonseparable functionals N12[25] and MN12-L[52], and also the revTPSS[50] functional. SOGGA11 is the first GGA correct to second order in the density gradient that provides good accuracy for a broad variety of chemical problems; SOGGA11-X is the most successful global-hybrid GGA for calculations on a broad variety of chemical problems. M11 is the first range-separated meta-GGA, and it is optimized for a broad variety of chemical problems; it shows significant improvement over the (already very successful) previous generation of Minnesota functionals for the databases examined in the article in which it is

presented. M11-L is the first dual-range local meta-GGA and also the first local functional to have as good an average accuracy as hybrid functionals for many chemical properties. More importantly it has good overall performance for multi-reference systems, which is expected to be a very important advantage for treating transition metals. The N12 functional is the first xcF depending only on the spin-labeled electron densities and their reduced gradients that simultaneously provides good accuracy for the four key energetic and structural properties of solids and molecules, namely, solid-state cohesive energies and lattice constants and molecular atomization energies and bond lengths. The MN12-L functional is a new local exchange-correlation energy functional that has significantly improved across-the-board performance, including main-group and transition metal chemistry and solid-state physics. The recent revTPSS functional is a revised version of the TPSS meta-GGA functional, constructed to be correct to the second order and to improve especially the lattice constants for solid-state calculations.

5.4 Theory and Computational Details

5.4.1 Theory

The WABS[6] method is briefly mentioned in Section 1, and we shall discuss it in detail here. For all the ΔE calculations in this paper, the HS state is a state with $S = n/2$, where n is the number of unpaired electrons; whereas the LS state is a state with lower S. A state with $S = n/2$ can be well represented by a single Slater determinant with $M_S = n/2$, and thus it can be treated naturally by Kohn-Sham DFT. The LS state, however, often cannot be represented naturally by a single Slater determinant, and such states constitute particularly difficult cases for calculations with approximate

xcFs. In other cases we observe LS states that are treated well by a single Slater determinant; see Section 5 for a detailed discussion. The unbalance of the accuracy expected for the many LS states that cannot be represented by a single Slater determinant as compared to the higher accuracy expected for HS states leads to systematic errors in calculated ΔEs since an accurate treatment of the excitation energy requires the LS and HS states to be described equally well.

If one does not fully optimize the Kohn–Sham Slater determinant, the results are sensitive to the choice constraints imposed, and it is hard to impose the same kinds of constraints molecules that one can impose in high-symmetry situations like atoms. Therefore, since our ultimate objective as chemists is accurate calculations on molecules, our first step in the solution of this problem is to allow the self-consistent-field process to break all the spatial symmetries in the calculations of both the HS and LS states, leading to the variationally lowest results one can possibly obtain. For the LS state, this yields the low-M_S broken-symmetry (BS) solution. There exist two strategies regarding how to utilize this stable solution:

(i) Use the low-M_S BS solution *as is*, and calculate the ΔE as the energy difference between the HS state and the low-M_S BS state.

(ii) Assume that the low-M_S BS state is a linear combination of the HS state and the actual LS state, and attempt to extract the energy of the LS state based on this assumption.

Strategy (i) will be called the variational method; it should work well if the LS state can be well represented by a single Slater determinant. However, this is often not true. In strategy (ii), which is the WABS method, the system is usually further

classified into weakly coupled cases and strongly coupled cases.[7,8] The former usually involves two or more distant spin centers with weak coupling between the centers.[7] The atoms we study in this paper fall into the second type because: (i) for a single atom there are no spin centers far apart in space; (ii) the couplings between spins in different MOs of a single atom are usually much greater than the couplings between centers in binuclear or polynuclear transition metal complexes.

For the WABS calculations in this paper, we use the formula proposed by Yamaguchi[8]

$$\Delta E_{WABS} = \frac{2S_{HS}\left(E_{HS} - E_{BS}\right)}{< S^2 >_{HS} - < S^2 >_{BS}} \tag{5.3}$$

(See the Appendix for a derivation.) Here S_{HS} is the total spin of the HS state, $< \hat{S}^2 >_{\mathrm{HS}}$ and $< \hat{S}^2 >_{\mathrm{BS}}$ are calculated expectation values of S^2, and BS denotes the low-M_S BS state. Equation 3 is based on the inference that a large spin contamination results from multi-determinantal character of the actual LS state that leads to a significant mixing of the LS and HS states in the calculated BS state. Therefore, to extract the real excitation energies, the energy difference calculated from the gap between HS and BS states should be scaled by a factor proportional to the spin contamination. In contrast, for systems with little or no spin contamination in the calculated LS state, the BS solution should be used with strategy (i).

In practice we allow symmetry breaking in the HS state as well as the LS state so that all SCF calculations are converged to a stable solution. Thus the HS state may also have broken-symmetry; in general both the variational method and the WABS method involve broken-symmetry solutions. Again, we emphasize that this is

consistent with the goal of present work to test the qualities of xcFs in real world transition metal chemistry applications, where high spatial symmetry is not present.

The s-d orbital transitions in 4d elements lead to complications in applying this method. First, some orbitals have mixed s and d character so there are noninteger occupations of s and d subshells in some states, and in these cases the spin contamination could originate from the partial occupations, from "pure" multi-reference character in d orbital configurations, or from both. WABS was originally formulated conceptually without considering noninteger subshell occupations, and we find that it can lead to little improvement or even worse results when orbitals are partially occupied. Furthermore, the spatial orbitals of the LS and HS states involving s-d transitions differ more than those without s-d transitions, which raises a concern as to whether the assumption of having the same orbitals in the two states is a safe assumption.

To clarify the questions above and to emphasize that complications in the spin states of transition metals should be analyzed on a case-by-case basis, in Section 5.1 we separate the ΔE cases into ones involving large partial subshell occupations and those involving smaller or no partial subshell occupations and also into cases with and without s-d transitions. For each scenario we further compare the results with and without use of WABS post processing.

5.4.2 Computational Details

All the density functional calculations were performed with a locally modified version of *Gaussian 09*.[67] For each state we performed a broken-symmetry calculation, using the spin-unrestricted formalism and not requiring symmetry

orbitals. Furthermore, a stability test was carried out for each calculation, and the orbitals were optimized (if instability was found) until the SCF solution was stable. For integrals over all space of the energy density, we used the "ultrafine" grid in the *Gaussian 09* software; this is a pruned grid with 99 radial shells and 590 angular points in each shell. To calculate 5s and 4d subshell occupation numbers, natural bond orbital (NBO) analysis[68-75] was performed using the *NBO 3.1* package with *Gaussian 09*. The scalar relativistic effect is included by using the Douglas-Kroll-Hess (DKH) second-order scalar relativistic Hamiltonian.[76-78]

We considered five all-electron basis sets specifically designed for DKH calculations of 4d elements. First we compared three triple zeta basis sets: the cc-pVTZ-DK basis set of Petersen et al.[79] and basis sets by Hirao[80] and Huzinaga.[81] We carried out calculations for all three bases for a subset of the density functionals used in this paper, and we found that almost all the density functionals showed a reduced error as compared to experiment when the cc-pVTZ-DK basis is used. Next, although one would expect core correlation effects to be less for 4d elements than for 3d ones, we tested the cc-pwCVTZ-DK[79] basis set, which includes 4s4p correlation, for a subset of ten methods, in particular HF, SVWN, B88, PBE, B3LYP, LC-ωPBE, HSE, ωB97X-D, M06-L, and M06. Table 5.3 compares the results obtained from cc-pVTZ-DK and cc-pwCVTZ-DK calculations, showing that they agree within 0.2 kcal/mol. Finally we considered the ANO basis of Roos et al.;[82] it is much larger than the cc-pVTZ-DK basis, but Petersen et al. found that it performs comparably to cc-pwCVTK-DK in CCSD(T) calculations. Therefore the more manageable cc-pVTZ-

DK basis was selected for our benchmark purposes, and all the remaining results reported here were obtained with the cc-pVTZ-DK basis set.

5.5 Results AND Discussion

5.5.1 5s and 4d subshell occupations

The density functional calculations do not always yield integer occupancies for the 4d and 5s subshells because we always find variationally stable solutions, as mentioned above. Therefore we first consider the 5s subshell occupations. Tables 5.4 and 5.5 show, for each density functional and for Hartree-Fock theory, the mean signed deviation (called ε) and mean unsigned deviation (called δ) of the occupation number n_{5s} of the 5s subshell from the integer value characterizing the dominant determinant (according to the experimentally based tables of Moore[5]) for the 32 spin states we studied. (The 4d occupancy usually has an equal but oppositely signed error to that for the 5s, although in a few cases there is some small 5p occupancy of order 0.01.) We label the mean noninteger 5s occupancy as ε, and we label the mean absolute noninteger 5s occupancy as δ. Note that ε and δ should not necessarily be interpreted as errors because the exact Kohn–Sham orbitals need not be symmetry orbitals. Nevertheless it is not clear whether presently available approximate density functionals might build in noninteger occupancies as a way to mimic configuration interaction effects of wave function theory or whether these noninteger occupancies should be viewed in a negative light. In the present work, our goal is to evaluate the functionals based on energetic comparison to experiment, and such comparisons do not suffer from such ambiguities. However, we will see that the noninteger

occupancies are very helpful in understanding some of the results if we interpret a positive ε as a bias toward s orbitals and a negative ε as a bias toward d orbitals, and so we shall use this interpretation.

Table 5.4 shows that 43 out of the 61 functionals have negative ε for 5s occupancy, which implies an overstabilization of 4d orbitals relative to 5s. Furthermore, almost all of the 19 local functionals produce negative ε, the exceptions being B88, mPWLYP, and BLYP, which have small positive ε of 0.01, 0.02, and 0.01. This is consistent with a previous study of 3d elements by Hirao et al. al.[10] Adding a small amount of Hartree–Fock exchange alleviates this bias, resulting in six global-hybrid GGAs with an ε that rounds to 0.00. This was also pointed out by previous study[83], which, however, was based on Slater exchange rather than Kohn-Sham exchange. Density functionals with a large percentage of Hartree–Fock exchange seem to overcorrect the bias of local functionals and are biased towards occupation of 5s orbitals, as most clearly observed in M05-2X, M06-2X, and BMK, but the bias is smaller than the bias in the other direction of the first 30 functionals in Table 5.4.

Whereas Table 5.4 has the functionals in order of increasing ε, Table 5.5 has them in order of increasing δ. The result is that almost all the entries in the first half (31) of the 61 entries of Table 5.5 are hybrid functionals, with the only exception being VS98, which is in position 26 with an ε of 0.08. It is also notable that the pure Hartree–Fock exchange functional is positioned near the very bottom of the ordered list. These observations confirm the conventional wisdom that appropriate amount of

Hartree–Fock exchange for an unbiased description of the 5s and 4d orbitals is neither zero nor 100%.

Whereas Tables 5.4 and 5.5 show averages of the noninteger 5s occupancies over spin states for each functional, Table 5.6 shows averages of the noninteger 5s occupancies as averaged over all functionals for each of the 32 spin states. Table 5.6 also shows the experimental multiplicity $2S + 1$ and experimental 5s occupation numbers. We find that, for a given spin state, all the methods tend to produce errors with the same sign (either positive or negative). The results show that there are six spin states (in red) with an ε more negative than –0.10, implying a strong bias towards occupation of 4d orbitals, and there are three states (in blue) with an ε more positive than 0.10, implying a strong bias towards occupation of 5s orbitals. The 5s/4d occupations are more properly described in the remaining 23 spin states.

We should be careful to distinguish *actual 5s occupancy* (an output variable obtained by NBO analysis of the orbitals) from *nominal 5s occupancy change* (an input variable, as part of the initial guesses for the HS and LS SCF processes, based on the dominant configurations of the experimental states). In addition to the *deviation from an integer* of the actual in 5s occupancy *in each of the 32 spin states* involved in the multiplicity-changing transitions, it is also important to consider *changes* in the nominal 5s occupancy *in each of the 16 transitions*. By taking account of both considerations, we divide the 16 ΔE cases into four groups:

In ***group 1***, neither the LS nor the HS state has from a large-magnitude ε, and there is no change in nominal s and d occupancies involved in the excitation. This group contains the ΔE of Mo, Mo^+, Ru, and Rh^+. In all these cases it turns out that <

$\hat{S}^2>$ for the low-M_S BS state is close to what one expects for a 50:50 mixture of the HS and LS states, that is, there is large spin contamination. For the 4d transition metals in this study, we did not find any cases involving a change in nominal 5s occupancy that had a small error in the 5s occupancies of both the HS and LS states but large spin contamination (although this does occur for some other transition metals).

In ***group 2***, neither the LS nor the HS state has a large-magnitude ε, but the multiplicity-changing excitation does involve a nominal s–d transition. This group contains Y, Tc^+, Ru^+, Pd, and Pd^+. In these cases it turned out that the $<\hat{S}^2>$ values are close to those for pure spin states.

In ***group 3***, one of the two states suffers from a large-magnitude ε. We find that all such cases also happen to involve a nominal s–d transition. This group contains Y^+, Zr, Nb, Tc, and Rh.

In ***group 4***, both the LS and HS states have a large-magnitude ε. This group contains only Zr^+ and Nb^+, and neither of them involves a nominal s–d transition.

Next, results for these four groups will be discussed separately, after which a brief summary and further discussion will be provided. Finally we will discuss the overall performance of the functionals and methods and make recommendations.

5.5.2. Group 1 cases

Since all the spin states in this group present neither nonintegral subshell occupation nor s-d transitions, group 1 cases are the most "pure" ones for discussing the performance of density functionals for spin states and the usefulness of WABS methods. The results are presented in Table 5.7, with the four columns of numbers

corresponding to the MSEs and MUEs before and after WABS treatment, where MSE is the mean signed error in ΔE and MUE is the mean unsigned error in ΔE.

A first observation is that before post processing with the WABS treatment, i.e., employing the variationally stable states without reinterpretation by the WABS method, all the methods overestimate ΔE, resulting in a positive MSE value. Also we find (not shown) that all the LS states have a calculated $<\hat{S}^2>$ close to the one of a state with a half-and-half linear combination of the HS and the LS states. Since for group 1, all the experimental ΔE values are negative (meaning the LS state is higher than the HS one), this puts the broken-symmetry low-M_S variational solution half way between the HS state and the actual LS state and result in a *less negative* excitation energy; this explains the positive MSE. Furthermore there is no fractional s occupancy in either of the spin states involved in the transition, and the LS and the HS states tend to have very similar spatial orbitals. This then is precisely the situation that the WABS post processing method was originally designed to treat.

After WABS treatment, the MSEs for various functionals have both positive and negative values, and the MUE values are usually improved, as shown in the last column. In fact in 54 cases the MUE is lowered, in one case (M11-L) it stays the same, and in only four cases (MPW1K, HFPW91, B88, and HF) it increases. For group 1 then, the errors remaining after WABS treatment may be considered to be the "pure" spin-coupling errors of the corresponding density functionals, independent of whether or not they have a bias toward s or d occupancy, and we find the best functional to be O3LYP with an MUE of 1.9 kcal/mol. This is consistent with a

previous finding that O3LYP performs well in spin-state calculations.[9] Only slightly less accurate are MOHLYP, BP86, MPWB1K, and PW6B95.

It is usually said that Hartree–Fock theory has a bias towards HS states, and local density functionals have a bias toward LS states. The former can be rationalized by the fact that HF theory includes the Fermi hole but not the Coulomb hole; the latter can be rationalized by the fact that local functionals do not cancel self-interaction errors. The results in Table 5.7 are only partly consistent with this. HF does have a large negative ΔE as does HFPW91, but HFLYP has a positive MSE. This shows the important role of correlation energy changes in spin-flip transitions. Furthermore, Table 5.7 shows little correlation between the percentage of HF exchange and the sign of MSE.

To summarize, we find that much of the systematic error in ΔE for group 1 species originates from the multi-determinantal character of the LS state. Since the LS and HS states tend to have similar spatial orbitals, the WABS post processing treatment significantly improves the results. Comparison of the resulting excitation energies to experiment, as summarized in the WABS columns of in Table 5.7, reveals which functionals are well balanced in their treatment of different multiplicites.

5.5.3. Group 2 cases

In transition metal chemistry the simple situation discussed in Section 5.2 is commonly complicated by the possible overstabilization of s or d orbitals, which leads to partial occupations through hybridization. This could accidently favor either the LS or the HS state on a case-by-case basis. The entanglement of these effects, bias toward high *S* or low *S* and bias toward high s:d or low s:d; usually results in complex

and hard-to-interpret scenarios. However, group 2 species provide relatively clear cases in the sense that we find that both spin contaminations and nonintegral subshell occupation numbers are negligible for almost all methods in both states of each transition. The former seems to indicate that both the LS and the HS states are single-reference ones, and the latter means that the 5s and 4d orbitals are treated without the complication of hybridization.

Table 5.8 presents the calculated MSEs and MUEs of all the functionals for the group-2 excitation energies. Since a small amount of spin contamination exists for certain functionals in certain states, we also report in the last column the MUEs after WABS post processing. However, the comparison to the unprocessed results shows that the improvement by WABS is less than 2 kcal/mol, and for many cases the error increased after WABS treatment. Furthermore, in group 2 the $<\hat{S}^2>$ values are close to those for pure spin states, so the deviation from the pure-state values need not be dominated by a simple mixing of two states. Therefore, we do not recommend WABS corrections for group 2 calculations, and all the discussions of group 2, except where indicated otherwise, will be based on the variational results.

An MSE of -18.3 kcal/mol for Hartree–Fock theory implies a strong favoring of the HS state, which is consistent with the common expectation. If one compares the local functionals with their hybrid counterparts, however, the results are mixed. For most cases, an increased (although only by a small amount) favoring of the HS state is observed when the percentage X of Hartree–Fock exchange is raised, such as PBE vs. PBE0, PW91 vs. HFPW91, and BLYP vs. HFLYP. The same effect is also seen for OLYP vs. O3LYP and MPWLYP vs. MPW3LYP, even though the

correlation functional changes a little when X is raised in these cases. We also see apparent exceptions such as SOGGA11 vs. SOGGA11-X and M06-L vs. M06 vs. M06-2X; we note though that in these cases the local part is reoptimized significantly when X is changed.

Now turn to MUEs of the excitation energies. We find the top ten and most of the top half of the list are hybrid functionals, with the best being BHandH with 50 percent Hartree–Fock exchange. The best local functional for group 2 is BLYP with an MUE of 3.6 kcal/mol, and most local functionals are ranked near the bottom with an MUE larger than 5 kcal/mol. This is in contrast with group 1, where, after WABS correction, the top ten contains five local functionals and five hybrid functionals. Furthermore, no density functional appears in the top ten density functionals of both groups. If, however, we had included WABS postprocessing for group 2, MPWB1K, BP86, and RPBE would be in the top ten for both groups.

The large differences that we find in functional rankings between group 1, which does not involve an s–d transition, and group 2, which does involve of an s–d transition, seems to imply that excitations with and without s–d transitions are of distinctive character, and this should be carefully considered in assessing the quality of density functionals and in constructing representative subsets of 4d elements.

The conclusion that excitations with and without s–d transitions have a different character has profound implications for the many studies of multiplicity-changing transitions in polyatomic molecules. In molecules there is a continuum of s-d mixing due to changes in hybridization, and the hybridization state may change more or less upon a multiplicity-changing excitation, but in general the past attempts

to draw conclusions about the accuracies of various functionals for multiplicity-changing transitions have not taken account of this.

5.5.4. *Group 3 cases*

Now we turn to the more problematic group 3 cases, in which the 5s subshell has a noninteger occupation in either the LS or the HS state. We note that each calculated LS state in group 3, except Tc, suffers from a fair amount of spin contamination, but the calculated $<\hat{S}^2>$ value is still far from the one of a half-and-half linear combination of the HS and the LS states, and unlike group 1, the spin contamination values in group 3 depend heavily on the density functional being used. One should note there are actually two sources of spin contaminations for transition metals: (i) partial occupations of s or d orbitals, and (ii) multi-determinantal character in representing the electron configurations in the five d orbitals when $n/2 > M_S$. Furthermore, in complicated cases these two sources can be in effect at the same time. Spin contaminations from group 1 arise only from source (ii) since there is no partial occupation, and group 1 is most suitable for WABS treatment because the spatial orbitals of the LS and HS states are potentially very similar. In contrast, spin contaminations of LS states in group 3 mostly originate from source (ii), as revealed by Figure 5.1, where we plot the absolute error in $<\hat{S}^2>$ against δ for Y^+, Zr, Nb, and Rh and find a nearly linear dependence in all four cases; Tc is not plotted because for that case it is the HS state that has partial occupations and the spin contaminations for all functionals turn out to be negligible for Tc.

In the WABS method employing eq 3, the spin contamination is used as a sign of multi-configuration character in the BS state, and it is utilized to scale the LS–HS

gap proportionally, but this is only valid if the orbitals are the same (or almost the same) in the HS and BS solutions, and this is usually achieved only if no noninteger occupation of subshells is involved. The multiplicity-changing excitations in group 3 species all happen to involve an s–d transition, and just like group 2, the orbitals in the LS and HS states tend to differ more in this circumstance. In addition, one state has noninteger 4s occupancies, and the other does not. For these reasons one would not expect WABS post processing to offer meanful improvement for ΔE for group 3; and yet Table 5.9 does show improvement in MUE for most of the functionals, although it is usually less than 1 kcal/mol, and the errors even increase for some functionals. Additionally, the MUE in general increases as δ increases, which again is consistent with our conclusion that the main error in group-3 atoms and cations results from nonintger subshell occupations.

If we look at the MUEs either before or after WABS post processing, the best performing functional either way is SOGGA11-X with an error of 2.2 kcal/mol before and 1.6 kcal/mol after. If we order the functionals based on MUE after the WABS treatment, then 19 of the best 20 density functionals are hybrid functionals, with the only exception being M06-L with an MUE of 3.8 kcal/mol. Again using the WABS MUE, three functionals in the top ten for group 3 are also found in the best ten for group 2, namely, BHandH, BMK, and B1LYP, which could be due to the fact that group 2 and group 3 excitations both involve s–d transitions, and thus they share a common characteristic. However, as in group 2, there is no overlap between the best ten for group 3 the best ten for group 1.

5.5.5 Group 4 cases

Group 4 only includes Zr^+ and Nb^+**,** for which we found that the broken-symmetry solutions of both the LS and the HS states present high spin contamination. Furthermore, the calculated $<\hat{S}^2>$ values are very close to the ones for a half-and-half linear combination of the LS and the HS states, which is very similar to group 1. This seems to imply that results would be improved after applying WABS post processing. However, when one compares the calculated MUEs before and after WABS post processing in Table 5.10, we see that for more than 40 functionals the averaging procedure deteriorates the accuracy. Also note that no nominal s–d transition is involved in either cation, excluding possible impacts from this aspect. Thus if we compare group 1 and group 4, the main difference is the noninteger occupations of s and d subshells. Consequently, a possible explanation of the poor performance of WABS seems to be that the orbitals of the LS and HS states differ significantly from each other, and this contradicts the underlying assumptions of the WABS method.

Next we will discuss the MSE and MUE results of the variational calculations for group 4. First consider MSEs. The largest negative MSE is -6.2 kcal/mol for HF and is again consistent with the common conclusion that HF is biased toward the HS state. Also we find that most density functionals favor the LS state (i.e., they have a positive MSE). If one focuses on the MUE of each functional, then—surprisingly—HFLYP, a simple hybrid GGA with 100 percent of HF exchange, is the best performing functional with an MUE of merely 0.7 kcal/mol. This seems to be mainly due to its very small ε of 0.03. In general the absolute errors appear to decrease as ε decreases, but this is not as evident as in group 3 (where only one state has nonintger

subshell occupation), especially when we notice that in the best 10 functionals, five, namely TPSSh, revTPSS, B98, ωB97X, and TPSS, have ε greater than or equal to 0.19.

We conclude that the situations for the group 4 species are too complicated for a general interpretation, and they serve as typical examples where multi-reference character (suggested by a very large spin contamination) is not properly treated by averaging due to having very different orbitals of the LS and the HS states. Although the key factor in improving the accuracy seems to be connected with a proper description of s and d orbitals to eliminate partial occupations, this is not as conclusive as in group 3. In general one should consider the best functionals in this group to achieving their success or partial success fortuitously, and it is recommended not to include this group in assessment or design of functionals for transition metals due to the entanglement of several effects.

5.6. Overall performance

We shall briefly summarize our observations here, with an attempt to gain some insights for an appropriate assessment of the overall performance of all the methods.

Group 1 contains the clearest cases of where WABS post processing can help because the error is dominated by multideterminental character of the LS states. Since WABS post processing significantly improves the accuracy of almost all functionals, we conclude that only WABS-corrected results should be used to assess the intrinsic error of each functional for spin states in this group. Group 2 and group 3 share some similarities in that both involve s–d transitions in multiplicity-changing excitations.

The former group has little spin contamination, and all of its states are single-reference ones. The spin contaminations of group 3, although non-negligible, are smaller than for group 1 and, as distinct from group 1, seem to result mainly from noninteger subshell occupations. WABS post processing improves the results very little for groups 2 and 3 and also generally does not change the trends of the results. Therefore we use the variational results for these groups for the final analysis. Group 4 has large spin contaminations for LS states, but WABS post processing worsens the results; also most functionals working well in this group should be considered to be working by fortuitous cancellation of errors. This leads us to exclude this group from our final assessment, and further leads to a database of 28 states, with 14 ΔEs and 8 IPs.

Another important observation is that the noninteger subshell occupations tend to be closely associated with the energy errors. In groups 1 and 2, only small partial occupations are observed so all the functionals are assessed equally. In groups 3 and 4, most of the best functionals appear to be those with the smallest noninteger subshell occupations. To generalize, it seems that it is necessary to achieve a balanced description of the orbitals before one compares the errors in multiplicity-changing energies, and if a certain functional achieves good accuracy in excitation energy on the basis of significant overstabilization of s or d orbitals, its success should perhaps be considered as resulting from fortuitous cancellation of errors.

Based on this analysis, a final assessment of the overall performance of all the methods is summarized in Table 5.11. The data used to calculate the errors in this table are composed of WABS results for group 1 and variational results for groups 2

and 3. The column called δ is the mean unsigned deviation from the dominant experimental configuration of 5s occupations in 28 spin states. The columns called "MSE", "MUE(14)", and "MUE(22)" contain respectively the MSE of 14 Δ*E*s, the MUE of 14 Δ*E*s, and MUE of 14 Δ*E*s plus 8 IPs.

First we consider the MSE results of Table 5.11. As expected, HF exchange strongly favors HS states with an MSE of -12.0 kcal/mol. Correlation functionals usually favor the LS state, as shown by comparison of the MSE of HF (-12 kcal/mol) with the MSE of HFLYP (1.5 kcal/mol) or HFPW91 (-5.5 kcal/mol) or by comparison of the MSE of B88 (-11.6 kcal/mol) with the MSE of BPW91 (-3.6 kcal/mol) or of BLYP (2.1 kcal/mol). Also an increased favoring of the HS state is observed when the percentage of Hartree–Fock exchange is increased. This can be most clearly seen in the series of BLYP, B1LYP, and BHandHLYP functionals.

Next we compare MUE(14) and MUE(22) for all the density functionals. This comparison shows that these two columns tend to show very similar trends, and therefore we will base our discussion on MUE(22), which is the overall mean unsigned error of all the Δ*E*s and IPs included in the final analysis based on the considerations above. As expected, the two purely exchange functionals, namely HF and B88, both have large energetic errors, in particular, 18.8 and 11.5 kcal/mol. The best functional is SOGGA11-X with an MUE of 3.1 kcal/mol and a δ of merely 0.01. B1LYP also achieves an MUE of 3.1 kcal/mol but with a slightly larger δ of 0.04. All of the 14 best functionals are hybrid functionals.

Nine of the 10 best performing functionals have a δ equal to or smaller than 0.06, with the only exception being PW6B95. Actually the δ of 0.18 for PW6B95 is,

along with OPBE, the largest of all the 59 tested methods. The best three local functionals, according to excitation energy errors, are revTPSS, RPBE, and TPSS, all of which have large δ in the range 0.11–0.15. Actually *most* local functionals produce δ equal to or larger than 0.10, with the three exceptions being VS98 (0.05), M11-L (0.08), and BLYP (0.09). Noninteger subshell occupation numbers are problematic; one could consider them to be an undesirable feature, but an alternative interpretation (which at present cannot be ruled out although there is also no evidence to support it) is that noninteger subshell occupancies are a positive feature and represent inclusion of effects that would be labeled as configuration interaction in wave function theory.

If one uses the interpretation that noninteger subshell occupation numbers are to be avoided and considers them in conjunction with the energetic errors, the best local functional appears to be BLYP, which is especially interesting because some of its hybrid variants, namely, B1LYP, B3V5LYP, B3LYP, CAM-B3LYP, and B3LYP*, are ranked in the top ten best functionals. However if one does not penalize noninteger subshell occupancies the best local functional would be considered to be revTPSS.

Because, as discussed above, Tables 5.7 and 5.8 provide very clearcut tests of the functionals we might ask which functional has a high rating by all three of the following criteria: column MUE (WABS) in Table 5.7, column MUE (Var.) in Table 5.8, and column MUE(22) in Table 5.11. We find six functionals are in the top 20 for all three of these columns: B3LYP*, B3V5LYP, B3LYP, BHandH, MPWKCIS1K, and SOGGA11-X; and MPW3LYP is always in the top 21. Of these, the highest

ranked in the overall MUE(22) column are SOGGA11-X, B3V5LYP, and MPW3LYP.

Another interesting observation is that the simpler GGA and hybrid GGA functionals tend to perform better than meta-GGA and hybrid meta-GGA functionals. At the meta-GGA or hybrid meta-GGA level, there is only one functional with a low MUE in excitation energies and a low δ, namely BMK. Other than BMK, other meta-GGAs and hybrid meta-GGAs with relatively small MUEs, such as PW6B95 and several variants of TPSS, are all observed to have very large δ; ones with small δ, including M05, M06, and M06-2X, all perform unsatisfactorily for excitation energies.

Finally, we compare the conclusions reached here to those in a closely related study, namely a study[9] of p-block excitation energies that allowed an assessment the accuracy of self-consistent calculations on states of different multiplicity without the complications of broken symmetry, multireference character, or d orbitals. Therefore the tests were interpreted as a rather clean test of high-spin bias vs. low-spin bias. Of the functionals included here, the ones that performed best overall in Ref. 9 are O3LYP, TPSS, M06-2X, and CAM-B3LYP. Table 5.9 shows that three of these are also above average for 4d transition metals, but M06-2X becomes poor, which is consistent with our previous experience that caused us to recommend that M06-2X not be used for transition metals.

5.7. Conclusions

We summarize this paper with the following remarks:

(i) For subshell occupation numbers, Section 5.1 shows that local functionals tend to overstabilize 4d orbitals over 5s orbitals, and HF exchange tends to alleviate this bias. For excitation energy differences, Table 5.10 shows that correlation functionals in DFT usually favors the LS state, while HF exchange favors the HS state. Therefore, to achieve a well-balanced description of both occupations and excitation energies in 4d transition metals, an appropriate percentage of HF exchange is necessary.

(ii) GGAs and their hybrid variants perform better than functionals built at the meta-GGA and hybrid meta-GGA levels, which seems to leave room for further improvements of present meta-GGAs and hybrid meta-GGAs.

(iii) The ranking of functions in the final overall assessment is not well correlated with the percentage of HF exchange.

(iv) SOGGA11-X and B1LYP offer good accuracy both in subshell occupations and excitation energies and have the lowest mean unsigned error in the final overall evaluation, B3V5LYP and MPW3LYP perform almost as well as B1LYP, and B3LYP, CAM-B3LYP, BMK, and PW6B95 rank in the next four positions. Thus these eight functionals are recommended for accurate calculations of spin states and ionization potentials of 4d elements.

Appendix

The derivation of eq 3 begins with the assumption that the orbitals in the HS and LS states are similar so that the BS state is a linear combination of determinants with the same orbitals (but different spin-coupling) as the HS state. In such a case we can use the phenomenological Heisenberg Hamiltonian,

$$\hat{H} = J\hat{S}^2 \tag{5.A1}$$

in which J is a phenomenological constant and $\hat{S}$ is the total electron spin, and for which the expectation value of the energy is

$$E = J\left\langle \hat{S}^2 \right\rangle \tag{5.A2}$$

and the energy eigenvalues are

$$E = J\,S(S+1) \tag{5.A3}$$

where S is total spin quantum number. In the present article we always have S_{LS} equal to $S_{\mathrm{HS}} - 1$. Therefore

$$E_{\mathrm{HS}} = J\,S_{\mathrm{HS}}(S_{\mathrm{HS}}+1) \tag{5.A4}$$

$$E_{\mathrm{LS}} = J\,S_{\mathrm{HS}}(S_{\mathrm{HS}}-1) \tag{5.A5}$$

and

$$\Delta E = E_{\mathrm{HS}} - E_{\mathrm{LS}} = 2J\,E_{\mathrm{HS}} \tag{5.A6}$$

But eq A2 yields

$$J = \frac{E_{\mathrm{HS}} - E_{\mathrm{LS}}}{\left\langle \hat{S}^2 \right\rangle_{\mathrm{HS}} - \left\langle \hat{S}^2_{\mathrm{LS}} \right\rangle} \tag{5.A7}$$

Combining eqs. A6 and A7 and relabeling the LS state as BS yields eq 3.

References for Chapter 5

(1) Kohn, W.; Sham, L. *Phys. Rev.* **1964**, *140*, A1133.

(2) Barth, U.; Hedin, L. A. *J. Phys. C* **1972**, *5*, 1629.

(3) Seidl, A.; Görling, A.; Vogl, P.; Majewski, J. A.; Levy, M. *Phys. Rev. B* **1996**, *53*, 3764.

(4) Cramer, C. J.; Truhlar, D. G. *Phys. Chem. Chem. Phys.* **2009**, *11*, 10757.

(5) Moore, C. E. *Atomic Energy Levels*; National Bureau of Standards: Washington, DC, 1949–1958, *Vols. 1–3*.

(6) (a) Noodleman, L.; *J. Chem. Phys.* **1981**, *74*, 5737. (b) Bachler, V.; Olbrich, G.; Neese, F.; Wieghardt, K. *Inorg. Chem.* **2002**, *41*, 4179..

(7) Neese, F. *Coord. Chem. Rev.* **2009**, *253*, 526.

(8) (a) Yamaguchi, K.; Takahara, Y.; Fueno, T. In Smith Jr., V.H. ; Schaefer III., H.F. ; Morokuma, K. (Eds.), *Applied Quantum Chemistry*; D. Reidel: Boston, 1986, p155. (b) Caballol, R.; Castell, O.; Illas, F.; de P. R. Moreira, I.; Malrieu, J. P. *J. Phys. Chem.* **1997**, *101*, 7860. (c) Shoji , M.; Koizumi, K.; Kitagawa, Y.; Kawakami, T.; Yamanaka, S.; Okumura, M.; Yamaguchi, K. *Chem. Phys. Lett.* **2006**, *432*, 343.

(9) Yang, K.; Peverati, R.; Truhlar, D. G.; Valero, R. *J. Chem. Phys.* **2011**, *135*, 044118.

(10) Yanagisawa, S.; Tsuneda, T.; Hirao, K. *J. Chem. Phys.* **2000**, *112*, 545.

(11) Gáspár, R. *Acta Phys. Hung.* **1974**, *35*, 213.

(12) Vosko, S. H.; Wilk, L.; Nusair, M. *Can. J. Phys.* **1980**, *58*, 1200.

(13) Becke, A. D. *Phys. Rev. A* **1988**, *38*, 3098.

(14) Lee, C.; Yang, W.; Parr, R. G. *Phys. Rev. B* **1988**, *37*, 785.

(15) Perdew, J. P. *Phys. Rev. B* **1986**, *33*, 8822.

(16) Perdew, J. P. In *Electronic Structure of Solids '91*, edited by Ziesche P.; Eschrig, H. Akademie Verlag: Berlin, 1991, pp 11–20.

(17) Hamprecht, F. A.; Cohen, A.; Tozer, D. J.; Handy, N. C. *J. Chem. Phys.* **1998**, *109*, 6264-71.

(18) Boese, A. D.; Handy, N.C. *J. Chem. Phys.* **2001**, *114*, 5497.

(19) Adamo, C.; Barone, V. *J. Chem. Phys.* **1998**, *108*, 664.

(20) Handy, N. C.; Cohen, A.J. *Mol. Phys.* **2001**, *99*, 403.

(21) Perdew, J. P.; Burke, K.; Ernzerhof, M. *Phys. Rev. Lett.* **1996**, *77*, 3865.

(22) Hammer, B.; Hansen, L. B.; Norskov, J. K. *Phys. Rev. B* **1999**, *59*, 7413.

(23) Zhao, Y.; Truhlar, D. G. *J. Chem. Phys.* **2008**, *128*, 184109.

(24) Peverati, R.; Zhao, Y.; Truhlar, D. G. *J. Phys. Chem. Lett.* **2011**, *2*, 1911.

(25) Peverati, R.; Truhlar, D. G. *J. Chem. Theory. Comput.*, **2012**, *8*, 2310.

(26) Adamo, C.; Barone, V. *Chem. Phys. Lett.* **1997**, *274*, 242.

(27) Stephens, P. J.; Devlin,; Chabalowski, C. F.; Frisch, M. J. *J. Phys. Chem.* **1994**, *98*, 11623.

(28) Reiher, M.; Salomon, O.; Hess, B. A. *Theor. Chem. Acc.* **2001**, *107*, 48.

(29) Becke, A.D. *J. Chem. Phys.* **1993**, *98*, 5648.

(30) Hertwig, R. H.; Koch, W. *Chem. Phys. Lett.* **1997**, *268*, 345.

(31) Keal, T.W.; Tozer, D.J. *J. Chem. Phys.* **2005**, *123*, 121103.

(32) Schmider, H. L.; Becke, A. D. *J. Chem. Phys.* **1998**, *108*, 9624.

(33) Becke, A.D. *J. Chem. Phys.*, **1993**, *98*, 1372-77.

(34) Schultz, N. E.; Zhao, Y.; Truhlar, D. G. *J. Phys. Chem. A* **2005**, *109*, 11127.

(35) Lynch, B. J.; Fast, P. L.; Harris, M.; Truhlar, D. G. *J. Phys. Chem. A* **2000**, *104*, 4811.

(36) Zhao, Y.; Truhlar, D. G. *J. Phys. Chem. A* **2004**, *108*, 6908.

(37) Zhao, Y.; Lynch, B. J.; Truhlar, D. G. *J. Phys. Chem. A* **2004**, *108*, 4786.

(38) Hoe, M. W.; Cohen, A. J.; Handy, N. C. *Chem. Phys. Lett.* **2001**, *341*, 319.

(39) Adamo C.; Barone, V. *J. Chem. Phys.* **1999**, *110*, 6158.

(40) Peverati, R.; Truhlar, D. G. *J. Chem. Phys.* **2011**, *135*, 191102.

(41) Yanai, T.; Tew, D.P.; Handy, N.C. *Chem. Phys. Lett.* **2004**, *393*, 51.

(42) Heyd, J.; G. E. Scuseria, G. E.; Ernzerhof, M. *J. Chem. Phys.* **2003**, *118*, 8207.

(43) Henderson, T. M.; Izmaylov, A. F.; Scalmani, S.; Scuseria, G. E. *J. Chem. Phys.* **2009**, *131*, 044108.

(44) Iikura, H.; Tsuneda, T.; Yanai, T.; Hirao, K. *J. Chem. Phys.* **2001**, *115*, 3540.

(45) Vydrov, O. V.; Scuseria, G. E. *J. Chem. Phys.* **2006**, *125*, 234109.

(46) Chai, J.; Head-Gordon, M. *J. Chem. Phys.* **2008**, *128*, 084106.

(47) Chai, J.; Head-Gordon, M. *Phys. Chem. Chem. Phys.* **2008**, *10*, 6615.

(48) Zhao, Y.; Truhlar, D. G. *J. Chem. Phys.* **2006**, *125*, 194101.

(49) Peverati, R.; Truhlar, D. G. *J. Phys. Chem. Lett.*, **2012**, *3*, 117.

(50) Perdew, J. P.; Ruzsinszky, A.; Csonka, G. I.; Constantin, L. A.; Sun, J. *Phys. Rev. Lett.* **2009**, *103*, 026403.

(51) Tao, J.; Perdew, J. P.; Staroverov, V. N.; Scuseria, G. E. *Phys. Rev. Lett.* **2003**, *91*, 146401.

(52) Van Voorhis, T.; Scuseria, G. E. *J. Chem. Phys.* **1998**, *109*, 400.

(53) Peverati, R.; Truhlar, D. G. *Phys. Chem. Chem. Phys.*, online at dx.doi.org/10.1039/c2cp42025b.

(54) Boese, A. D.; Martin, J. M. L. *J. Chem. Phys.* **2004**, *121*, 3405.

(55) Zhao, Y.; Schultz, N. E.; Truhlar, D. G. *J. Chem. Phys.* **2005**, *123*, 161103.

(56) Zhao, Y.; Schultz, N. E.; Truhlar, D. G. *J. Chem. Theory Comput.* **2006**, *2*, 364.

(57) Zhao, Y.; Truhlar, D. G. *Theor. Chem. Acc.* **2008**, *120*, 215.

(58) Zhao, Y.; Truhlar, D. G. *J. Phys. Chem. A* **2006**, *110*, 13126.

(59) Zhao, Y.; Truhlar, D. G. *J. Chem. Theory Comput.***2008**, *4*, 1849.

(60). Krieger, J. B.; Chen, J.; Iafrate, G. J.; Savin, A. in *Electron Correlations and Materials Properties*, edited by A. Gonis, and N. Kioussis, Plenum: New York, 1999, pp 463.

(61) Zhao, Y.; González-García, N.; Truhlar, D. G. *J. Phys. Chem. A* **2005**, *109*, 2012.

(62) Zhao Y.; Truhlar, D. G. *J. Phys. Chem. A* **2005**, *109*, 5656.

(63) Zhao, Y.; Lynch, B. J.; Truhlar, D. G. *Phys. Chem. Chem. Phys.* **2005**, *7*, 43.

(64) Staroverov, V. N.; Scuseria, G. E.; Tao, J.; Perdew, J. P. *J. Chem. Phys.***2003**, *119*, 12129.

(65) Boese, A. D.; Handy, N. C. *J. Chem. Phys.* **2002**, *116*, 9559.

(66) Peverati, R.; Truhlar, D. G. *J. Phys. Chem. Lett.* **2011**, *2*, 2810.

(67) Frisch, M. J.; Trucks, G. W.; Schlegel, H. B. et al., *GAUSSIAN09*, Revision C.1, Gaussian, Inc., Wallingford, CT, 2009.

(68) Foster, J. P.; Weinhold, F. *J. Am. Chem. Soc.***1980**, *102*, 7211.

(69) Reed, A. E.; Weinhold, F. *J. Chem. Phys.*, **1983**, *78*, 4066.

(70) Reed, A. E.; Weinstock, R. B.; Weinhold, F. *J. Chem. Phys.***1985**, *83*, 735.

(71) Reed, A. E.; Weinhold, F. *J. Chem. Phys.***1985**, *83*, 1736.

(72) Carpenter, J. E. Ph. D. thesis, University of Wisconsin, Madison, WI, 1987.

(73) Carpenter, J. E.; Weinhold, F. *J. Mol. Struct. (Theochem)* **1988**, *46*, 41.

(74) Reed, A. E.; Curtiss, L. A.; Weinhold, F. *Chem. Rev.***1988**, *88*, 899.

(75) Weinhold, F; Carpenter, J. E. In *The Structure of Small Molecules and Ions*, Ed. R. Naaman and Z. Vager, Plenum: New York, 1988, pp 227-36.

(76) Douglas M.; Kroll, N. M. *Ann. Phys.* **1974**, *82*, 89.

(77) Hess, B. A. *Phys. Rev. A* **1986**, *33*, 3742.

(78) Jansen, G.; Hess, B. A. *Phys. Rev. A* **1989**, *39*, 6016.

(79) Peterson, K.A.; Figgen, D.; Dolg, M.; Stoll, H. *J. Chem. Phys.***2007**, *126*, 124101.

(80) Tsuchiya, T., Abe, M.; Nakajima, T.; Hirao, K. *J. Chem. Phys.* **2001**, *115*, 4463.

(81) Huzinaga, S.; Klobukowski, M. *Chem. Phys. Lett.* **1993**, *212*, 260.

(82) Roos, O.; Lindh R.; Malmqvist, P.A.; Veryazov, V.; Widmark, P. O. *J. Phys. Chem. A* **2005**, *109*, 6575.

(83) Gunnarsson, O.; Jones, R. O. *Phys. Rev. B.* **1985**, *31*, 7588.

Table 5.1. Reference data (after removal of spin-orbit coupling) from experiments for all excitation energies and ionization potentials in kcal/mol

	Y	Zr	Nb	Mo	Tc	Ru	Rh	Pd
$\Delta E(M)^a$	31.27	13.93	-3.27	-30.79	-30.07	-18.71	-9.46	18.77
$\Delta E(M^+)^b$	2.40	-12.15	-15.90	-43.46	-9.90	26.16	-23.34	71.71
IP[c]	150.53	160.33	156.11	163.71	167.83	169.86	172.11	192.24

[a] the excitation energy of neutral atom, with the sign being positive if the lower energy state has a lower spin
[b] the excitation energy of the singly positive cation, with the same sign convention
[c] the ionization potential

Table 5.2. All the density functionals tested in this paper (Hartree–Fock is tested but not listed here)

Type	Name	References
LSDA	GKSVWN3[a]	11, 1, 12
GGA	B88[b]	13
	BLYP	13, 14
	BP86	13, 15
	BPW91	13, 16
	HCTH/407	17, 18
	mPWLYP	14, 19
	OLYP	14, 20
	OPBE	20, 21
	PBE[c]	21
	PW91	16
	RPBE	22
	SOGGA	23
	SOGGA11	24
NGA	N12	25
Global-hybrid GGA	B1LYP	26
	B3LYP	27
	B3LYP*	28
	B3PW91	29
	B3V5LYP	30
	B97-3	31
	B98	32
	BHandH	33
	BHandHLYP	33
	HFLYP[d]	14
	HFPW91[d]	16
	MOHLYP	34
	MPW1K	35
	MPW3LYP	36
	MPWB1K	37
	MPWLYP1M	34
	O3LYP	38

	PBE0[e]	39
	SOGGA11-X	40
Range-separated hybrid GGA	CAM-B3LYP	41
	HSE	42, 43
	LC-mPWLYP[f]	44
	LC-ωPBE	45
	ωB97X	46
Range-separated hybrid GGA-D	ωB97X -D	47
Meta-GGA	M06-L	48
	M11-L	49
	revTPSS	50
	TPSS	51
	VS98[g]	52
Meta-NGA	MN12-L	53
Global-hybrid meta-GGA	BMK	54
	M05	55
	M05-2X	56
	M06	57
	M06-2X	57
	M06-HF	58
	M08-HX	59
	M08-SO	59
	MPWKCIS1K	19, 60, 61
	PW6B95	62
	TPSS1KCIS	50, 60, 64
	TPSSh	64
	τHCTHhyb	65
Range-separated hybrid meta-GGA	M11	66

[a] Gáspár-Kohn-Sham for exchange and VWN3 for correlation (keyword SVWN in Gaussian)

[b] Exchange functional with no correlation functional.

[c] Also called PBEPBE

[d] Hartree–Fock exchange with correlation functional.

[e] Also known as PBE1, PBE1PBE, or PBEh.

[f] Obtained by applying Hirao's long-range correction[43] to the indicated GGA.

[g] Also known as VSXC.

Table 5.3. Comparison of excitation energies (in kcal/mol) calculated with cc-pVTZ-DK and cc-pwcVTZ-DK basis sets

							cc-pVTZ-DK								
Functional	Y	Y^+	Zr	Zr^+	Nb	Nb^+	Mo	Mo^+	Tc	Tc^+	Ru	Ru^+	Rh	Rh^+	Pd	Pd^+
B3LYP	23.8	1.5	7.7	-7.4	-7.7	-14.2	-23.1	-28.3	-18.6	-5.5	-13.1	27.1	-5.5	-11.8	19.9	70.8
B88	13.1	-0.5	-4.8	-9.7	-18.9	-20.2	-36.1	-38.0	-32.9	-26.8	-22.9	5.2	-9.2	-13.3	11.1	55.7
HF	17.5	-4.5	0.3	-17.0	-16.7	-23.5	-33.3	-44.4	-23.3	-32	-17.0	8.4	-10.6	-18.9	-1.6	54.2
HSE	18.3	-2.0	-0.6	-10.6	-17.3	-19.5	-33.8	-35.1	-23.7	-12.4	-17.3	22.7	-7.9	-13.2	18.7	70.4
LC-ωPBE	19.0	-3.1	-1.0	-10.0	-18.2	-20.0	-29.5	-33.9	-21.4	-5.7	-16.3	28.9	-3.6	-11.8	23.5	77.6
M06	38.8	10.1	21.7	-6.9	5.5	-16.0	-8.0	-31.0	-15.4	1.0	-3.1	34.8	-0.6	-12.1	25.5	81.2
M06-L	28.6	6.1	13.7	-7.5	2.6	-12.9	-16.4	-28.8	-23.6	0.1	-11.4	37.6	-4.7	-16.9	21.1	76.1
ωB97X-D	29.3	0.4	13.4	-9.3	-3.1	-17.7	-15.5	-30.9	-17.0	-0.6	-7.1	35.3	-1.0	-11.1	26.1	80.6
PBE	17.9	-0.4	-0.6	-8.6	-14.5	-18.3	-30.0	-33.4	-24.1	-10.7	-15.9	23.0	-2.3	-11.7	21.9	71.4
SVWN	20.7	0.2	0.7	-9.7	-16.0	-20.5	-31.3	-35.1	-23.2	-9.7	-13.9	24.5	1.6	-9.8	26.9	77.1
								cc-pwcVTZ-DK								
B3LYP	23.8	1.5	7.6	-7.4	-7.7	-14.2	-23.1	-28.3	-18.6	-5.5	-13.1	27.1	-5.5	-11.8	19.9	70.8
B88	13.1	-0.5	-4.8	-9.7	-18.8	-20.2	-36.1	-38.0	-32.9	-26.8	-22.9	5.2	-9.2	-13.3	11.1	55.7
HF	17.4	-4.5	0.3	-17.1	-16.7	-23.5	-33.3	-44.2	-23.3	-32	-17.0	8.4	-10.6	-19.0	-1.6	54.2
HSE	18.2	-2.0	-0.6	-10.6	-17.3	-19.5	-33.8	-35.1	-23.8	-12.4	-17.3	22.6	-7.9	-13.2	18.7	70.4
LC-PBE	19.1	-3.1	-1.0	-10.1	-18.4	-20.1	-29.3	-33.9	-21.4	-5.7	-16.3	28.9	-3.6	-11.8	23.5	77.6
M06	38.8	10.0	21.6	-6.9	5.5	-16.0	-8.0	-31.0	-15.4	1.0	-3.1	34.8	-0.6	-12.1	25.5	81.0
M06L	28.6	6.1	13.9	-7.5	2.6	-12.9	-16.4	-28.8	-23.6	0.1	-11.4	37.5	-4.7	-16.9	21.1	76.1
ωB97X-D	29.5	0.4	13.4	-9.3	-3.1	-17.7	-15.5	-30.9	-17.0	-0.6	-7.1	35.3	-1.0	-11.1	26.1	80.6
PBE	17.9	-0.4	-0.6	-8.6	-14.5	-18.3	-30.1	-33.3	-24.0	-10.7	-15.9	23.0	-2.3	-11.7	21.9	71.4
SVWN	20.6	0.2	0.7	-9.7	-16.1	-20.5	-31.3	-35.1	-23.2	-9.7	-13.9	24.5	1.6	-9.8	27.0	77.3

Table 5.4. Mean noninteger occupancy of the 5s subshell occupations for each method[a]

Functional	ε	Functional	ε	Functional	ε
N12	-0.17	MOHLYP	-0.05	M08-SO	-0.01
MN12-L	-0.16	PBE	-0.05	M06-HF	0.00
OPBE	-0.14	PW91	-0.05	B3V5LYP	0.00
PW6B95	-0.13	MPW1K	-0.05	B3LYP*	0.00
SOGGA11	-0.11	M11	-0.05	B3LYP	0.00
MPWB1K	-0.10	M05	-0.04	LC-mPWLYP	0.00
M11-L	-0.10	M06	-0.04	MPW3LYP	0.00
OLYP	-0.09	HFLYP	-0.04	SOGGA11-X	0.00
O3LYP	-0.08	BP86	-0.04	BHandHLYP	0.00
TPSS	-0.08	M06-L	-0.03	MPWLYP1M	0.01
revTPSS	-0.08	τHCTHhyb	-0.03	B88	0.01
LC-ωPBE	-0.07	HSE	-0.03	CAM-B3LYP	0.01
TPSSh	-0.07	GKSVWN3	-0.03	BLYP	0.01
BPW91	-0.07	M08-HX	-0.03	BHandH	0.01
HCTH/407	-0.07	B98	-0.02	B1LYP	0.01
TPSS1KCIS	-0.06	VS98	-0.02	M06-2X	0.02
B3PW91	-0.06	ωB97X	-0.02	BMK	0.02
RPBE	-0.06	MPWKCIS1K	-0.02	mPWLYP	0.02
HFPW91	-0.06	ωB97XD	-0.01	M05-2X	0.03
SOGGA	-0.06	B97-3	-0.01		
PBE0	-0.05	HF	-0.01		

Table 5.5. Mean unsigned deviation (δ) of 5s subshell occupations from that of the dominant experimental configuration

Functional	δ	Functional	δ	Functional	δ
BMK	0.02	B3LYP*	0.07	M11-L	0.12
ωB97X-D	0.03	B3LYP	0.07	MOHLYP	0.13
LC-mPWLYP	0.03	M08-HX	0.07	TPSSh	0.13
SOGGA11-X	0.03	M11	0.07	RPBE	0.13
BHandH	0.03	VS98	0.08	SOGGA	0.13
BHandHLYP	0.03	HSE	0.08	MPWB1K	0.13
ωB97X	0.04	HFPW91	0.08	HCTH/407	0.13
CAM-B3LYP	0.04	M06-HF	0.09	BPW91	0.14
M08-SO	0.04	MPWLYP1M	0.09	OLYP	0.14
M05-2X	0.05	mPWLYP	0.09	SOGGA11	0.14
B97-3	0.05	BLYP	0.09	M06-L	0.15
B98	0.05	MPW1K	0.09	revTPSS	0.15
HFLYP	0.05	PBE0	0.1	HF	0.16
MPWKCIS1K	0.05	B3PW91	0.11	TPSS	0.16
B1LYP	0.05	LC-ωPBE	0.11	B88	0.17
M05	0.06	GKSVWN3	0.11	PW6B95	0.17
M06	0.06	TPSS1KCIS	0.12	OPBE	0.19
τHCTHhyb	0.06	PBE	0.12	N12	0.20
B3V5LYP	0.06	PW91	0.12	MN12-L	0.24
MPW3LYP	0.06	O3LYP	0.12		
M06-2X	0.07	BP86	0.12		

Table 5.6. Multiplicity, 5s subshell occupancies, and ε for each level[a]

	Y		Y^+		Zr		Zr^+	
Multiplicity	2	4	1	3	3	5	2	4
Exp. n_{5s}	2	1	2	1	2	1	1	1
ε	-0.08	-0.02	-0.54	-0.05	-0.12	-0.03	-0.14	-0.21
	Nb		Nb^+		Mo		Mo^+	
Multiplicity	4	6	3	5	5	7	4	6
Exp. n_{5s}	2	1	0	0	1	1	0	0
ε	-0.29	-0.02	0.26	0.10	0.05	-0.03	0.04	0.00
	Tc		Tc^+		Ru		Ru^+	
Multiplicity	4	6	5	7	3	5	4	6
Exp. n_{5s}	1	2	0	1	1	1	0	1
ε	0.01	-0.46	0.07	-0.03	-0.07	0.02	0.00	0.00
	Rh		Rh^+		Pd		Pd^+	
Multiplicity	2	4	1	3	1	3	2	4
Exp. n_{5s}	0	1	0	0	0	1	0	1
ε	0.30	0.00	0.00	0.00	0.00	0.00	0.00	0.00

[a] n_{5s} is the occupancy of the 5s subshell, and ε is the mean signed deviation, averaged over the 59 calculations of that occupancy, from the integer value that characterizes the configuration that is experimentally found to be dominant

Table 5.7. MSE and MUE of Δ*E* for group 1 by the variational and WABS methods

	Var.		WABS			Var.		WABS	
Functional	MSE	MUE	MSE	MUE	Functional	MSE	MUE	MSE	MUE
O3LYP	8.1	8.1	0.4	1.9	revTPSS	6.0	6.2	-2.4	4.8
MOHLYP	9.2	9.2	2.1	2.1	B3PW91	4.0	6.0	-4.6	4.9
BP86	8.2	8.2	0.8	2.1	MPWLYP1M	11.4	11.4	4.9	4.9
MPWB1K	8.3	8.3	0.7	2.2	TPSS1KCIS	5.7	6.5	-2.6	5.1
PW6B95	9.3	9.3	2.2	2.2	MPW1K	3.8	5.0	-5.2	5.2
LC-ωPBE	6.2	6.2	-1.7	2.3	OPBE	3.6	5.3	-5.2	5.2
RPBE	7.1	7.1	-0.7	2.3	HFPW91	4.2	4.2	-5.3	5.3
OLYP	8.8	8.8	1.4	2.3	mPWLYP	11.7	11.7	5.3	5.3
PBE	6.3	6.3	-1.6	2.4	BHandHLYP	10.8	10.8	3.6	5.5
PW91	6.6	6.6	-1.2	2.4	BMK	11.8	11.8	5.8	5.8
BPW91	6.1	6.1	-1.9	2.8	B97-3	12.3	12.3	6.1	6.1
GKSVWN3	6.6	6.8	-0.8	2.8	B98	12.7	12.7	6.5	6.5
B3LYP*	9.9	9.9	2.9	2.9	M08-HX	11.2	11.2	4.9	6.6
M08-SO	9.0	9.0	2.3	3.0	ωB97X-D	12.9	12.9	6.9	6.9
B3V5LYP	10	10	3.0	3.2	HCTH/407	11.6	11.6	4.8	6.9
B3LYP	10	10	3.0	3.2	VS98	9.1	9.1	1.6	7.2
BHandH	9.2	9.2	1.9	3.3	LC-mPWLYP	13.2	13.2	7.4	7.4
MPWKCIS1K	6.6	6.6	-1.6	3.5	B88	1.5	6.3	-7.9	7.9
SOGGA	4.6	5.8	-3.7	3.7	M06-L	10.7	10.7	2.9	8.2
SOGGA11-X	9.8	9.8	2.8	3.8	HFLYP	11.1	11.1	3.5	8.3
MPW3LYP	10.6	10.6	3.8	3.9	τHCTHhyb	14.2	14.2	8.4	8.4
TPSS	6.8	6.8	-1.2	4.0	HF	0.7	2.4	-10	10.0
SOGGA11	10.5	10.5	4.2	4.2	MN12-L	13.8	13.8	7.2	10.1
M11	5.2	5.2	-2.7	4.2	M06	15.5	15.5	9.9	10.3
B1LYP	10.6	10.6	3.7	4.3	M11-L	11.7	11.7	3.7	11.7
PBE0	4.2	5.6	-4.4	4.4	M05-2X	17.0	17.0	12.3	12.3
HSE	4.2	5.7	-4.4	4.4	ωB97X	17.6	17.6	12.7	12.7
N12	9.2	9.2	2.6	4.4	M05	18.8	18.8	14.1	14.1
CAM-B3LYP	11.2	11.2	4.6	4.6	M06-2X	18.5	18.5	14.1	14.1
BLYP	11.2	11.2	4.6	4.6	M06-HF	18.8	18.8	14.1	14.1
TPSSh	5.8	5.9	-2.6	4.8					

Table 5.8. MSE and MUE of Δ*E* for the variational method and MUE of Δ*E* for the WABS method for group 2

	Var.		WABS		Var.		WABS
Functional	MSE	MUE	MUE	Functional	MSE	MUE	MUE
BHandH	-1.6	1.6	1.7	LC-mPWLYP	4.0	4.8	6.0
BMK	1.6	2.4	3.5	VS98	1.9	4.9	3.5
MPWKCIS1K	-2.1	2.6	1.0	M06-HF	5.0	5.0	8.6
MPW3LYP	-0.2	2.7	2.0	MOHLYP	1.3	5.1	3.3
B3V5LYP	-0.6	2.8	1.6	GKSVWN3	0.3	5.2	3.7
B1LYP	-0.7	2.8	1.9	M08-SO	3.0	5.6	7.8
B3LYP*	-0.4	3.0	1.6	SOGGA	-3.7	5.7	4.4
B3LYP	-0.4	3.0	1.7	LC-ωPBE	1.1	6.0	4.5
CAM-B3LYP	1.2	3.1	3.1	M06-L	5.1	6.2	7.1
BHandHLYP	-1.0	3.1	2.8	B97-3	5.4	6.5	7.5
SOGGA11-X	2.9	3.2	5.0	B98	5.6	6.7	7.6
TPSS1KCIS	-1.4	3.3	1.5	O3LYP	2.6	7.1	5.3
MPWLYP1M	0.0	3.3	2.5	ωB97X-D	6.5	7.3	8.5
mPWLYP	0.1	3.5	2.6	M08-HX	7.6	7.8	9.7
BLYP	-0.3	3.6	2.1	OPBE	0.5	8.0	6.3
MPWB1K	0.1	3.6	2.0	OLYP	3.4	8.1	6.1
PBE0	-3.4	3.7	2.3	SOGGA11	2.9	8.1	6.4
PW6B95	0.9	3.7	2.6	τHCTHhyb	8.3	8.3	10.5
B3PW91	-3.2	3.8	2.5	HCTH/407	8.4	8.4	11.6
MPW1K	-3.8	3.8	2.4	MN12-L	4.7	8.6	11.1
BP86	-2.1	3.8	2.0	M06	8.7	8.7	11.3
TPSSh	-2.1	3.9	2.2	M06-2X	9.0	9.0	11.7
RPBE	-2.1	3.9	2.0	M11	5.3	9.5	8.1
HFLYP	-1.2	3.9	4.8	N12	4.1	10.2	9.7
HSE	-4.1	4.1	2.6	ωB97X	11.3	11.3	13.9
PBE	-2.9	4.2	2.7	M05-2X	11.4	11.4	14.1
PW91	-2.9	4.2	2.7	M11-L	11.4	13.0	13.6
revTPSS	-2.3	4.2	2.5	M05	14.7	14.7	17.1
HFPW91	-3.6	4.3	2.9	B88	-15.9	15.9	15.0
TPSS	-2.0	4.3	2.5	HF	-18.3	18.3	17.1
BPW91	-3.7	4.8	3.5				

Table 5.9. MSE and MUE of Δ*E* for the variational method, MUE of Δ*E* for the WABS method, and δ of the 5s subshell occupation for group 3

	Var.		WABS	Var.		Var.		WABS	Var.
Functional	MSE	MUE	MUE	δ^a	Functional	MSE	MUE	MUE	δ^a
SOGGA11-X	2.2	2.2	1.6	0.03	MPWKCIS1K	-3.8	7.3	7.0	0.15
BMK	3.0	3.0	1.8	0.06	O3LYP	0.0	7.4	6.9	0.41
BHandH	-0.6	3.1	2.1	0.05	TPSS1KCIS	-2.6	7.4	6.4	0.47
BHandHLYP	0.2	3.3	2.5	0.06	BP86	-1.6	7.5	6.6	0.41
HCTH/407	4.2	4.2	5.2	0.21	HFLYP	1.6	7.6	7.3	0.22
M06-L	4.1	4.2	3.8	0.43	RPBE	-2.0	7.7	6.8	0.44
B98	3.8	4.3	3.6	0.11	OLYP	1.0	7.8	7.7	0.45
LC-mPWLYP	3.4	4.3	3.3	0.05	B88	-8.0	8.1	11.2	0.45
M08-SO	2.3	4.4	5.7	0.08	PBE0	-4.7	8.2	7.5	0.38
B1LYP	1.2	4.4	3.1	0.09	HSE	-5.0	8.2	7.3	0.31
B97-3	3.9	4.5	3.9	0.14	PW91	-2.9	8.2	7.5	0.42
CAM-B3LYP	1.9	4.6	3.4	0.08	B3PW91	-4.8	8.3	8.0	0.42
MPW3LYP	1.4	4.6	3.6	0.13	PBE	-3.1	8.3	7.6	0.42
ωB97X-D	3.8	4.8	4.0	0.10	HF	-5.7	8.4	8.8	0.40
B3V5LYP	0.8	5.2	4.0	0.18	M05-2X	8.8	8.8	9.4	0.10
MPWB1K	-1.2	5.3	4.2	0.07	MPW1K	-6.2	8.9	8.9	0.35
MPWLYP1M	2.4	5.4	4.8	0.21	M11	0.4	8.9	7.5	0.23
B3LYP	0.8	5.4	4.1	0.19	BPW91	-3.9	9.1	8.7	0.48
MN12-L	5.2	5.2	4.2	0.17	M06-2X	9.2	9.2	9.6	0.18
B3LYP*	0.8	5.7	4.6	0.21	GKSVWN3	-2.0	9.2	8.6	0.29
mPWLYP	2.5	5.7	5.2	0.20	SOGGA	-4.5	9.3	9.7	0.44
PW6B95	0.2	5.7	4.7	0.09	ωB97X	9.4	9.4	8.7	0.03
τHCTHhyb	5.8	5.8	5.1	0.11	M06	9.6	9.6	8.8	0.14
BLYP	1.7	6.0	5.4	0.24	LC-ωPBE	-4.2	10.0	9.7	0.39
VS98	0.2	6.7	5.9	0.15	OPBE	-3.9	10.2	10.4	0.56
M08-HX	3.2	6.7	6.4	0.18	M05	10.7	10.7	10.1	0.10
MOHLYP	1.5	6.8	6.6	0.40	HFPW91	-6.7	10.7	11.0	0.27
revTPSS	-3.0	6.9	5.9	0.44	SOGGA11	-0.4	10.7	10.6	0.47
TPSSh	-3.4	7.0	6.1	0.44	N12	-3.9	12.7	12.4	0.35
M11-L	4.2	7.1	6.4	0.41	M06-HF	11.9	11.9	14.0	0.27
TPSS	-2.6	7.3	6.3	0.45					

[a] δ denotes the mean unsigned deviation of the 10 occupancies in group 3 of the 5s subshell from the integer values corresponding to the dominant configuration of the experimental state.

Table 5.10. MSE and MUE of Δ*E* for the variational method, MUE of Δ*E* for the WABS method, and δ of the 5s subshell occupation for group 4

	Var.		WABS	Var.		Var.		WABS	Var.
	MSE	MUE	MUE	δ^a		MSE	MUE	MUE	δ^a
HFLYP	-0.3	0.7	5.9	0.03	LC-ωPBE	-1.0	3.1	6.7	0.22
BMK	-0.7	0.9	6.4	0.08	B3V5LYP	3.2	3.2	2.0	0.11
PW6B95	0.6	1.7	4.6	0.07	B3LYP*	3.2	3.2	2.3	0.12
TPSSh	1.6	1.9	3.2	0.19	B3LYP	3.2	3.2	2.0	0.11
LC-mPWLYP	1.9	1.9	2.9	0.06	MPW3LYP	3.2	3.2	2.0	0.11
revTPSS	1.9	1.9	2.7	0.21	OLYP	3.3	3.3	4.4	0.25
BHandH	-0.9	2.0	6.7	0.06	O3LYP	2.5	3.3	4.4	0.23
BHandHLYP	2.0	2.0	2.7	0.06	B88	-0.9	3.4	6.4	0.34
B98	1.8	2.2	2.9	0.20	GKSVWN3	-1.1	3.5	6.9	0.14
ωB97X	0.9	2.2	3.9	0.21	B1LYP	3.5	3.5	1.6	0.10
TPSS	2.2	2.2	2.3	0.23	SOGGA	-1.2	3.7	7.0	0.20
ωB97X-D	0.5	2.3	4.6	0.12	M06L	3.8	3.8	0.8	0.42
TPSS1KCIS	2.3	2.3	2.5	0.14	M052X	3.2	4.0	5.7	0.26
CAM-B3LYP	2.3	2.3	2.3	0.08	MPWKCIS1K	0.0	4.0	5.3	0.03
M05	0.0	2.6	5.0	0.36	M08-SO	0.9	4.3	5.8	0.22
HSE	-1.0	2.6	6.8	0.08	VS98	-1.5	4.4	7.2	0.27
M06	2.6	2.7	3.4	0.35	OPBE	-1.7	4.5	7.7	0.30
MPWB1K	-1.7	2.7	7.7	0.07	HCHT/407	3.3	4.5	6.4	0.31
SOGGA11-X	-2.6	2.7	8.8	0.12	MOHLYP	4.6	4.6	4.2	0.25
BP86	2.7	2.7	3.3	0.17	MPWLYP1M	4.6	4.6	2.5	0.15
B97-3	2.8	2.8	2.7	0.11	HFPW91	-4.7	4.7	11.7	0.07
SOGGA11	-1.2	2.8	7.1	0.29	BLYP	4.8	4.8	2.5	0.16
B3PW91	-0.1	2.9	5.5	0.13	mPWLYP	4.9	4.9	2.7	0.16
RPBE	1.8	2.9	3.8	0.22	M08-HX	0.2	4.9	6.2	0.32
BPW91	0.9	2.9	4.1	0.21	M11-L	5.7	5.7	3.7	0.38
MPW1K	-1.7	2.9	7.7	0.10	HF	-6.2	6.2	14.2	0.31
N12	0.6	2.9	4.3	0.18	M11	-2.0	6.6	8.7	0.15
τHCTHhyb	1.4	3.0	3.8	0.24	MN12-L	6.9	6.9	4.4	0.21
PBE0	-0.9	3.0	6.6	0.12	M06-2X	9.7	9.7	8.5	0.29
PBE	0.6	3.0	4.6	0.19	M06-HF	18.1	18.1	19.9	0.24
PW91	0.8	3.0	4.3	0.19					

[a] δ denotes the mean unsigned deviation of the four occupancies in group 4 of the 5s subshell from the integer values corresponding to the dominant configuration of the experimental state.

Table 5.11 Overall performances of all the methods against groups 1-3

	δ^a	MSE	MUE(14)^b	MUE(22)^c		δ^a	MSE	MUE(14)^b	MUE(22)
SOGGA11-X		2.9	3.4	3.1	PBE		-2.7	4.4	5.5
B1LYP		1.5	3.0	3.1	LC-mPWLYP		5.2	5.4	5.5
B3V5LYP		1.1	2.9	3.3	BP86		-1.1	3.7	5.5
MPW3LYP		1.8	3.1	3.5	PW91		-2.5	4.3	5.6
B3LYP		1.2	3.0	3.6	MPW1K		-5.4	5.5	5.6
CAM-B3LYP		2.7	3.6	3.6	ωB97X-D		6.1	6.4	5.9
PW6B95		1.2	3.2	3.7	BPW91		-3.6	5.1	6.1
BMK		3.6	3.6	3.7	M06-L		4.7	6.2	6.3
BHandH		-0.1	2.3	3.9	LC-ωPBE		-1.8	5.7	6.4
B3LYP*		1.2	3.0	3.9	SOGGA		-4.3	6.1	6.8
MOHLYP		2.1	4.1	4.0	SOGGA11		2.2	7.3	6.8
TPSS1KCIS		-2.2	4.3	4.1	OPBE		-2.9	7.4	6.9
TPSSh		-2.9	4.3	4.2	M08-HX		5.7	7.7	6.9
MPWKCIS1K		-2.7	3.9	4.3	τHCTHhyb		8.0	8.0	7.0
revTPSS		-2.7	4.4	4.5	MN12-L		7.5	8.9	7.3
BHandHLYP		0.9	3.5	4.6	M11		1.5	6.8	8.1
TPSS		-2.1	4.3	4.6	HCTH/407		6.9	7.9	8.1
O3LYP		1.3	4.9	4.6	M06		10.0	10.1	8.8
RPBE		-1.6	3.8	4.6	M06-2X		11.6	11.6	9.6
PBE0		-4.5	4.7	4.8	SVWN		-0.9	5.2	10.4
MPWLYP1M		2.6	4.0	4.8	HFPW91		-5.5	6.5	10.4
BLYP		2.1	4.0	4.9	ωB97X		11.7	11.7	10.5
HSE		-4.8	4.8	5.0	HFLYP		1.5	6.7	10.5
VS98		1.3	5.4	5.1	M11-L		7.3	10.5	10.6
B98		5.7	5.8	5.1	N12		2.7	10.8	10.6
MPWB1K		-0.2	2.8	5.2	M05-2X		11.4	11.9	10.6
B97-3		5.6	5.8	5.2	M06-HF		12.1	12.1	11.4
OLYP		2.5	5.6	5.3	B88		-11.6	11.6	11.5
M08-SO		3.0	5.7	5.4	M05		13.7	13.7	12.1
MPWLYP		2.8	4.3	5.4	HF		-12.0	12.1	18.8
B3PW91		-4.6	5.1	5.4					

[a] δ denotes the mean unsigned deviation of the 28 occupancies of the 5s subshell from the integer values corresponding to the dominant configuration of the experimental state.
[b] MUE over 14 excitation energies
[c] MUE over 14 excitation energies and eight ionization potentials

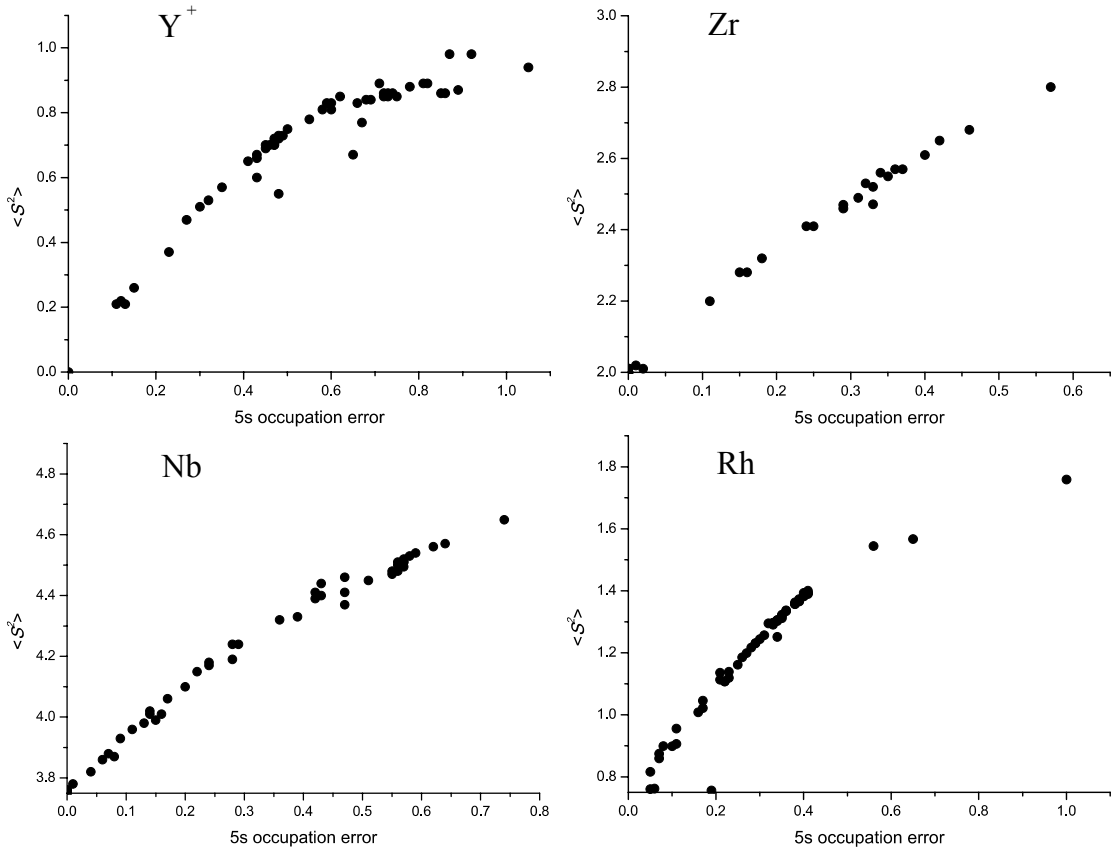

Figure 5.1. Plots of calculated $<\hat{S}^2>$ values against the absolute error in 5s subshell occupations for Y+, Zr, Nb, and Rh.

Chapter 6

Noncollinear Density Functional Theory for Open-Shell and Multi-Configurational Systems I: Dissociation of MnO and NiO and Barrier Heights of O_3, BeH_2, and H_4

6.1 Introduction

Kohn-Sham density functional theory[1] is based on representing the electron density as the square magnitude of a single Slater determinant. The energy is computed by a variational principle in which the energy is minimized with respect to variations of the orbitals in the Slater determinant. However the Slater determinant is not a wave function for the real system (it is a wave function for a system with the same density as the real system but with noninteracting electrons), and consequently one should not overinterpret the Slater determinant. For example, it is not required to have the correct expectation value of the spin density or of $\hat{S}^2$, where $\hat{S}$ is total electron spin.[2] Therefore the variational determination of the ground-state energy should be carried out without spin or symmetry constraints in the Slater determinant.[3]

In wave function theory it is very convenient to use symmetry-adapted configuration state functions that are linear combinations of Slater determinants. Because one can use multiple Slater determinants, it is not a restriction to take the spin-orbitals used in the Slater determinants as collinear, i.e., to have the form of a spatial function times spin function α or spin function β, where α and β are quantized along a single

arbitrary laboratory-fixed axis. When one is restricted to a single determinant, as in Hartree-Fock theory or Kohn-Sham density functional theory, though, this is a restriction, and an unconstrained varational optimization should allow each spin-orbital ψ_j to be an arbitrary linear combination

$$\psi_j = \phi_{j1}(\mathbf{r})\alpha + \phi_{j2}(\mathbf{r})\beta \tag{6.1}$$

where ϕ_{ji} is a complex spatial function, and ψ_j is called a general spin-orbital (GSO). General spin-orbitals arise naturally in relativistic wave function theory and relativistic density functional theory, where they may be used to treat spin-orbit coupling.[4–6] They have also been employed with the Hartree-Fock wave function method, where the result is called generalized Hartree-Fock[7-9] and with nonrelativistic (or single-component scalar relativistic) density functional theory,[10–21,23-28] where the result is usually called noncollinear Kohn-Sham (NKS) theory. Most NKS calculations reported so far have been used to study magnetic solids and unligated and ligated metal clusters formed by transition metals.[10–12,16,23, 26] Here we present some examples to show their usefulness for diatomic molecule potential curves and for three systems with no transition metals but with significant multiconfigurational character. In particular we present calculations on MO (M = Mn, Ni), O_3, H_4, and BeH_2. The goal of the paper to learn whether noncollinear solutions are more stable than collinear ones for a variety of kinds of multireference systems, to see if the noncollinear solutions yield smoother potential energy curves or significantly different reaction barriers, and to illustrate the orientations of the noncollinear spin vectors in some cases.

From the point of view of wave function theory, for example from the point of view of generalized Hartree–Fock theory, we note that a noncollinear determinant can be rewritten as a linear combination of collinear ones, and optimizing a noncollinear is may be considered to provide a limited optimization of multideterminantal character. While the noncollinear determinant has more variational flexibility than a collinear determinant, it has less flexibility than a linear combination of many collinear determinants with completely independent coefficients. However, from the point of view of Kohn–Sham density functional theory, a noncollinear determinant plays a more canonical role. In particular, the Kohn-Sham method is defined to involve the variational optimization of a single determinant, and a noncollinear determinant represents the limit of complete optimization in the general case, although in specific cases the variationally optimized determinant might correspond to the special case of a collinear determinant. The examples in the present article will show both kinds of cases, that is, cases where the colllinear determinant is stable and cases where it is not.

We will use the following notation. Complete optimization of the Slater determinant with GSOs will be called NKS. Optimization with the restriction to collinear spin-orbitals will be called unrestricted Kohn-Sham (UKS), analogous to unrestricted Hartree-Fock; we note that this kind of optimization is often simply called the broken-symmetry method, but this term can be ambiguous because it usually refers to a multi-step process for extracting an energy estimate from the broken-symmetry solutions. Furthermore the NKS solution may also break symmetry. UKS, although it usually breaks spatial symmetry (if present), makes the Slater determinant an eigenfunction of $\hat{S}_Z$ with eigenvalue M_S but does not give eigenfunctions of $\hat{S}^2$. Optimization with the

restrictions of (i) collinear spin-orbitals, (ii) eigenfunctions of $\hat{S}^2$ with $M_S = S > 0$, (iii) $2M_S$ singly occupied orbitals, and (iv) the rest of the orbitals double occupied may be called restricted open-shell Kohn-Sham; this is not recommended and is not employed here. Finally we will use the shorthand term "multireference" to denote systems that require more than one symmetry-adapted configuration state function for an adequate treatment by wave function theory, as reviewed elsewhere.[29]

6.2 Systems

Bond dissociations of metal oxide diatomics provide some of the simplest examples of a process that cannot be treated adequately by UKS. Consider, e.g., MnO. The ground state has $S = 5/2$, and so UKS would involve a determinant with $M_S = 5/2$. But the ground states of the dissociation products are Mn($S = 5/2$) and O($S = 1$). To treat this with an unrestricted but collinear single Slater determinant would require a determinant with $M_S = 7/2$ or a determinant with $M_S = 3/2$. Similarly NiO($S = 1$) should dissociate to Ni($S = 1$) plus O($S = 1$), for which requires $M_S = 1$ or 0 at the equilibrium geometry and $M_S = 2$ at the dissociation limit. In this article we will examine the question: can NKS treat this kind of potential curve qualitatively correctly?

Next we will consider three examples that do not involve a transition metal or a dissociation process, but rather contain multi-configurational transition states:

(a) The potential energy surface of ozone. Ozone, although it is a closed-shell singlet, is a classic example of a problem that profits in wave function theory from a multi-configurational self-consistent-field treatment.[30–35] In particular,

ozone has significant biradical character which is best described in wave function theory by mixing doubly excited configurations with the dominant configuration.

(b) Insertion of Be into H_2. This is another popular test for handling multi-reference character.[36]

(c) H_4, which also has been widely used to test the ability of various quantum chemistry methods in treating multi-reference character.[37] In the present study, we are comparing the energy difference between a TS of square geometry with four H-H distances of 2.0 bohrs, and a lower-energy geometry with three identical H-H distances of 2.0 bohrs.

Here we ask: can NKS provide an improved description of these multi-configurational transition states, relative to UKS?

6.3 Methods

All the DFT calculations were performed with a locally modified version of *VASP 5.3* [38,39] using the projector augmented wave (PAW)[40] method and either the PBE[45] or the PBE0[43] exchange–correlation functional. (The functionals are used without modification, and the local modifications of *VASP* are not required for the present calcuations.) Since VASP does not provide PAW potentials for each exchange-correlation functional, we used the latest PAW potentials generated from the PBE functional, which can be downloaded from the VASP website; these potentials also contain the kinetic energy densities, which are necessary for meta-GGA calculations. The unit cell is of size 10×11×12 Å, and the cut-off energy is 1000 eV. It has been shown

previously that *VASP* calculations using PAW potentials are able to reproduce DFT calculations using high-quality Gaussian-type basis sets,[41] and our tests also showed that collinear DFT results obtained from *VASP* and *Gaussian 09* agree within 0.5 kcal/mol.

In carrying out the calculations we found it essential to use the feature in *VASP* that allows one to initialize the SCF iterations with a determinant that breaks the spin symmetry in an appropriate way. This is achieved in VASP by specifying the initial spin magnetic moment on each atom.

For ozone we carried out complete-active-space second-order perturbation[42] calculations with *Molpro*[47, 48] with 12 electrons in 9 active orbitals and the aug-cc-pV5Z basis set to optimize the geometries of both ozone and cyclic ozone, and we obtained nine intermediate geometries (table 6.1) by linear interpolation. Single-point CASPT2 calculations were then performed to construct the reference potential energy curve, providing a relativistic approximation of the reaction barrier height. For H_4 and BeH_2, the geometries used for the calculations and the reference barrier heights in Table 6.2 are taken from previous studies.[36, 37]

6.4 Results

6.4.1 MnO and NiO Dissociation

We first performed calculations on two transition metal oxides using the PBE0 exchange-correlation functional, and the results are given in Figs. 1 and 2. Figure 6.1 compares the dissociation curves of MnO obtained by UKS (for M_S = 5/2 and 7/2) to that obtained by NKS. The zero of energy is taken as the sum of energies of the two atoms in their ground states (sextet for Mn and triplet for O). First consider the two UKS

calculations. Near equilibrium the ground state of MnO is a sextet, which, however, dissociates to a wrong limit composed of a sextet Mn and a singlet O. This limit is about 20 kcal/mol higher than the correct one, and the error is precisely equal to the triplet–singlet gap of oxygen atom calculated by PBE0. The error originates from the fact that, to correctly describe an isolated sextet Mn atom together with an isolated triplet atom with a single Slater determinant within the collinear spin scheme, the determinant must have M_S = 7/2. This, however, contradicts the requirement of M_S = 5/2 to treat the ground state near equilibrium. The above can be verified by examining the UKS curve (also shown in Fig. 6.1) for the octet state of MnO, which is the excited state near equilibrium, but correctly dissociates to the limit of Mn(S = 5/2) + O(S = 1). Thus UKS is intrinsically incapable of describing the spin coupling through the process of dissociation. Although one may attempt to describe the dissociation behavior by combining the two UKS curves, the merged results fail to provide any insight into the intermediate region, which in real applications is often the most chemically important one for reaction mechanism or catalysis studies.

Next we consider the NKS curve. It is clear that by relaxing the constraint of collinear spins, the resulting Kohn-Sham orbitals have more flexibility to describe the whole energy curve. Since no constraints on spin states are present in our NKS calculations, the SCF iterations can converge to the lowest-energy state. Hence near equilibrium NKS delivers results identical to the M_S = 5/2 UKS calculation, while at long bond lengths it also correctly predicts the dissociation behavior. Also notable is the smooth transition at intermediate bond lengths from the sextet to the octet. This shows

that NKS can describe the dissociation of this transition metal system smoothly along the whole reaction path.

We note that the NKS calculations are not automatic. During our attempt to locate the lowest-energy solution, we found that an NKS calculation initiated with a UKS configuration would generally stay in the UKS variational space without further spin symmetry breaking. Only when the initial guess properly breaks the symmetry would the SCF successfully converge to a real NKS solution. We did find, however, that once the symmetry is broken, the SCF iterations would usually converge to the same NKS solution, regardless the specific spin configuration in use.

By comparing the local spin magnetic moments on each atom we obtain additional insights relevant to the goal of illustrating the orientations of the noncollinear spin vectors in some cases where the molecular orbitals of Kohn-Sham density functional theory become noncollinear when fully optimized. The atomic magnetic moments are defined by integration of the magnetization over the space within a certain radius around the atoms. (Thus these moments are not equal to expectation values of spin operators. The normalization is such that the magnetic moment of a single electron would be $2m_s$, i.e., unity rather than one half.) Parts (a) and (b) of Fig. 6.3 provide these atomic magnetic moments for MnO at an internuclear distance of 6 Å. Parts (a) and (b) in Fig. 6.3 compare the MnO results obtained by UKS and NKS. The UKS results clearly show that at the dissociation limit the magnitude of the local spin magnetic moment on the Mn atom is 4.2, consistent with that of a sextet state ($2S = 5$); it also shows that the O atom is in the singlet state rather than the triplet state, verifying the deficiency of collinear spins. This intrinsic difficulty is alleviated in NKS by relaxing the spins as shown in (b), and

both Mn and O atoms are in their ground state, while remaining describable by a single determinant of $M_S = 5/2$. Notice that parts (a) and (b) of Fig. 6.3 both correspond to $M_S = 5/2$, and yet the solutions differ in energy by 20 kcal/mol. This is a clear demonstration of the dependence of the energy on the relaxing the collinear constraint. (The magnetic moments in Fig. 3 serve as pictorial aids to illustrate how NKS relaxes the spin collinearity constraint to achieve the lowest-energy broken-symmetry SCF solution, but they do not describe the physical situation, just as the UKS polarized spin densities on each hydrogen atom for the dissociated H_2 molecule do not describe experimental observables.)

Similar results for dissociation curves are observed in Fig. 6.2, comparing the UKS and NKS dissociation curves for NiO. For bond distances of 4.0 Å to 5.5 Å we also find that NKS leads to a solution that is slightly lower in energy than the UKS one. This implies that NKS not only offers extra variational freedom for the NiO system to avoid spin frustration, but also it leads to a slightly different SCF solution that is not located within the UKS variational space. The local magnetic moments are drawn for NiO at bond distances of 6.0 Å in Fig. 6.3 (c) and (d) and at bond distances of 4.5 Å in Fig. 6.3 (e) and (f).

These are just two examples of the kind of transition-metal-containing systems with complicated spin states that are problematic for collinear KS. These systems could include metal dimers, metal clusters, and oxo-metal cores in important metal-organic species. As we previously showed,[26] NKS can provide new possibilities in modeling the complicated low-lying spin states with both computational convenience and theoretical simplicity.

NKS does not always lead to a lower-energy SCF solution than UKS since the variational space of UKS is essentially completely contained in that of NKS. Consider, for example, MnO. One can observe that for bond distances of 1.5 to 2.0 Å the NKS solution exactly matches the UKS solution, implying that the UKS treatment is sufficient. Nevertheless, without an NKS calculation or a stability test of the UKS solution, one could not predict the stability in advance, and thus an NKS calculation or a stability analysis is required to demonstrate attainment of the variational minimum energy. (Since generalized Hartree-Fock theory (GHF) also uses noncollinear spin orbitals, it can lead to qualitatively similar results as those obtained by NKS. GHF has been discussed in various places in the literature, but these studies did not approach the problem of noncollinear spin orbitals from the perspective of variational instabilities. We did not pursue this issue for GHF because, due to not having a correlation functional, GHF is quantitatively wrong for descriptions of the systems discussed in this paper.)

6.4.2 Barrier heights of ozone, BeH_2, and H_4

Now we turn to several systems without transition metals, starting by considering ozone. It is well known that a cyclic high-energy structure exists for ozone, and by considering a linear synchronous path[44] parameterized by the progress variable λ between normal and cyclic ozone, we can test the ability of UKS and NKS to handle highly multi-configurational systems. The results are compared in Table 6.1 and Fig. 6.4, tabulating the energy changes along the path from the high-energy cyclic ozone ($\lambda = 1.0$) to the low-energy normal ozone ($\lambda = 0.0$). First consider the UKS results with the PBE[45] exchange-correlation functional; these calculations yield a barrier height 6 kcal/mol lower than the CASPT2 barrier. This is no surprise since generalized gradient approximations

like PBE are well known to underestimate barrier heights.[49] However, we also find that PBE0, with 25% Hartree-Fock exchange, offers no improvement. Next we turn to NKS. We find no energy lowering for either the normal ozone or the cyclic one when collinear spins are allowed to relax. However, for PBE one finds an energy lowering of 0.1 to 3.1 kcal/mol in intermediate structures with $\lambda = 0.3$ to 0.7. Similar energy lowering is also observed for PBE0 results in the λ range of 0.5 to 0.8, with the magnitude ranging from 0.1 to 4.8 kcal/mol. Thus the more complete variational optimization of the Slater determinant changes the shape of the calculated reaction barrier. Since UKS already underestimates the barrier height, NKS results present even larger errors by further stabilizing the transitions states. So if we were to judge the accuracy of the exchange-correlation functionals for this multi-reference system by comparison to the reference values, one would draw an incorrect conclusion. Despite the larger error of NKS with the exchange-correlation functionals employed here, it provides a more stabilized SCF solution, and the most stabilized solution would provide the correct prediction if the unknown exact exchange-correlation functional were used, and the resulting exact SCF solution would be NKS-stable. Thus if better agreement with experiment is obtained by imposing symmetry constraints on the spin orbitals, it just represents cancellation of errors due to the exchange–correlation functional with those due to incomplete optimization. In the long term we would prefer to use exchange-correlation functionals designed to give good results with full variational optimization. However at this moment we are limited to GGA and hybrid GGA functionals due to the present lack of software capable of performing NKS with completely general functionals, e.g., with meta-GGA functionals. To facilitate understanding of the PBE noncollinear results in Fig. 6.4 and

Table 6.1, we calculated the magnetic moments on each oxygen atom for the transition state ($\lambda = 0.7$) as shown in Fig. 6.5 (a) and (b). These figures show that by using noncollinear spin orbitals, the system is able to be variationally stabilized to avoid spin frustration due to spin collinearity constraints.

Next we consider another system with a multi-reference transition state, namely, the insertion of Be into H_2. The results are tabulated in Table 6.2, showing that the most stable UKS results obtained by PBE and PBE0 underestimate the barrier heights by 14.7 kcal/mol and 22.9 kcal/mol, respectively; this again contradicts the common expectation that hybrid GGAs predict higher barrier heights than GGAs. In this case one observes a further stabilization of 13.3 kcal/mol and 8.4 kcal/mol with NKS for PBE and PBE0 respectively. The large stabilization by use of noncollinear spins should further be considered in combination with the fact that most widely popular exchange-correlation functionals were previously designed and tested with collinear-spin Kohn-Sham orbitals. To advance the development of better functionals, many of the multi-configurational systems need to be reexamined with greater attention to the stability of the solutions of the Kohn-Sham equations. By comparing the local magnetic moments on each atom in Fig. 6.5 (c) and (d), one sees that the local spin on two hydrogen atoms are further relaxed to align noncollinearly with PBE NKS calculations.

As a third example we show a system where NKS, even with the presently available functionals, leads to both more stabilized states and better accuracy. The energy differences between square and linear H4, a widely used test model for treating multireference systems, are shown in Table 6.3. UKS gives similar results for PBE and PBE0, with barrier heights 17-18 kcal/mol higher than the reference data, while NKS

leads to significantly lower absolute energies for the transition state, with errors for PBE and PBE0 being -8.6 kcal/mol and -8.4 kcal/mol, respectively. In Fig. 6.5 (e) and (f) we show that although the magnitudes of local magnetic moments of PBE NKS calculations remain the same as those from PBE UKS calculations, NKS leads to a further lowering of energy by allowing the noncollinear alignments.

6.4.3 Cases Stable to Noncollinearity

Finally we mention cases where no further stabilization is found when the collinear constraint is relaxed. The first example is the reaction barrier of $Cl + H_2 \rightarrow HCl + H$, in which we performed NKS calculations from multiple initial guesses for the transition states with no lower-energy SCF solutions found. This example can represent a wide collection of reactions where the transition states, contrary to some misconceptions, do not have significant multireference character. Next we want to make clear that not all multireference systems are unstable when spin is allowed to be noncollinear. Test cases we have tried that do not reveal any difference between UKS and NKS include the barrier height of the D_{4h} transition state for automerization of cyclobutadiene (C_4H_4) between rectangular D_{2h} minimum-energy structures,[36] as well as the barrier height of the D_{8h} transition state for double-bond shifting in cyclooctatetrane (C_8H_8) between D_{4h} localized double-bond structures.[46] For these multi-reference systems, both the transition states and the minimum-energy states are stable with respect to the spin orbitals becoming noncollinear. We also tested the dissociation curve of H_2, which at large internuclear separations is another well-known multireference system, and where we were unable to find instability of the UKS solutions. Thus it is not obvious where the

noncollinear relaxation will lower the energy, and readers should be aware that not all multireference systems are alike. In fact, analysis of the stability to noncollinear relaxation may provide a useful tool for classifying different kinds of multi-reference character. Since one is unable to predict the stability of a system with respect to noncollinear spin symmetry breaking beforehand, the safest procedure is to try NKS rather than only UKS to achieve the lowest possible SCF solution.

6.5 Conclusions

We have compared UKS and NKS results for dissociation of transition metal oxides as well as barrier heights for multireference systems. NKS provides direct and accurate descriptions of the dissociation processes of MnO and NiO, which are highly challenging processes for UKS due to their spin couplings. Stabilization of multireference transitions states of ozone, BeH_2, and H_4 by noncollinear relaxation of Slater determinants leads to different conclusions about the accuracy of exchange-correlation functionals than would be drawn from constrained ("unrestricted") optimizations.

It is well known that one can use currently available functionals in noncollinear calculations, as is done here and in all the noncollinear references that we cite both here and in Ref. 26. It is also well known that current functionals are not exact and need further development to achieve good accuracy across the broad spectrum of systems of chemical and physical interest.[50] Development and assessment of new exchange-correlation functionals intended for multi-reference systems can benefit by taking account of the energy lowering possible with noncollinear spin orbitals. It is difficult to completely decouple the error due to using inexact exchange-correlation functionals from that due to incomplete optimization of the Slater determinant, but one should always bear

in mind that assessment of exchange-correlation functionals without the complication of possible errors due to constraints on the optimization requires the use of the stable and variationally optimized solutions.

References for Chapter 6

(1) Kohn, W.; Sham, L. *J. Phys. Rev*. **1965**, *140*, A1133.

(2) Jacob, C. R.; Reiher, M. *Int. J. Quantum Chem*. **2012**, *112*, 3661.

(3) Görling, A. *Phys. Rev. A* **1993**, *47*, 2783.

(4) von Barth, U.; Hedin, L. *J. Phys. C* **1972**, *5*, 1628.

(5) Rajagopal, A. K.; Callaway, J. *Phys. Rev. B* **1973**, *7*, 1912.

(6) van Wüllen, C. *J. Comput. Chem*. **2002**, *23*, 779.

(7) Fukutome, H. *Int. J. Quantum Chem*. **1981**, *20*, 955.

(8) Löwdin, P.-O.; Mayer, I. *Adv. Quantum. Chem*. **19**8**2**, *24*, 79.

(9) Jiménez-Hoyos, C. A.; Henderson, Thomas M.; Scuseria, G. E. *J. Chem. Theory Comput.* **2011***, 7*, 2667.

(10) Sandratskii, L. M.; Goletskii, P. G. *J. Phys. F* **1986**, *16*, L43.

(11) Kubler, J.; Hock, K.-H.; Sticht, J.; Williams, A. R. *J. Phys. F* **1988**, *18*, 469.

(12) Hobbs, D.; Kresse, G.; Hafner, J. *Phys. Rev. B* **2000**, *62*, 11556.

(13) Yamanaka, S.; Yamaki, D.; Shigeta, Y.; Nagao, H.; Yamaguchi, K. *Int. J. Quantum Chem*. **2001**, *84*, 670.

(14) Soler, J. M.; Artacho, E.; Gale, J. P.; Garcia, A.; Junquera, J.; Ordejón, P.; Sánchez-Portal, D. *J. Phys. Condens. Mat*. **2002**, *14*, 2745.

(15) Yamanaka, S.; Yamaguchi, K. *Bull. Chem. Soc. Jpn*. **2004**, *77*, 1269.

(16) Scalmani, G.; Frisch, M. J. *J. Chem. Theory Comput*. **2012**, *8*, 2193.

(17) Uhl, M.; Sandratskii, L. M.; Kübler, J. *J. Magnetism Magnetic Mat*. **1992**, *103*, 314.

(18) Oda, T.; Pasquarello, A.; Car, R. *Phys. Rev. Lett*. **1998**, *80*, 3622.

(19) Hobbs, D.; Hafner, J.; Spisak, D. *Phys. Rev. B* **2003**, *68*, 014407.

(20) Longo, R. C.; Noya, E. G.; Gallego, L. J. *Phys. Rev. B* **2005**, *72*, 174409.

(21) Xie, Y.; Blackman, J. A. *Phys. Rev. B* **2006**, *73*, 214436.

(21) Sharma, S.; Dewhurst, J. K.; Ambrosch-Draxl, C.; Kurth, S.; Helbig, N.; Pittalis, S.; Shallcross, S.; Nordström, L.; Gross, E. K. U. *Phys. Rev. Lett*. **2007**, *98*, 196405.

(23) Peralta, J. E.; Scuseria, G. E.; Frisch, M. J. *Phys. Rev. B* **2007***, 75,* 125119.

(24) Longo, R. C.; Alemany, M. M. G.; Ferrer, J.; Vega, A.; Gallego, L. J. *J. Chem. Phys*. **2008**, *121*, 114315.

(25) Ruiz-Dias, P.; Dorantes-Davila, J.; Pastor, G. M. *Eur. Phys. J. D* **2009**, *52*, 175.

(26) Luo, S.; Rivalta, I.; Batista, V.; Truhlar, D. G. *J. Phys. Chem. Lett.* **2011**, *2*, 2629.

(27) Scalmani, G.; Frisch, M. J.; *J. Chem. Theory Comput.* **2012**, *8*, 2193.

(28) Bulik, I. W.; Scalmani, G.; Frisch, M. J.; Scuseria, G. E. *Phys. Rev. B* **2013***, 85,* 35117.

(29) Truhlar, D. G. *J. Comp. Chem.* **2007**, *28*, 73.

(30) Hay, P. J.; Dunning, T.-H.; Goddard, W. A. *J. Chem. Phys*. **1975**, *62*, 3912.

(31) Laidig, W. D.; Schaefer, H. F. III *J. Chem. Phys*. **1981,** *74*, 3411.

(32) Adler-Golden, S. M.; Langhoff, S. R.; Bauschlicher, C. W. Jr.; Carney, G. D. *J. Chem. Phys*. **1985**, *83*, 255.

(33) Ljubic, I.; Sablijic, A. *J. Phys. Chem. A* **2002**, *106*, 4745.

(34) Chang, W.-T.; Weng, C.; Goddard, J. D. *J. Phys. Chem. A* **2007**, *111*, 4792.

(35) Zhao, Y.; Tishchenko, O.; Gour, J. R.; Li, W.; Lutz, J. J.; Piecuch, P.; Truhlar, D. G. *J. Phys. Chem. A* **2009**, *113*, 5786.

(36) Jiang, W.; Jeffery, C. C.; Wilson, A. K. *J. Phys. Chem*. A **2012**, *116*, 9969.

(37) Becke, A. D. *J. Chem. Phys.* **2013**, *139*, 021104.

(38) Kresse, G.; Furthmuller, J. *Comp. Mater. Sci.* **1996**, *6*, 15.

(39) Kresse, G.; Furthmuller, J. *Phys. Rev. B* **1996**, *54*, 11169.

(40) Blochl, P. E. *Phys. Rev. B* **1994**, *50*, 17953.

(41) Paier, J.; Hirschl, R.; Marsman, M.; Kresse, G. *J. Chem. Phys.* **2005**, *122*, 234102.

(42) Anderson, K.; Malmqvist, P. –Å; Roos, B. O.; Sadlej, A. J.; Wolinski, K. *J. Phys. Chem.* **1990**, *94*, 5483.

(43) Adamo, C.; Barone, V. *J. Chem. Phys.* **1999**, *110*, 6158.

(44) Halgren, T. A.; Lipscomb, W. N. *Chem. Phys. Lett.* **1977**, *49*, 225.

(45) Perdew, J. P.; Burke, K.; Ernternof, M. *Phys. Rev. Lett.* **1996**, *77*, 3865.

(46) Karadakov, P. B. *J. Phys. Chem. A* **2008**, *112*, 12707.

(47) Werner, H.-J.; Knowles, P. J.; Knizia, G.; Manby, F. R.; Schütz, M. *WIREs Comput. Mol. Sci*. **2012**, *2*, 242.

(48) *MOLPRO*, version 2012.1, a package of *ab initio* programs, Werner, H.-J.; Knowles, P. J.; Knizia, G.; Manby, F. R.; Schütz, M. and others, see http://www.molpro.net.

(49) Yang, K.; Zheng, J.; Zhao, Y.; Truhlar, D. G. *J. Chem. Phys.* **2010**, 132, 164117.

(50) Peverati, R.; Truhlar, D. G. *Phil. Trans. Roy. Soc. A*, in press, dx.doi.org/10.1098/rsta.2012.0476; available online at http://arxiv.org/abs/1212.0944.

Table 6.1. Energies Changes (kcal/mol) from Cyclic Ozone (x = 1.0) to Ozone (x = 0.0) Calculated by UKS and NKS with PBE and PBE0 with $M_S = 0$

x	CASPT2	UPBE	NPBE	UPBE0	NPBE0
1[a]	0	0	0	0	0
0.9[b]	1.9	2.2	2.2	2.4	2.4
0.8	6.8	8.1	8.1	8.4	8.3
0.75	10.3	12.9	12.0	12.5	12.0
0.7	14	16.6	13.5	16.2	15.0
0.65	19.5	14.6	11.8	14.2	12.5
0.6	22.8	7.3	7.1	9.4	4.6
0.55	21.7	2.9	2.7	4.3	0.0
0.5	19.3	-1.4	-1.6	0.2	-4.5
0.4	-1.0	-4.0	-5.8	-3.6	-7.6
0.3	-16	-14.9	-15.2	-17.5	-17.5
0.2	-26.2	-26.7	-26.7	-26.8	-26.8
0.1	-31.9	-33.6	-33.6	-31.9	-31.9
0[c]	-33.8	-36.4	-36.4	-33.1	-33.1

[a] equilateral triangle with R(O–O) = 1.448 Å and bond angle equal to 60 deg.

[b] The central oxygen atom is located at the origin, and the Cartesian coordinates of the other two atoms are (-($x|\lambda$), ($y|\lambda$), 0) and (($x|\lambda$), ($y|\lambda$), 0). Here ($q|\lambda$) = ($q|\lambda = 0$) + $\lambda[(q|\lambda = 1) - (q|\ \lambda = 0)]$, where $q = x$ or y. In Å, ($x|\lambda = 0$) = 1.091, ($x|\lambda = 1$) = 0.724, ($y|\lambda = 0$) = 0.674, ($y|\lambda = 1$) = 1.254.

[c] R(O–O) is 1.282 Å, and the bond angle equals 116.6 deg.

Table 6.2. Barrier Heights for Insertion of Be into H_2 (kcal/mol) Calculated by UKS and NKS with PBE and PBE0 with $M_S = 0$

	UKS	NKS
PBE	100.9	87.6
PBE0	91.8	83.4
Ref.	114.7[a]	

[a] From Ref. 36.

Table 6.2. Barrier Heights for H_4 (kcal/mol) Calculated by UKS and NKS with PBE and PBE0 with $M_S = 0$

	UKS	NKS
PBE	116.1	89.5
PBE0	116.8	86.1
Ref.	99.1[a]	

[a] From Ref. 37.

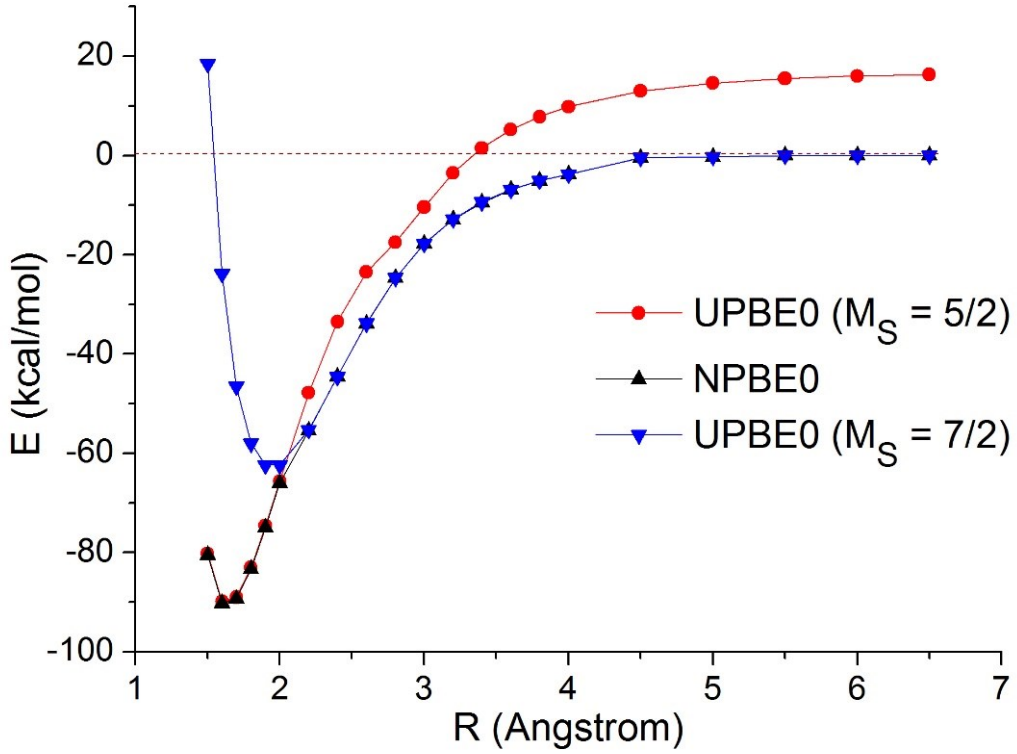

Figure 6.1 Dissociation curve of MnO calculated with PBE0 using UKS and NKS. The NKS curve corresponds to $M_S = 5/2$.

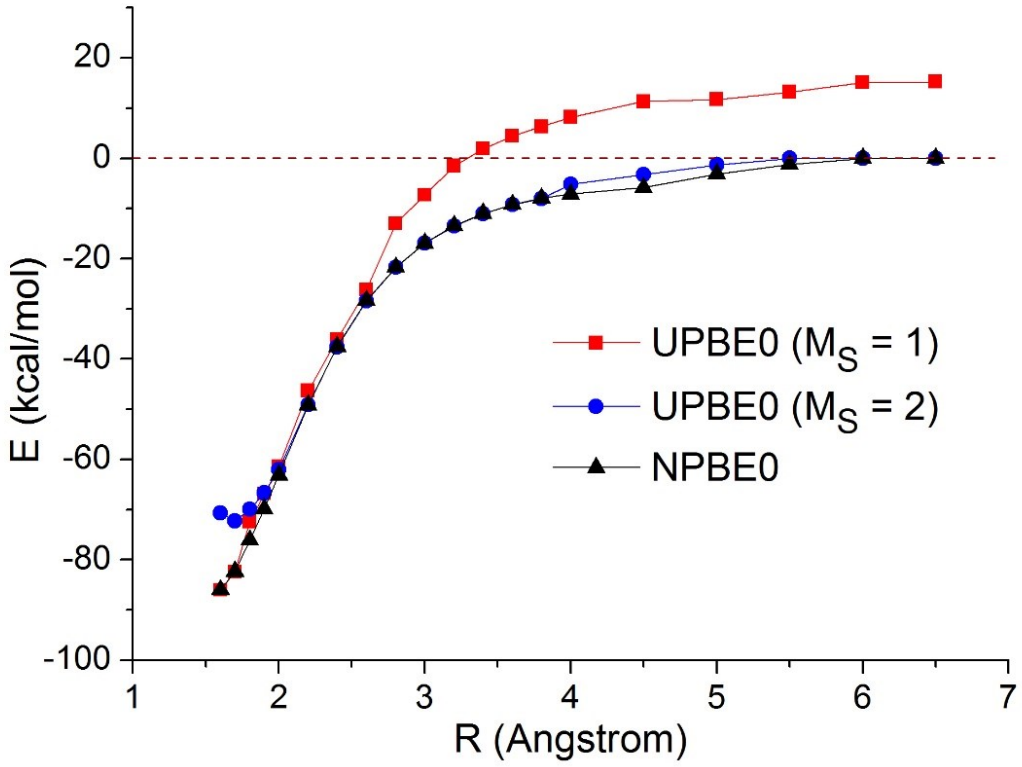

Figure 6.2 Dissociation curve of NiO calculated with PBE0 using UKS and NKS. The NKS curve corresponds to $M_S = 1$.

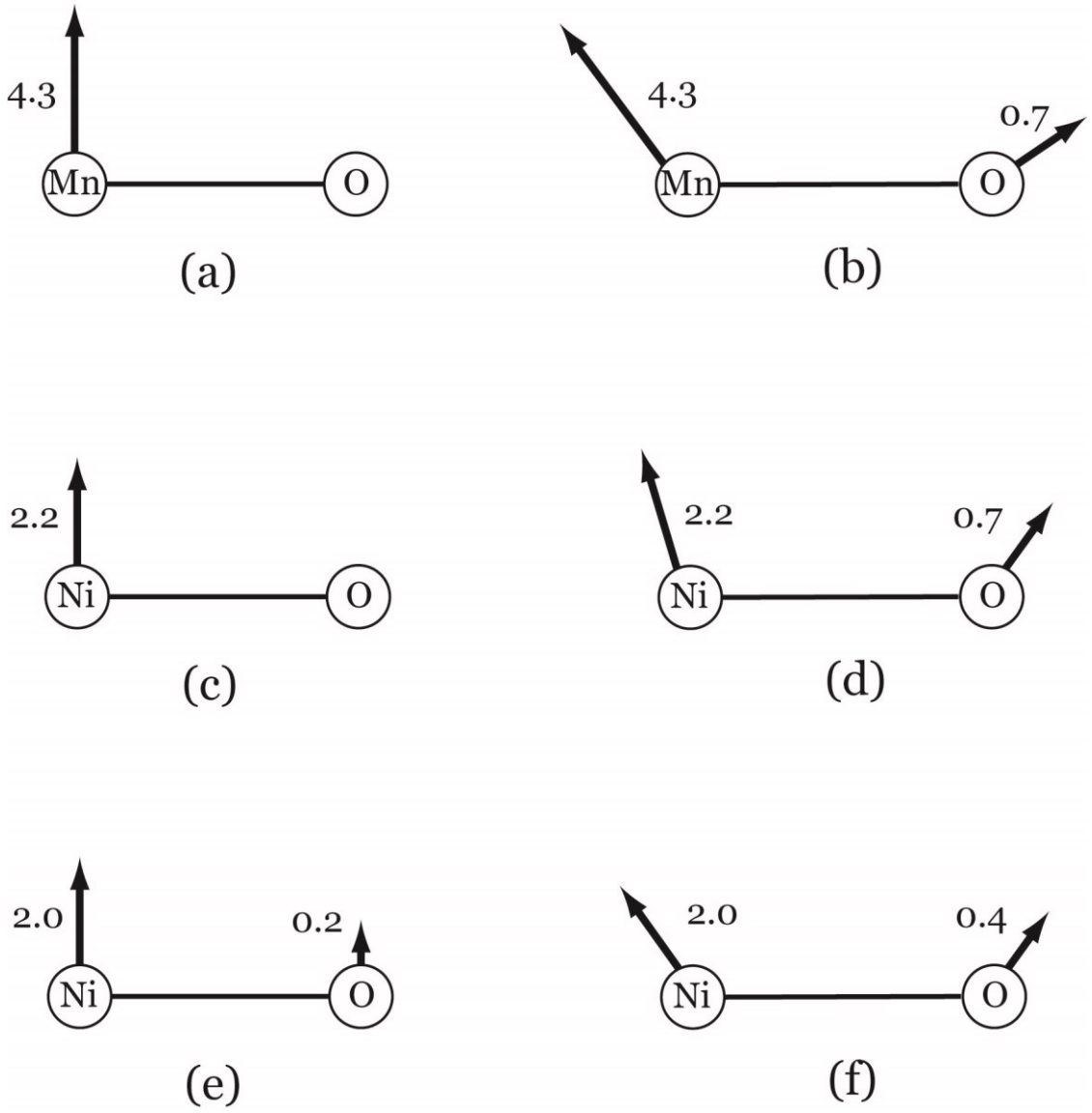

Figure 6.3 Local spin magnetic moments calculated by PBE0. Bond distances of 6.0 Å: (a) MnO by UKS with $M_S = 5/2$, (b) MnO by NKS with $M_S = 5/2$, (c) NiO by UKS with $M_S = 1$ (d) NiO by NKS with $M_S = 1$. Bond distances of 4.5 Å: (e) NiO by UKS with $M_S = 1$ (f) NiO by NKS with $M_S = 1$.

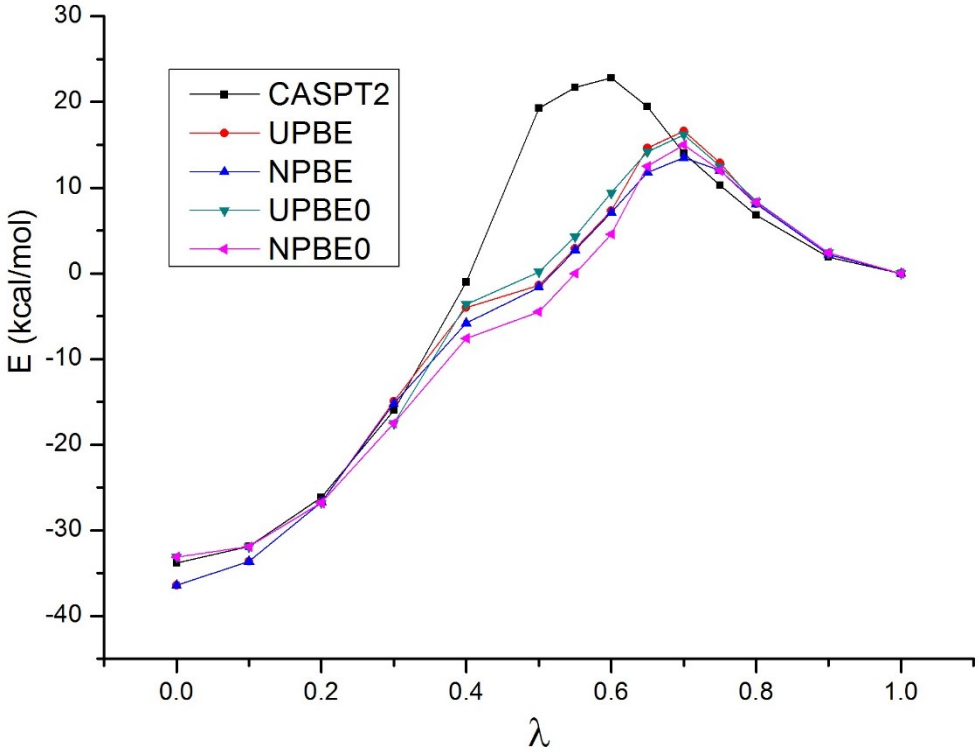

Figure 6.4 Energies Changes (kcal/mol) from Cyclic Ozone (x = 1.0) to Ozone (x = 0.0) Calculated by UKS and NKS with PBE and PBE0 with $M_S = 0$.

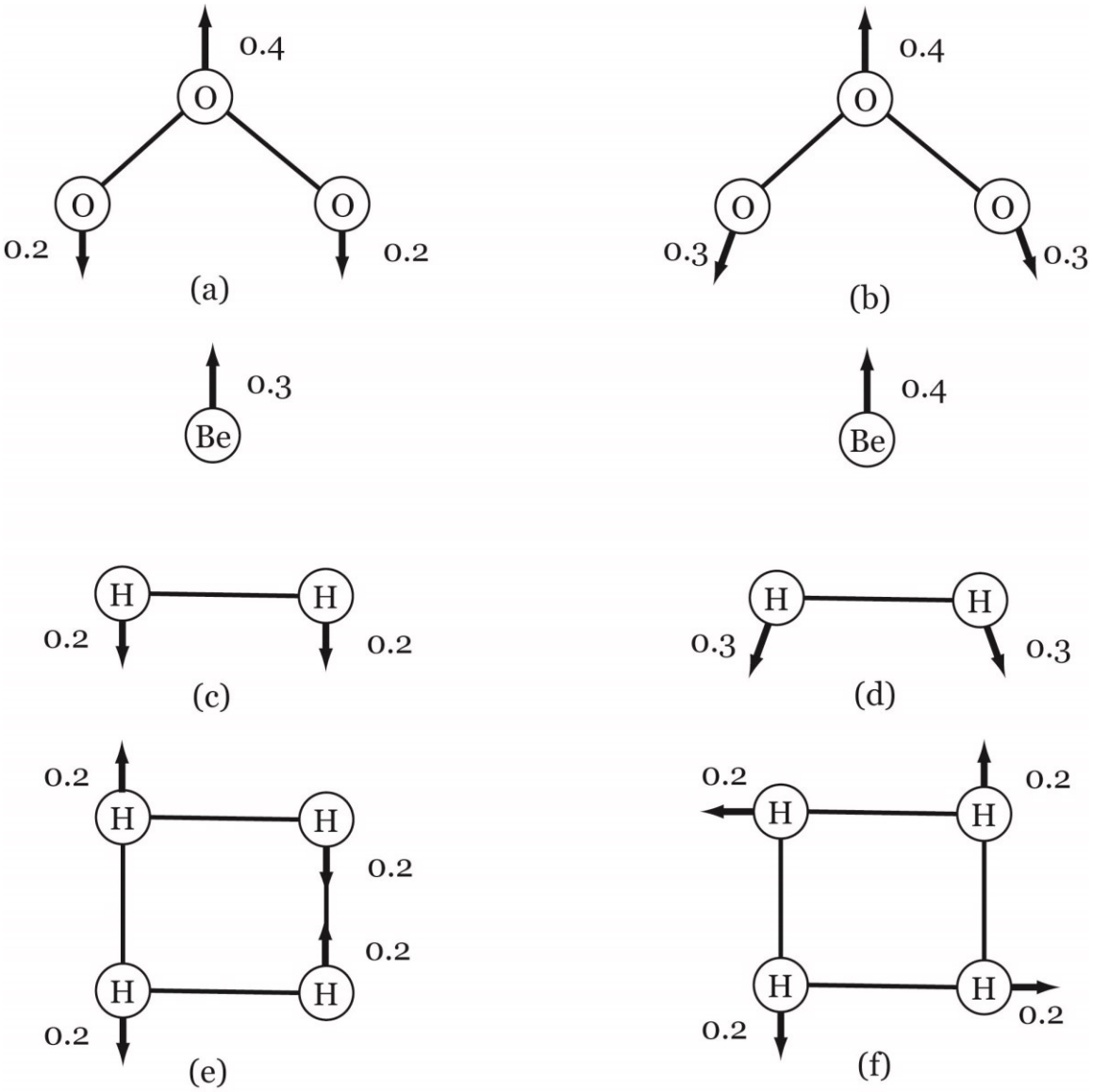

Figure 6.5 Local spin magnetic moments calculated by PBE. (a) ozone at $\lambda = 0.7$ by UKS with $M_S = 0$. (b) ozone at $\lambda = 0.7$ by NKS with $M_S = 0$. (c) BeH_2 at transition state by UKS with $M_S = 0$. (d) BeH_2 at transition state by NKS with $M_S = 0$. (e) square H_4 by UKS with $M_S = 0$. (f) square H_4 by NKS with $M_S = 0$.

Chapter 7

Noncollinear Density Functional Theory for Open-Shell and Multi-Configurational Systems II: A Biomimetic Oxomanganese Synthetic Trimer Inspired by the Oxygen Evolving Complex of Photosystem II (PS II)

7.1 Introduction

The photoenzymatic oxidation of water to dioxygen by the oxygen-evolving complex (OEC) of photosystem II (PS II) is a key step in the biological utilization of solar energy.[1–5] The necessity to fully understand the electronic structure of the high-valent polynuclear oxomanganese complex that constitutes the catalyst has stimulated considerable work on studies of oxomanganese complexes with structural features common to the OEC of PS II.[2–8] Density functional theory[9] (DFT) in the self-consistent-field (SCF) formalism of Kohn and Sham[10] (KS) has greatly advanced our ability to model transition metal chemistry,[11] but it is limited by the need to approximate its central quantity, the exchange-correlation functional[9,10] (xcF), and the complexes under consideration have continued to pose challenges that are only partially solved.

In the KS formulation, DFT represents the density by a single Slater determinant with each electron in an up-spin or down-spin orbital. When the orbitals are not required to be doubly occupied, this is called an unrestricted determinant

(UD); some states, such as open-shell singlets or doublets with three unpaired electrons, cannot be described by a UD (we will call them non-UD-describable). If all minority-spin electrons (β electrons) are in doubly occupied orbitals, a UD always has $M_S = \pm S$, where M_S is the spin-component along the up–down axis, and S is total spin; if, however, the UD has different orbitals for spin-up and spin-down electrons, the UD is not a spin eigenfunction. The KS orbitals are found by an iterative SCF calculation. If the resulting orbitals occupied by the minority spins all have a high overlap with a corresponding majority-spin orbital (as in the variationally lowest-energy UD for Li atom, where the two 1s orbitals are very similar), although the symmetry is broken, in this article we will call this a spin-contaminated state to avoid confusion; it can still be a good approximation to a spin eigenfunction that is an eigenfunction of the real Hamiltonian. If, however, the corresponding orbitals are very different, for example if they are located on different centers, the solution is not a good approximation to any one real state, and it will be called a broken-symmetry (BS) state. A procedure,[11-13] which we will call the weighted-average BS method (because it treats the BS state as a weighted average of pure spin states) has shown the ability to reproduce some spectroscopic results on non-UD-describable low-spin (LS) systems with good accuracy, [13-21] and has gained increasing popularity.[22]

In the treatment of LS states in polynuclear transition metal complexes by the weighted-average BS method, the LS state is not calculated self-consistently, but rather its energy is obtained by diagonalization of an effective Hamiltonian using coupling parameters that are calculated from other spin states (usually one state with the highest spin, together with one or more BS states formed by flipping the spins at

some center, see Figure 7.2 (b) for a simple illustration). (The BS states represent a mixture of the HS state and one or more non-UD-describable lower-spin states.) In this paper we differentiate the use of BS determinants in DFT, which can be called BS-DFT, from the more specific weighted-average BS method, which is a specific procedure for the construction of an energetic ladder; it involves the use of both BS-DFT and spin-symmetry-adapted DFT. Furthermore, even if it yields approximately correct energies in some cases, the weighted-average BS method, or any other method based on single determinants formed from only spin-up and spin-down orbitals, does not provide a self-consistent approximation to wave functions for which the spins at the various atomic centers are not collinear (i.e., parallel or antiparallel).

An example of a complex where these considerations are very relevant is

$$\left[\left(\mathrm{Mn^{IV}}\right)_3\mathrm{O}_4\left(\mathrm{bpy}\right)_4\left(\mathrm{OH}_2\right)_2\right]^{4+} \qquad \mathbf{1}$$

which has Mn centers linked by μ-oxo bridges as in the "3 + 1 Mn tetramer"[4,5] of the OEC; this complex has been experimentally determined to have a LS (S = ½) ground state with more than one unpaired orbital and a HS (S = 3/2) first excited state with an energy difference ΔE (= $E_{LS} - E_{HS}$) of –0.2 kcal/mol.[7] (Another system, $\left[\left(\mathrm{Mn^{IV}}\right)_3\mathrm{O}_4\right]^{4+}$, that also has a triangular Mn_3 core and a non-UD-describable LS ground state has ΔE = –0.3 kcal/mol.[6]) In the present article we consider the structure [23]

$$\left[\left(\mathrm{Mn^{IV}}\right)_3\mathrm{O}_4\mathrm{L}_4\left(\mathrm{OH}_2\right)_2\right]^{4+} \qquad \mathbf{1s}$$

which is shown in Fig. 7.1, where L is *N, N'*-bis(methylene)-*Z*-1,2-ethenediamine). This is a simplified version of **1**.

Label the three Mn atoms as A, B, and C, and let S_{AB} be the total spin of the two closest Mn atoms A and B, which are the ones in the $(\mu\text{-O})_2Mn_2$ unit. Since A and B are closer to each other than to C, which is coupled to them by a O-Mn-O linkage, the EPR measurements[7] were interpreted by first coupling the spins of centers A and B and then coupling the total spin of AB with the spin of C. This analysis led to the AB subsystem of the LS state being in an $S_{AB} = 1$ state, with equivalent Mn^{IV} ions (that are likely to be both in a local HS state with $S_A = S_B = 3/2$ since this arrangement avoids pairing of d electrons on any Mn center). In addition, the total spin of the complex in the ground state was determined to be $S = ½$ and $S_C = 3/2$. The HS spin state with S = 3/2 is an excited state, again with all three Mn^{IV} ions also in the local HS state ($S_A = S_B = S_C = 3/2$), but the AB subsystem being an $S_{AB} = 0$ state. Based on this analysis, neither the HS nor the LS state of the system is UD-describable.

If one tries to force KS DFT to describe a $S_{AB} = 1$ subsystem, then d electrons must be paired in either A or B, leading to $S_A = 1/2$, $S_B = 3/2$ or $S_A = 3/2$, $S_B = 1/2$, with opposite signs for M_S. (See Figure 7.2(a)). This is the best result for the observed LS state that can be directly obtained by KS DFT without using the weighted-average BS method (note that this calculation uses BS-DFT and results in a BS state, but it does not include calculations of a series of spin states to obtain the effective Hamiltonian and then indirectly obtain the energy of the LS state so it is not an example of the weighted-average BS method). As expected, this state with paired d

orbitals is high in energy; it was found previously,[23] using the B3LYP[24] density functional, to give an LS state that is 22 kcal/mol higher than the HS state. This occurs because pairing two of the d electrons on one of the centers raises the energy much higher than the real LS state.

7.2 Theory

In order to understand the self-consistent treatment of the LS state that we will present here, we must consider the description of open-shell systems in wave function theory (WFT) and in a more complete version[25,26] of open-shell DFT. In WFT one builds wave functions as a superposition of configuration state functions (CSFs) that are themselves usually either single determinants or symmetry-adapted linear combinations of determinants. Each determinant is an antisymmetrized product of spin orbitals, each of which is a product of a spatial orbital (depending on electron position **r**) and an eigenfunction of spin angular momentum corresponding to spin up (α) or down (β) along a chosen axis. One such determinant is not general enough to describe an arbitrary open-shell system, but a linear combination of α and β can represent spin angular momentum in an arbitrary direction, and therefore a linear combination of CSFs can represent a state with arbitrary magnetic properties. But reliable WFT calculations are impractical for large, complex systems, so we turn to DFT, which is usually carried out by the KS formalism based on a single reference determinant with the same electron density as the molecule under consideration. This would be exact if the exact xcF were known, but it isn't.

However the main practical limitation of DFT is not always the approximate nature of the xcF. Since the electron density is represented by a single determinant,

the generalization of the magnetic state must occur at the spin orbital level rather than by a superposition of CSFs, and a better treatment of open-shell systems involves generalizing the spin orbitals $\phi(\mathbf{r})\alpha$ or $\phi(\mathbf{r})\beta$ to more general spinors[25-27]

$$\theta = \phi_\alpha(\mathbf{r})\alpha + \phi_\beta(\mathbf{r})\beta \tag{7.1}$$

Such a determinant is even more unrestricted than a UD, and it is called a general determinant (GD); GDs can also be used in WFT.[28-31] Since θ (usually a complex function) can represent a spin in an arbitrary direction, the spins need not be aligned along a single axis, and the generalization is therefore called noncollinear DFT. [32,33] Noncollinear DFT has been applied to metals,[27,34,35] metal alloys,[36] and bare metallic clusters,[37–41] but its utility to overcome the limitations of the weighted-average BS method[16] has not been sufficiently appreciated for transition metal chemistry.

7.3 Computational Details

The complex **1s** provides a prime example of an organometallic system where a noncollinear treatment can be useful. We show this by calculations with the *Quantum Espresso* program[42] with the local spin density approximation[43, 44] for the xcF, a norm-conserving pseudopotential[45] with a nonlinear core correction,[46] a supercell of (70 bohr^3), a cutoff energy of 190 Ry, and the Makov-Payne correction[47] to account for the net charge of +4.

Spin-orbit coupling is neglected. Spin symmetry is not enforced; if it were, the magnitude *S* of total spin would be ½ (LS) or 3/2 (HS). (The calculated value of $\langle S^2 \rangle$ is not reported here since the calculation of this quantity is not currently supported in the software we used.)

Geometries were optimized by ADF[48] using collinear calculations with the TZ2P basis for the spin state with $S_{AB} = 3$ and $S = 3/2$ (the (+,+,-) state in Figure 7.2(b)). This choice is justified below; it yields A–B, B–C, and A–C distances of respectively 2.63, 3.20, and 3.20 Å, in good agreement with x-ray[7] results.

7.4 Results and Discussions

Our noncollinear solutions have all three Mn^{IV} ions in the local HS state ($S_A = 3/2$, $S_B = 3/2$, and $S_C = 3/2$). In LS ground state, the component of spin of the AB subsystem along the AB-to-C direction is approximately −1, whereas in the HS excited state, the component of spin of the AB subsystem along the AB-to-C axis is approximately 0. The energetic results are in Table 7.1, and the local spins are in Table 7.2 and Fig. 7.2.

Consider first the collinear BS calculations, which are carried out using the weighted-average BS method that is described in detail elsewhere.[11-21] This method involves calculations on four UDs (Figure 7.2 (b)), and phenomenological magnetic coupling constants J_{AB}, J_{BC}, and J_{AC} are calculated from the energy differences of these four calculations; then the first excitation energy is obtained by direct diagonalization of an effective spin Hamiltonian. We used both *ADF* and *Quantum Espresso* to independently perform these BS calculations, giving consistent results of $\Delta E = -1.5$ and −1.6 kcal/mol, respectively. While the energetic results are reasonably close to experiment, as also reported by others,[20] the LS state is not calculated directly in this method, but rather is obtained from a set of calcuations on nonphysical states, in all of which the spins are collinear (up or down with respect to single axis). For HS state of the weighted-average BS method, which is represented as either (+,-,+) or

(-,+,+) in Figure 7.2, the spins on A and B cannot be simultaneously antiferromagnetically coupled to C, resulting in a kind of spin frustration. If a variational calculation that allows the spins to be noncollinear shows that indeed they are noncollinear in the LS or HS state or both, then the UD calculations upon which the weighted-average BS method rests do not contain the correct physics.

Consider next the calculations in which we allowed noncollinear spins. The magnetic moments used to initiate the SCF calculation are specified as 120 degrees between A-B, A-C and B-C, all in the *xz* plane. The HS and LS states are obtained by adding a penalty function to the total Hamiltonian to restrain the value of M_S to be approximately 3/2 and 1/2. Other initial magnetic moments configuration (for example, 140 degrees between A-B and 110 degrees between A-C and B-C) have also been tested and lead to the same HS and LS (this shows that the final SCF state is not an arbitrary artifact of the initialization of the iterations). Both the HS and LS states can be directly calculated self-consistently, and we find noncollinear spins in both states and ΔE equal to –0.2 kcal/mol, in good agreement with the experiment. Furthermore, centers A and B are treated nearly symmetrically, all three atomic spins are greater than one (avoiding the pairing of d orbitals), and spin frustration is eliminated.

When the spins are allowed to be noncollinear, the energy is lowered by 7 kcal/mol relative to the best result that could be directly calculated by collinear DFT without BS (Figure 7.2 (a)). For the HS state, noncollinear DFT also gives a state that is lower than the lowest HS obtained by BS-DFT, the (+, -, +) state in Figure 7.2 (b); in particular, the lowering in this case is 2 kcal/mol.

Take the LS state as an example for more detailed discussion; when projected onto the *xz* plane (the *y* components are negligible in our self-consistent solution), the angle between the spin of A and that of B is 135 deg, the angle between the spin of B and that of C is 113 deg, and the angle between the spin of C and that of A is 112 degrees. Because they are all greater than 90 deg, all three spin couplings can be described as more antiferromagnetic than ferromagnetic. Furthermore, since the local spins at the three atomic centers are not even approximately collinear, no version of KS DFT can approximate the wave function of such an LS state, and any KS calculation, including the previous and present BS calculations, since they are based entirely on collinear spins, contains a physically incorrect description.

Finally we return to the choice of state used to optimize the geometry. Comparison of Fig. 7.2(b) to Fig. 7.2(c), and noting that flipping all the signs in any of the Fig. 7.2(b) models does not change the state, we see that of the four states in Fig. 7.2(b), the (+,+,-) one is the one that most resembles the actual LS ground state. Thus, we chose the (+,+,-) state for geometry optimization.

The use of better density functionals for noncollinear calculations and the optimization of geometries with noncollinear calcuations may further improve the quality of the calcuations, and we look forward to being able to do those kinds of calculations, but the present calculations already demonstrate that noncollinear DFT provides a practical way to perform self-consistent calculations on organometallic complexes with noncollinear magnetic states. We conclude that both the HS and LS state of the Mn_3 core in the OEC have noncollinear spins that can be treated self-consistently, and this brings a new element into the description of the magnetic

coupling. Although the collinear weighted-average BS method in recent years has provided practical case-by-case workarounds for some specific systems, we anticipate that noncollinear spins may be a more powerful method for theoretical modeling of transition metal chemistry, and the collinear model of open-shell states should be used with caution, especially in cases where the spin systems are strongly coupled.

References for Chapter 7

(1) Renger, G. Biological Exploitation of Solar Energy by Photosynthetic Water Splitting. *Angew. Chem. Int. Ed.* **1987***, 26*, 643-660.

(2) Kessissoglou, D. P. Homo- and Mixed-Valence EPR-Active Trinuclear Manganese Complex. *Coord. Chem. Rev*. **1999**, *185–186*, 837-858.

(3) Mukhopadhyay, S.; Mandal, S. K.; Bhoduri, S.; Armstrong, W. H. Manganese Clusters with Relevance to Photosystem II. *Chem. Rev.* **2004**, *104*, 3981-4026.

(4) Sproviero, E. M.; Gascón, J. A.; McEvoy, J. P.; Brudvig, G. W.; Batista, V. S. Computational Studies of the O_2-Evolving Complex of Photosystem II and Biomimetic Oxomanganese Complexes. *Coord. Chem. Rev*. **2008**, *252*, 395-415.

(5) Luber, S.; Rivalta, I.; Umena, Y.; Kawakami, K.; Shen, J.-R.; Kamiya, N.; Bruce, D.; Brudvig, G.; Batista, V. S. S_1-State Model of the O_2-Evolving Complex of Photosystem II. *Biochemistry* **2011**, *50*, 6308-6311.

(6) Auger, N.; Girerd, J.-J.; Corbella, M.; Gleizes, A.; Zimmerman, J.-L. Synthesis, Structure, and Magnetic Properties of the Stable Triangular $[Mn(IV)_3O_4]^{4+}$ core. *J. Am. Chem. Soc*. **1990**, *112*, 448-450.

(7) Sarneski, J. E.; Thorp, H. H.; Brudvig, G. W.; Crabtree, R. H.; Shulte, G. K. Assembly of High-Valent Oxomanganese Clusters in Aqueous Solution. Redox Equilibrium of Water-Stable $Mn_3O_4^{4+}$ and $Mn_2O_2^{3+}$ Complexes. *J. Am. Chem. Soc*. **1990**, *112*, 7255-7260.

(8) Marlin, D. S.; Bill, E.; Weyhermüller, T.; Rentschler, E.; Weighardt, K. Long-Distance Magnetic Interaction between a $Mn^{III}Mn^{IV}$ ($S = 1/2$) Core and an Organic Radical: A Spectroscopic Model for the $S_2Y_Z^{\bullet}$ State of Photosystem II. *Angew. Chem. Int. Ed*. **2002**, *41*, 4775-4779.

(9) Kohn, W.; Becke, A. D.; Parr, R. G. Density Functional Theory of Electronic Structure. *J. Phys. Chem*. **1996**, *100*, 12974-12980.

(10) Kohn, W.; Sham, L. J. Self-Consistent Equations Including Exchange and Correlation Effects. *Phys. Rev.* **1965**, *140*, A1133-A1138.

(11) Noodleman, L. Valence Bond Description of Antiferromagnetic Coupling in Transition Metal Dimers. *J. Chem. Phys.* **1981**, *74*, 5737–5743.

(12) Noodleman, L.; Davidson, E. R. Ligand Spin Polarization and Antiferromagnetic Coupling in Transition Metal Dimers. *Chem. Phys.* **1986**, *109*, 131-143.

(13) Neese, F. Prediction of Molecular Properties and Molecular Spectroscopy with Density Functional Theory: From Fundamental Theory to Exchange-Coupling. *Coord. Chem. Rev.* **2009**, *253*, 526-563.

(14) Noodleman, L.; Case, D. A. Density-Functional Theory of Spin Polarization and Spin Coupling in Iron-Sulfur Clusters. *Adv. Inorg. Chem.* **1992**, *38*, 423-470.

Noodleman, L.; Peng, C. Y.; Case, D. A.; Mouesca, J. M. Orbital interactions, electron delocalization and spin coupling in iron-sulfur clusters. *Coord. Chem. Rev.* **1995**, *144*, 199-244.

(15) Ruiz, E.; Rodriguez-Fortea, A.; Cano, J.; Alvarez, S.; Alemany, P. About the Calculation of Exchange Coupling Constants in Polynuclear Transition Metal Complexes. *J. Comput. Chem.* **2003**, *24*, 982-989.

(16) Shoji, M.; Koizumi, K.; Kitagawa, Y.; Kawakami, T.; Yamanaka, S.; Okumura, M.; Yamaguchi, K. A General Algorithm for Calculation of Heisenberg Exchange Integrals J in Multispin Systems. *Chem. Phys. Lett.* **2006**, *432*, 343-347.

(17) Pantazis, D. A.; Orio, M.; Petrenko, T.; Zein, S.; Bill, E.; Lubitz, W.; Messinger, J.; Neese, F. A New Quantum Chemical Approach to the Magnetic Properties of Oligonuclear Transition-Metal Complexes: Application to a Model for the Tetranuclear Manganese Cluster of Photosystem II. *Chem.–Eur. J.* **2009**, *15*, 5108–5123.

(18) Pantazis, D. A.; Orio, M.; Petrenko, T.; Zein, S.; Lubitz, W.; Messinger, J.; Neese, F. Structure of the Oxygen-Evolving Complex of Photosystem II: Information on the S_2 State Through Quantum Chemical Calculation of its Magnetic Properties. *Phys. Chem. Chem. Phys.* **2009**, *11*, 6788-6798.

(19) Schinzel, S.; Schraut, J.; Arbuznikov, A. V.; Siegbahn, P. E. M.; Kaupp, M. Density Functional Calculations of ^{55}Mn, ^{14}N and ^{13}C Electron Paramagnetic Resonance Parameters Support an Energetically Feasible Model System for the

S_2 State of the Oxygen-Evolving Complex of Photosystem II. *Chem.–Eur. J.* **2010**, *16*, 10424-10438.

(20) Baffert, C.; Orio, M.; Pantazis, D. A.; Duboc, C.; Blackman, A. G.; Blondin, G.; Neese, F.; Deronzier, A.; Collomb, M. Trinuclear Terpyridine Frustrated Spin System with a $Mn^{IV}_3O_4$ Core: Synthesis, Physical Characterization, and Quantum Chemical Modeling of Its Magnetic Properties. *Inorg. Chem.* **2009**, *48*, 10281-10288.

(21) Valero, R.; Costa, R.; Moreira, I. de P.R.; Truhlar, D. G.; Illas, F. Performance of the M06 Family of Exchange-Correlation Functionals for Predicting Magnetic Coupling in Organic and Inorganic Molecules, *J. Chem. Phys.* **2008**, *128*, 114103/1-8.

(22) Cramer, C. J.; Truhlar, D. G. Density Functional Theory for Transition Metals and Transition Metal Chemistry. *Phys. Chem. Chem. Phys*. **2009**, *11*, 10757-10816.

(23) Sproviero, E. M.; Gascon, J. A.; McEvoy, J. P.; Brudvig, G. W.; Batista, V. S. Characterization of Synthetic Oxomanganese Complexes and the Inorganic Core of the O_2-Evolving Complex in Photosystem II: Evaluation of the DFT/B3LYP level of theory. *J. Inorg. Biochem.* **2006**, *100*, 786-800.

(24) Stephens, P. J.; Devlin, F. J.; Chabalowski, C. F.; Frisch, M. J. Ab Initio Calculation of Vibrational Absorption and Circular Dichroism Spectra Using Density Functional Force Fields. *J. Phys. Chem*. **1994**, *98*, 11623-11627.

(25) von Barth, U.; Hedin, L. A Local Exchange-Correlation Potential for the Spin Polarized Case. I. *J. Phys. C* **1972**, *5*, 1629-1642.

(26) Rajagopal, A. K.; Callaway, J. Inhomogeneous Electron Gas. *Phys. Rev. B* **1973**, *7*, 1912-1919.

(27) Sandratskii, L. M.; Guletskii, P. G. Symmetrised Method for the Calculation of the Band Structure of Noncollinear Magnets. *J. Phys. F. Met. Phys*. **1986**, *16*, L43-L48.

(28) Fukutome, H. Unrestricted Hartree–Fock theory and its Applications to Molecules and Chemical Reactions. *Int. J. Quantum Chem.* **1981***, 20*, 955-1065.

(29) Löwdin, P.-O.; Mayer, I. Some Studies of the General Hartree–Fock Method. *Adv. Quantum Chem.* **1992***, 24*, 79-114.

(30) Hammes-Schiffer, S.; Andersen, H. C. The Advantages of the General Hartree–Fock Method for Future Computer Simulation of Materials. *J. Chem. Phys.* **1993***, 99*, 1901-1913.

(31) Yamaguchi, K.; Yamanaka, S.; Nishino, M.; Takano, Y.; Kitagawa, Y.; Nagao, H.; Yoshioka, Y. Symmetry and Broken Symmetries in Molecular Orbital Descriptions of Unstable Molecules II. Alignment, Frustration, and Tunneling of Spins in Mesoscopic Molecular Magnets. *Theor. Chem. Acc.* **1999***, 102*, 328-345.

(32) Yamanaka, S.; Yamaki, D.; Shigeta, Y.; Nagao, H.; Yamaguchi, K. Noncollinear Spin Density Functional Theory for Spin-Frustrated and Spin-Degenerate Systems. *Int. J. Quantum Chem.* **2001**, *84*, 670-676.

(33) van Wüllen, C. Spin Densities in Two-Component Relativistic Density Functional Calculations: Noncollinear Versus Collinear Approach. *J. Comput. Chem*. **2002**, *23*, 779-785.

(34) Gebauer, R.; Baroni, S. Magnons in Real Materials from Density-Functional Theory. *Phys. Rev. B* **2000**, *61*, R6459-R6462.

(35) Sharma, S.; Dewhurst, J. K.; Ambrosch-Draxl, C.; Kurth, S.; Helbig, N.; Pittalis, S.; Shallcross, S.; Nordström, L.; Gross, E. K. U. First-Principles Approach to Noncollinear Magnetism: Towards Spin Dynamics. *Phys. Rev. Lett.* **2007**, *98*, 196405/1-4.

(36) Sticht, J.; Höck, K.-H.; Kubler, J. Non-Collinear Itinerant Magnetism: The Case of Mn_3Sn. *J. Phys. Condens. Matter* **1989**, *1*, 8155-8170.

(37) Oda, T.; Pasquarello, A.; Car, R. Fully Unconstrained Approach to Noncollinear Magnetism: Application to Small Fe Clusters. *Phys. Rev. Lett*. **1998**, *80*, 3622-3625.

(38) Hobbs, D.; Kresse, G.; Hafner, J. Fully Unconstrained Noncollinear Magnetism Within the Projector Augmented-Wave Method. *Phys. Rev. B* **2000**, *62*, 11556-11570.

(39) Anton, J.; Fricke, B.; Engel, E. Noncollinear and Collinear Relativistic Density-Functional Program for Electric and Magnetic Properties of Molecules. *Phys. Rev. A* **2004**, *69*, 012505/1-10.

(40) Longo, R. C.; Alemany, M. M. G.; Ferrer, J.; Vega, A.; Gallego, L. J. A Density-Functional Study of the Possibility of Noncollinear Magnetism in

Small Mn Clusters Using Siesta and the Generalized Gradient Approximation to Exchange and Correlation. *J. Chem. Phys*. **2008**, *121*, 114315/1-5.

(41) Soncini, A.; Chibotaru, L. F. Molecular Spintronics Using Noncollinear Magnetic Molecules. *Phys. Rev. B* **2010**, *81*, 132403/1-4.

(42) Giannozzi, P. et al. QUANTUM ESPRESSO: A Modular and Open-Source Software Project for Quantum Simulations of Materials.*J. Phys. Condens. Matter* **2009**, *21*, 395502/1-19.

(43) Slater, J. C. In *Quantum Theory of Molecular and Solids*, *Vol. 4*, McGraw-Hill: New York, 1974.

(44) Vosko, S. H.; Wilk, L.; Nusair, M. Accurate Spin-Dependent Electron Liquid Correlation Energies for Local Spin Density Calculations: A Critical Analysis. *Can. J. Phys.* **1980**, *58*, 1200-1211.

(45) Rappe, A. M.; Rabe, K. M.; Kaxiras, E.; Joannopoulos, J. D. Optimized Pseudopotentials. *Phys. Rev. B* **1990**, *41*, 1227-1230.

(46) Louie, S. G.; Froyen, S.; Cohen, M. L. Nonlinear Ionic Pseudopotentials in Spin-Density-Functional Calculations. *Phys. Rev. B* **1982**, *26*, 1738-1742.

(47) Makov, G.; Payne, M. C. Periodic Boundary Conditions in Ab Initio Calculations. *Phys. Rev. B* **1995**, *51*, 4014-4022.

(48) te Velde, G.; Bickelhaupt, F. M.; Baerends, E. J.; Fonseca Guerra, C.; van Gisbergen, S. J. A.; Snijders, J. G.; Ziegler, T. *J. Comput.Chem.* **2001**, *22*, 931–967. *ADF 2010*, SCM, Vrije Universiteit, Amsterdam, 2010.

Table 7.1. Calculated ΔE (kcal/mol) of **1s** by collinear BS DFT and noncollinear DFT

Software	Method	ΔE
ADF	Collinear BS	−1.5
Quantum Espresso	Collinear BS	−1.6
Quantum Espresso	Noncollinear	−0.2
Experiment		−0.2

Table 7.2. Magnitudes and directions of local spins on Mn atoms

State	Spin[a]			
	Total	Mn(A)	Mn(B)	Mn(C)
Noncollinear LS	0.45,–2	1.24,–114	1.25,111	1.22,–2
Noncollinear HS	1.45,0	1.25,–96	1.26,98	1.23,0

[a] S, θ, where S is the magnitude of the expectation value of the spin, and θ is the angle in degrees between $\mathbf{s}$ and the z axis; all spins are in the xz plane (see Fig. 7.2).

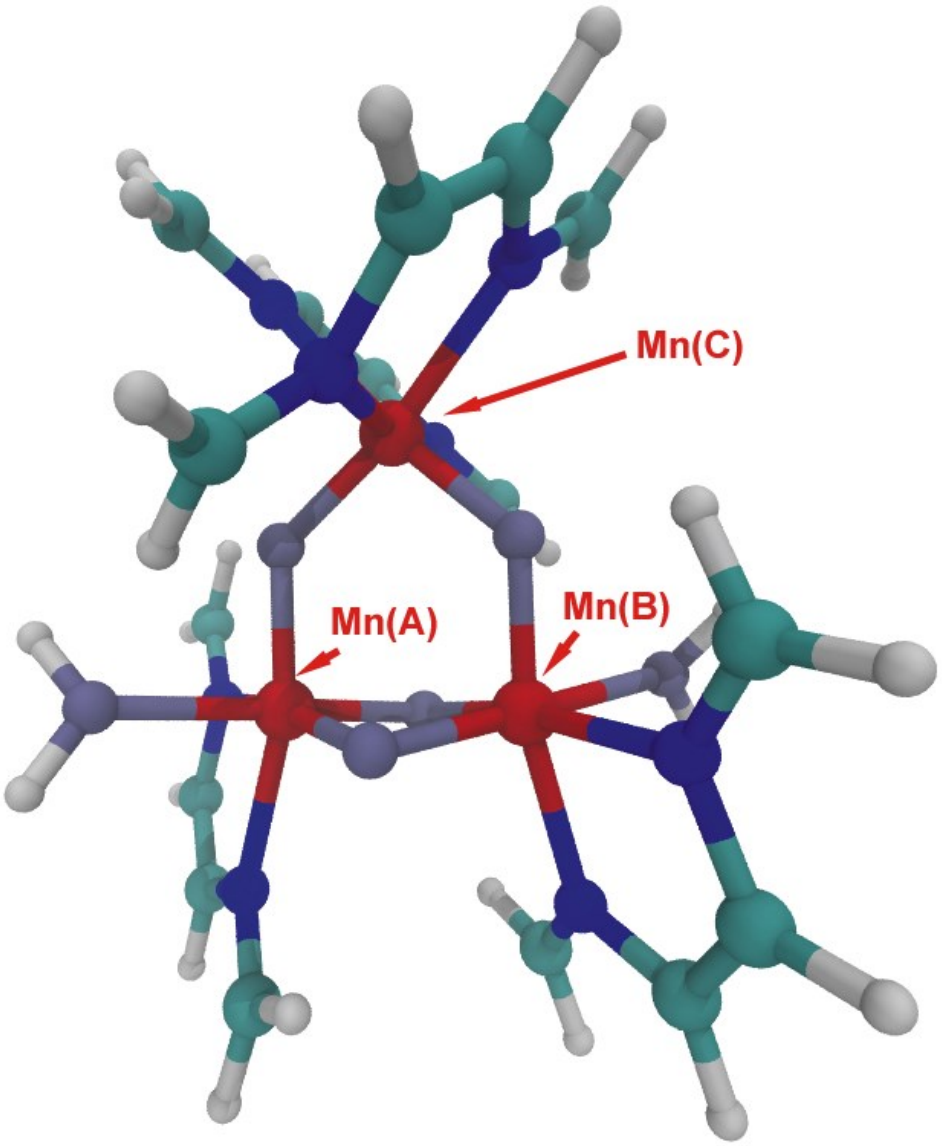

Figure 7.1. 1s.

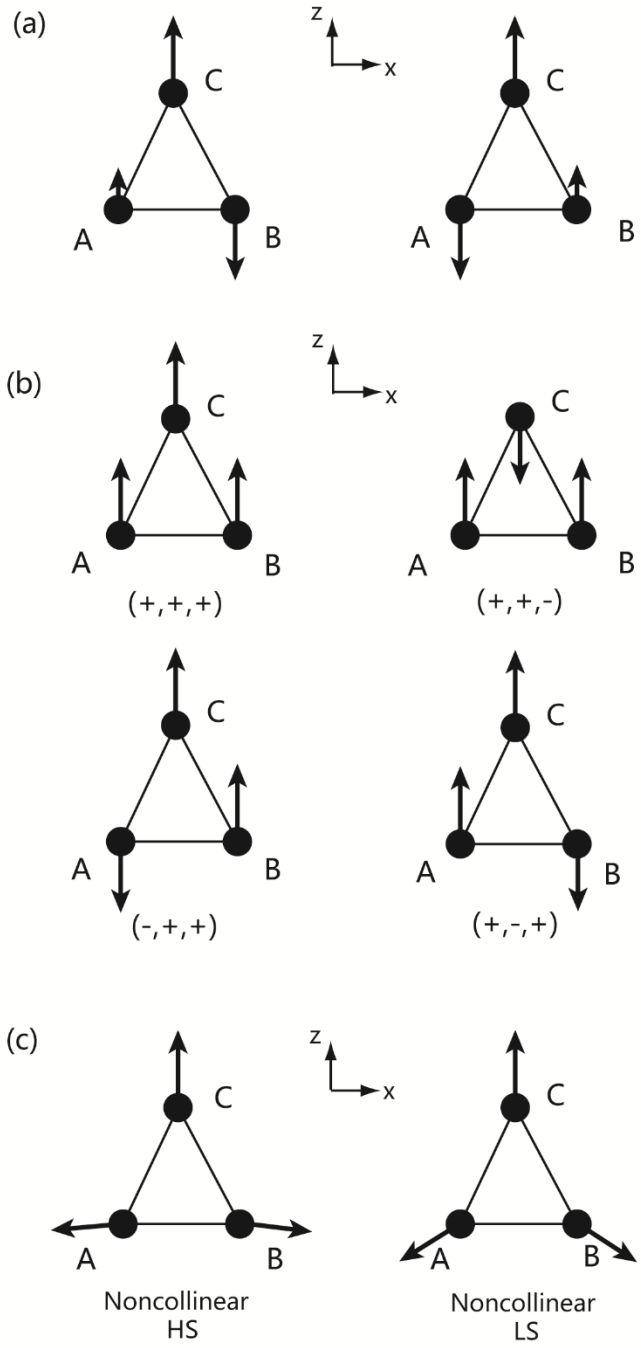

Figure 7.2. (a) The best LS that could be directly calculated by collinear DFT. A pair of d electrons on either A or B is forced to be paired. (b) Four spin states used for the collinear BS method, represented by their spin directions (+ is α spin, – is β spin) on three Mn atoms A, B, and C. Note that the (+,+, -) state is used for geometry optimization. (c) Directions of the Mn magnetic moments in 1s as projected onto the plane of the Mn3. The Mn3 is in the xz plane, with the x axis parallel to the A-B axis. Note that the spin directions in the LS state (ground state) are close to the (+,+,-) state, if the spins on the latter are all flipped.

Bibliography

(1) Abild-Pedersen, F.; Andersson, M. P. *Surf. Sci.* **2007**, *601*, 1747.

(2) Adamo, C.; Barone, V. *Chem. Phys. Lett.* **1997**, *274*, 242.

(3) Adamo, C.; Barone, V. *Chem. Phys. Lett.* **1998**, *298*, 113.

(4) Adamo, C.; Barone, V. *J. Chem. Phys.* **1998**, *108*, 664.

(5) Adamo, C.; Barone, V. *J. Chem. Phys.* **1999**, *110*, 6158.

(6) Adlergolden, S. M.; Langhoff, S. R.; Bauschlicher, C. W.; Carney, G. D. *J. Chem. Phys.* **1985**, *83*, 255.

(7) Alaei, M.; Akbarzadeh, H.; Gholizadeh, H.; de Gironcoli, S. *Phys. Rev. B* **2008**, *77*, 085414.

(8) Andersen, M.; Hornekaer, L.; Hammer, B. *Phys. Rev. B* **2012**, *86*, 085405.

(9) Andersson, K.; Malmqvist, P. A.; Roos, B. O.; Sadlej, A. J.; Wolinski, K. *J. Phys. Chem.* **1990**, *94*, 5483.

(10) Anton, J.; Fricke, B.; Engel, E. *Phys. Rev. A* **2004**, *69*, 012505.

(11) Auger, N.; Girerd, J. J.; Corbella, M.; Gleizes, A.; Zimmermann, J. L. *J. Am. Chem. Soc.* **1990**, *112*, 448.

(12) Bachler, V.; Olbrich, G.; Neese, F.; Wieghardt, K. *Inorg. Chem.* **2002**, *41*, 4179.

(13) Baffert, C.; Orio, M.; Pantazis, D. A.; Duboc, C.; Blackman, A. G.; Blondin, G.; Neese, F.; Deronzier, A.; Collomb, M. N. *Inorg. Chem.* **2009**, *48*, 10281.

(14) Balabanov, N. B.; Peterson, K. A. *J. Chem. Phys.* **2005**, *123*.

(15) Barth, U. v.; Hedin, L. *J. Phys. C* **1972**, *5*, 1629.

(16) Bast, R.; Jensen, H. J. A. A.; Saue, T. *Int. J. Quantum Chem.* **2009**, *109*, 2091.

(17) Bauernschmitt, R.; Ahlrichs, R. *J. Chem. Phys.* **1996**, *104*, 9047.

(18) Becke, A. D. *Phys. Rev. A* **1988**, *38*, 3098.

(19) Becke, A. D. *J. Chem. Phys.* **1993**, *98*, 5648.

(20) Becke, A. D. *J. Chem. Phys.* **1993**, *98*, 1372.

(21) Becke, A. D. *J. Chem. Phys.* **1996**, *104*, 1040.

(22) Becke, A. D. *J. Chem. Phys.* **1998**, *109*, 2092.

(23) Becke, A. D. *J. Chem. Phys.* **2013**, *139*, 021104.

(24) Blochl, P. E. *Phys. Rev. B* **1994**, *50*, 17953.

(25) Boese, A. D.; Handy, N. C. *J. Chem. Phys.* **2001**, *114*, 5497.

(26) Boese, A. D.; Handy, N. C. *J. Chem. Phys.* **2002**, *116*, 9559.

(27) Boese, A. D.; Martin, J. M. L. *J. Chem. Phys.* **2004**, *121*, 3405.

(28) Bulik, I. W.; Scalmani, G.; Frisch, M. J. *Phys. Rev. B* **2013**, *87*, 35117.

(29) Caballol, R.; Castell, O.; Illas, F.; Moreira, P. R.; Malrieu, J. P. *J. Phys. Chem. A* **1997**, *101*, 7860.

(30) Carpenter, J. E., University of Wisconsin, Madison, WI, 1987.

(31) Carpenter, J. E.; Weinhold, F. *J. Mo.l Struc. Theochem.* **1988**, *46*, 41.

(32) Chai, J. D.; Head-Gordon, M. *Phys. Chem. Chem. Phys.* **2008**, *10*, 6615.

(33) Chai, J. D.; Head-Gordon, M. *J. Chem. Phys.* **2008**, *128*, 084106.

(34) Chan, W. T.; Weng, C. E.; Goddard, J. D. *J. Phys. Chem. A* **2007**, *111*, 4792.

(35) Christoffersen, E.; Liu, P.; Ruban, A.; Skriver, H. L.; Norskov, J. K. *J. Catal.* **2001**, *199*, 123.

(36) Clark, T.; Chandrasekhar, J.; Spitznagel, G. W.; Schleyer, P. V. *J. Comput. Chem.* **1983**, *4*, 294.

(37) Cooper, V. R. *Phys. Rev. B* **2010**, *81*, 161104.

(38) Cramer, C. J.; Truhlar, D. G. *Phys. Chem. Chem. Phys.* **2009**, *11*, 10757.

(39) Curtiss, L. A.; Raghavachari, K.; Redfern, P. C.; Rassolov, V.; Pople, J. A. *J. Chem. Phys.* **1998**, *109*, 7764.

(40) Curtiss, L. A.; Redfern, P. C.; Raghavachari, K.; Pople, J. A. *J. Chem. Phys.* **2001**, *114*, 108.

(41) Doll, K. *Surf. Sci.* **2004**, *573*, 464.

(42) Douglas, M.; Kroll, N. M. *Anna. Phys.* **1974**, *82*, 89.

(43) Fast, P. L.; Corchado, J. C.; Sanchez, M. L.; Truhlar, D. G. *J. Phys. Chem. A* **1999**, *103*, 5129.

(44) Fast, P. L.; Sanchez, M. L.; Truhlar, D. G. *Chem. Phys. Lett.* **1999**, *306*, 407.

(45) Feibelman, P. J.; Hammer, B.; Norskov, J. K.; Wagner, F.; Scheffler, M.; Stumpf, R.; Watwe, R.; Dumesic, J. *J. Phys. Chem. B* **2001**, *105*, 4018.

(46) Ferrighi, L.; Hammer, B.; Madsen, G. K. H. *J. Am. Chem. Soc.* **2009**, *131*, 10605.

(47) Ferrighi, L.; Madsen, G. K. H.; Hammer, B. *J. Chem. Phys.* **2011**, *135*, 084704.

(48) Ferrighi, L.; Pan, Y. X.; Gronbeck, H.; Hammer, B. *J. Phys. Chem. C* **2012**, *116*, 7374.

(49) Foster, J. P.; Weinhold, F. *J. Am. Chem. Soc.* **1980**, *102*, 7211.

(50) Frisch, M. J.; Trucks, G. W.; Schlegel, H. B.; Scuseria, G. E.; Robb, M. A.; Cheeseman, J. R.; Scalmani, G.; Barone, V.; Mennucci, B.; Petersson, G. A.; Nakatsuji, H.; Caricato, M.; Li, X.; Hratchian, H. P.; Izmaylov, A. F.; Bloino, J.; Zheng, G.; Sonnenberg, J. L.; Hada, M.; Ehara, M.; Toyota, K.; Fukuda, R.; Hasegawa, J.; Ishida, M.; Nakajima, T.; Honda, Y.; Kitao, O.; Nakai, H.; Vreven, T.; Montgomery, J. A., Jr.; Peralta, J. E.; Ogliaro, F.; Bearpark, M.; Heyd, J. J.; Brothers, E.; Kudin, K. N.; Staroverov, V. N.; Kobayashi, R.; Normand, J.; Raghavachari, K.; Rendell, A.; Burant, J. C.; Iyengar, S. S.; Tomasi, J.; Cossi, M.; Rega, N.; Millam, J. M.; Klene, M.; Knox, J. E.; Cross, J. B.; Bakken, V.; Adamo, C.; Jaramillo, J.; Gomperts, R.; Stratmann, R. E.; Yazyev, O.; Austin, A. J.; Cammi, R.; Pomelli, C.; Ochterski, J. W.; Martin, R. L.; Morokuma, K.; Zakrzewski, V. G.; Voth, G. A.; Salvador, P.; Dannenberg, J. J.; Dapprich, S.; Daniels, A. D.; Farkas, O.; Foresman, J. B.; Ortiz, J. V.; Cioslowski, J.; Fox, D. J.; C01 ed.; Gaussian, Inc.: Wallingford, CT, 2009.

(51) Fukutome, H. *Int. J. Quantum Chem.* **1981**, *20*, 955.

(52) Gáspár, R. *Acta. Phys. Hung.* **1974**, *35*, 213.

(53) Gebauer, R.; Baroni, S. *Phys. Rev. B* **2000**, *61*, R6459.

(54) Giannozzi, P.; Baroni, S.; Bonini, N.; Calandra, M.; Car, R.; Cavazzoni, C.; Ceresoli, D.; Chiarotti, G. L.; Cococcioni, M.; Dabo, I.; Dal Corso, A.; de Gironcoli, S.; Fabris, S.; Fratesi, G.; Gebauer, R.; Gerstmann, U.; Gougoussis, C.; Kokalj, A.; Lazzeri, M.; Martin-Samos, L.; Marzari, N.; Mauri, F.; Mazzarello, R.; Paolini, S.; Pasquarello, A.; Paulatto, L.; Sbraccia, C.; Scandolo, S.; Sclauzero, G.; Seitsonen, A. P.; Smogunov, A.; Umari, P.; Wentzcovitch, R. M. *J. Phys. Condens. Mat.* **2009**, *21*, 395502/1.

(55) Goerigk, L.; Grimme, S.; Vol. 2011.

(56) Goerigk, L.; Grimme, S. *J. Chem. Theory Comput.* **2011**, *7*, 291.

(57) Goerigk, L.; Grimme, S. *Phys. Chem. Chem. Phys.* **2011**, *13*, 6670.

(58) Goerigk, L.; Kruse, H.; Grimme, S. *Chemphyschem* **2011**, *12*, 3421.

(59) Gorling, A. *Phys. Rev. A* **1993**, *47*, 2783.

(60) Grafenstein, J.; Hjerpe, A. M.; Kraka, E.; Cremer, D. *J. Phys. Chem. A* **2000**, *104*, 1748.

(61) Grimme, S. *J. Comput. Chem.* **2006**, *27*, 1787.

(62) Grimme, S. *J. Chem. Phys.* **2006**, *124*, 034108.

(63) Grimme, S. *WIRES Comput. Mol. Sci.* **2011**, *1*, 211.

(64) Grimme, S.; Antony, J.; Ehrlich, S.; Krieg, H. *J. Chem. Phys.* **2010**, *132*, 154104.

(65) Grimme, S.; Muck-Lichtenfeld, C. *Isr. J. Chem.* **2012**, *52*, 180.

(66) Gunnarsson, O.; Jones, R. O. *Phys. Rev. B* **1985**, *31*, 7588.

(67) Halgren, T. A.; Lipscomb, W. N. *Chem. Phys. Lett.* **1977**, *49*, 225.

(68) Hammer, B.; Hansen, L. B.; Norskov, J. K. *Phys. Rev. B* **1999**, *59*, 7413.

(69) Hammes-Schiffer, S.; Andersen, H. C. *J. Chem. Phys.* **1993**, *99*, 523.

(70) Hammes-Schiffer, S.; Andersen, H. C. *J. Chem. Phys.* **1993**, *99*, 1901.

(71) Hamprecht, F. A.; Cohen, A. J.; Tozer, D. J.; Handy, N. C. *J. Chem. Phys.* **1998**, *109*, 6264.

(72) Handy, N. C.; Cohen, A. J. *Mol. Phys.* **2001**, *99*, 403.

(73) Hartree, D. R.; Black, M. M. *Proc. Roy. Soc. A* **1933**, *139*, 311.

(74) Hay, P. J.; Dunning, T. H.; Goddard, W. A. *J. Chem. Phys.* **1975**, *62*, 3912.

(75) Henderson, T. M.; Izmaylov, A. F.; Scalmani, G.; Scuseria, G. E. *J. Chem. Phys.* **2009**, *131*,
044108.

(76) Hertwig, R. H.; Koch, W. *Chem. Phys. Lett.* **1997**, *268*, 345.

(77) Hess, B. A. *Phys. Rev. A* **1986**, *33*, 3742.

(78) Heyd, J.; Scuseria, G. E.; Ernzerhof, M. *J. Chem. Phys.* **2003**, *118*, 8207.

(79) Hobbs, D.; Hafner, J.; Spisak, D. *Phys. Rev. B* **2003**, *68*, 014407.

(80) Hobbs, D.; Kresse, G.; Hafner, J. *Phys. Rev. B* **2000**, *62*, 11556.

(81) Hoe, W. M.; Cohen, A. J.; Handy, N. C. *Chem. Phys. Lett.* **2001**, *341*, 319.

(82) Hohenberg, P.; Kohn, W. *Phys. Rev.* **1964**, *136*, B864.

(83) Huenerbein, R.; Schirmer, B.; Moellmann, J.; Grimme, S. *Phys. Chem. Chem. Phys.* **2010**, *12*, 6940.

(84) Huzinaga, S.; Kolbukowski, M. *Chem. Phys. Lett.* **1993**, *212*, 260.

(85) Iikura, H.; Tsuneda, T.; Yanai, T.; Hirao, K. *J. Chem. Phys.* **2001**, *115*, 3540.

(86) Jacob, C. R.; Reiher, M. *Int. J. Quantum Chem.* **2012**, *112*, 3661.

(87) Jansen, G.; Hess, B. A. *Phys. Rev. A* **1989**, *39*, 6016.

(88) Jiang, W. Y.; Jeffrey, C. C.; Wilson, A. K. *J. Phys. Chem. A* **2012**, *116*, 9969.

(89) Jimenez-Hoyos, C. A.; Henderson, T. M.; Scuseria, G. E. *J. Chem. Theory Comput.* **2011**, *7*, 2667.

(90) Johnson, E. R.; Becke, A. D. *Can. J. Chem.* **2009**, *87*, 1369.

(91) Kannemann, F. O.; Becke, A. D. *J. Chem. Theory Comput.* **2009**, *5*, 719.

(92) Karadakov, P. B. *J. Phys. Chem. A* **2008**, *112*, 12707.

(93) Karton, A.; Gruzman, D.; Martin, J. M. L. *J. Phys. Chem. A* **2009**, *113*, 8434.

(94) Karton, A.; Rabinovich, E.; Martin, J. M. L.; Ruscic, B. *J. Chem. Phys.* **2006**, *125*, 144108.

(95) Karton, A.; Tarnopolsky, A.; Lamere, J. F.; Schatz, G. C.; Martin, J. M. L. *J. Phys. Chem. A* **2008**, *112*, 12868.

(96) Keal, T. W.; Tozer, D. J. *J. Chem. Phys.* **2005**, *123*, 121103.

(97) Kendall, R. A.; Dunning, T. H.; Harrison, R. J. *J. Chem. Phys.* **1992**, *96*, 6796.

(98) Kessissoglou, D. P. *Coordin. Chem. Rev.* **1999**, *185-6*, 837.

(99) Knizia, G.; Adler, T. B.; Werner, H. J. *J. Chem. Phys.* **2009**, *130*, 054104.

(100) Kohn, W.; Becke, A. D.; Parr, R. G. *J. Phys. Chem.* **1996**, *100*, 12974.

(101) Kohn, W.; Sham, L. J. *Phys. Rev.* **1965**, *140*, A1133.

(102) Korth, M.; Grimme, S. *J. Chem. Theory Comput.* **2009**, *5*, 993.

(103) Kresse, G.; Furthmuller, J. *Comp. Mater. Sci.* **1996**, *6*, 15.

(104) Kresse, G.; Furthmuller, J. *Phys. Rev. B* **1996**, *54*, 11169.

(105) Kresse, G.; Joubert, D. *Phys. Rev. B* **1999**, *59*, 1758.

(106) Krieger, J. B.; Chen, J.; Iafrate, G. J.; Savin, A. In *Electron Correlation and Materials Properties*; Plenum: New York, 1999.

(107) Krishnan, R.; Binkley, J. S.; Seeger, R.; Pople, J. A. *J. Chem. Phys.* **1980**, *72*, 650.

(108) Kubler, J.; Hock, K. H.; Sticht, J.; Williams, A. R. *J. Phys. F* **1988**, *18*, 469.

(109) Laidig, W. D.; Schaefer, H. F. *J. Chem. Phys.* **1981**, *74*, 3411.

(110) Lee, C. T.; Yang, W. T.; Parr, R. G. *Phys. Rev. B* **1988**, *37*, 785.

(111) Lee, K.; Murray, E. D.; Kong, L. Z.; Lundqvist, B. I.; Langreth, D. C. *Phys. Rev. B* **2010**, *82*.

(112) Lee, S. J.; Mukerjee, S.; Ticianelli, E. A.; McBreen, J. *Electrochim. Acta.* **1999**, *44*, 3283.

(113) Li, R.; Peverati, R.; Isegawa, M.; Truhlar, D. G. *J. Phys. Chem. A* **2012**, *117*, 169.

(114) Liu, P.; Logadottir, A.; Norskov, J. K. *Electrochim. Acta.* **2003**, *48*, 3731.

(115) Ljubic, I.; Sabljic, A. *J. Phys. Chem. A* **2002**, *106*, 4745.

(116) Longo, R. C.; Alemany, M. M. G.; Ferrer, J.; Vega, A.; Gallego, L. J. *J. Chem. Phys.* **2008**, *128*, 114315/1.

(117) Longo, R. C.; Noya, E. G.; Gallego, L. J. *Phys. Rev. B* **2005**, *72*, 174409.

(118) Louie, S. G.; Froyen, S.; Cohen, M. L. *Phys. Rev. B* **1982**, *26*, 1738.

(119) Löwdin, P. O. *J. Math. Phys.* **1962**, *3*, 969.

(120) Lowdin, P. O.; Mayer, I. *Adv. Quantum. Chem.* **1992**, *24*, 79.

(121) Luber, S.; Rivalta, I.; Umena, Y.; Kawakami, K.; Shen, J. R.; Kamiya, N.; Brudvig, G. W.; Batista, V. S. *Biochemistry* **2011**, *50*, 6308.

(122) Lunell, S. *Chem. Phys. Lett.* **1972**, *13*, 93.

(123) Luo, S. J.; Rivalta, I.; Batista, V.; Truhlar, D. G. *J. Phys. Chem. Lett.* **2011**, *2*, 2629.

(124) Luo, S. J.; Truhlar, D. G. *J. Chem. Theory Comput.* **2012**, *8*, 4112.

(125) Lynch, B. J.; Fast, P. L.; Harris, M.; Truhlar, D. G. *J. Phys. Chem. A* **2000**, *104*, 4811.

(126) Lynch, B. J.; Truhlar, D. G. *J. Phys. Chem. A* **2003**, *107*, 3898.

(127) Lynch, B. J.; Zhao, Y.; Truhlar, D. G. *J. Phys. Chem. A* **2003**, *107*, 1384.

(128) Lynch, B. J.; Zhao, Y.; Truhlar, D. G. *J. Phys. Chem. A* **2005**, *109*, 1643.

(129) Madsen, G. K. H.; Ferrighi, L.; Hammer, B. *J. Phys. Chem. Lett.* **2010**, *1*, 515.

(130) Makov, G.; Payne, M. C. *Phys. Rev. B* **1995**, *51*, 4014.

(131) Mantina, M.; Valero, R.; Truhlar, D. G. *J. Chem. Phys.* **2009**, *131*, 064706.

(132) Marlin, D. S.; Bill, E.; Weyhermuller, T.; Rentschler, E.; Wieghardt, K. *Angew. Chem. Int. Edit.* **2002**, *41*, 4775.

(133) McWeeny, R.; Diercksen, G. *J. Chem. Phys.* **1968**, *49*, 4852.

(134) Modestov, A. D.; Tarasevich, M. R.; Filimonov, V. Y.; Davydova, E. S. *Electrochim. Acta.* **2010**, *55*, 6073.

(135) Moore, C. E. *Atomic Energy Levels*; National Bureau of Standards: Washington, DC, 1949-1958; Vol. 1-3.

(136) Mukhopadhyay, S.; Mandal, S. K.; Bhaduri, S.; Armstrong, W. H. *Chem. Rev.* **2004**, *104*, 3981.

(137) Murray, E. D.; Lee, K.; Langreth, D. C. *J. Chem. Theory Comput.* **2009**, *5*, 2754.

(138) Nakano, H.; Nakajima, T.; Tsuneda, T.; Hirao, K. In *Theory and Applications of Computational Chemistry: The First Forty Years*; Dykstra, C. A., Frenking, G., Kim, K. S., Scuseria, G. E., Eds.; Elsevier: Amsterdam, 2005, p 507.

(139) Neese, F. *Coordin. Chem. Rev.* **2009**, *253*, 526.

(140) Nishino, M.; Yamanaka, S.; Yoshioka, Y.; Yamaguchi, K. *J. Phys. Chem. A* **1997**, *101*, 705.

(141) Noga, J.; Kedzuch, S.; Simunek, J.; Ten-no, S. *J. Chem. Phys.* **2008**, *128*, 174103.

(142) Noodleman, L. *J. Chem. Phys.* **1981**, *74*, 5737.

(143) Noodleman, L.; Case, D. A. *Adv. Inorg. Chem.* **1992**, *38*, 423.

(144) Noodleman, L.; Davidson, E. R. *Chem. Phys.* **1986**, *109*, 131.

(145) Noodleman, L.; Han, W. G. *J. Biol. Inorg. Chem.* **2006**, *11*, 674.

(146) Noodleman, L.; Peng, C. Y.; Case, D. A.; Mouesca, J. M. *Coordin. Chem. Rev.* **1995**, *144*, 199.

(147) Oda, T.; Pasquarello, A.; Car, R. *Phys. Rev. Lett.* **1998**, *80*, 3622.

(148) Paier, J.; Hirschl, R.; Marsman, M.; Kresse, G. *J. Chem. Phys.* **2005**, *122*, 234102.

(149) Pantazis, D. A.; Orio, M.; Petrenko, T.; Zein, S.; Bill, E.; Lubitz, W.; Messinger, J.; Neese, F. *Chem.-Eur. J.* **2009**, *15*, 5108.

(150) Pantazis, D. A.; Orio, M.; Petrenko, T.; Zein, S.; Lubitz, W.; Messinger, J.; Neese, F. *Phys. Chem. Chem. Phys.* **2009**, *11*, 6788.

(151) Papajak, E.; Truhlar, D. G. *J. Chem. Theory Comput.* **2011**, *7*, 10.

(152) Peralta, J. E.; Scuseria, G. E.; Frisch, M. J. *Phys. Rev. B* **2007**, *75*, 125119.

(153) Perdew, J. P. *Phys. Rev. B* **1986**, *33*, 8822.

(154) Perdew, J. P. *Electronic Structure of Solids '91*; Akademie Verlag: Berlin, 1991.

(155) Perdew, J. P.; Burke, K.; Ernzerhof, M. *Phys. Rev. Lett.* **1996**, *77*, 3865.

(156) Perdew, J. P.; Burke, K.; Ernzerhof, M. *Phys. Rev. Lett.* **1997**, *78*, 1396.

(157) Perdew, J. P.; Kurth, S.; Zupan, A.; Blaha, P. *Phys. Rev. Lett.* **1999**, *82*, 2544.

(158) Perdew, J. P.; Ruzsinszky, A.; Csonka, G. I.; Constantin, L. A.; Sun, J. W. *Phys. Rev. Lett.* **2009**, *103*, 026403.

(159) Perdew, J. P.; Ruzsinszky, A.; Csonka, G. I.; Vydrov, O. A.; Scuseria, G. E.; Constantin, L. A.; Zhou, X. L.; Burke, K. *Phys. Rev. Lett.* **2008**, *100*, 136406.

(160) Perdew, J. P.; Yue, W. *Phys. Rev. B* **1986**, *33*, 8800.

(161) Peterson, K. A.; Figgen, D.; Dolg, M.; Stoll, H. *J. Chem. Phys.* **2007**, *126*, 124101.

(162) Peverati, R.; Truhlar, D. G. *J. Phys. Chem. Lett.* **2011**, *2*, 2810.

(163) Peverati, R.; Truhlar, D. G. *J. Chem. Phys.* **2011**, *135*, 191102.

(164) Peverati, R.; Truhlar, D. G. *J. Chem. Theory Comput.* **2012**, *8*, 2310.

(165) Peverati, R.; Truhlar, D. G. *J. Chem. Phys.* **2012**, *136*, 134704.

(166) Peverati, R.; Truhlar, D. G. *Phys. Chem. Chem. Phys.* **2012**, *14*, 13171.

(167) Peverati, R.; Truhlar, D. G. *Phys. Chem. Chem. Phys.* **2012**, *14*, 16187.

(168) Peverati, R.; Truhlar, D. G. *J. Phys. Chem. Lett.* **2012**, *3*, 117.

(169) Peverati, R.; Truhlar, D. G. *Philos. Tran. Roy. Soc. A* **2014**, *372*.

(170) Peverati, R.; Zhao, Y.; Truhlar, D. G. *J. Phys. Chem. Lett.* **2011**, *2*, 1991.

(171) Philipsen, P. H. T.; Baerends, E. J. *Phys. Rev. B* **1996**, *54*, 5326.

(172) Pople, J. A. *Rev. Mod. Phys.* **1999**, *71*, 1267.

(173) Pople, J. A.; Nesbet, R. K. *J. Chem. Phys.* **1954**, *22*, 571.

(174) Purvis, G. D.; Bartlett, R. J. *J. Chem. Phys.* **1982**, *76*, 1910.

(175) Raghavachari, K.; Trucks, G. W.; Pople, J. A.; Headgordon, M. *Chem. Phys. Lett.* **1989**, *157*, 479.

(176) Rajagopal, A. K.; Callaway, J. *Phys. Rev. B* **1973**, *7*, 1912.

(177) Rappe, A. M.; Rabe, K. M.; Kaxiras, E.; Joannopoulos, J. D. *Phys. Rev. B* **1990**, *41*, 1227.

(178) Reed, A. E.; Curtiss, L. A.; Weinhold, F. *Chem. Rev.* **1988**, *88*, 899.

(179) Reed, A. E.; Weinhold, F. *J. Chem. Phys.* **1983**, *78*, 4066.

(180) Reed, A. E.; Weinhold, F. *J. Chem. Phys.* **1985**, *83*, 1736.

(181) Reed, A. E.; Weinstock, R. B.; Weinhold, F. *J. Chem. Phys.* **1985**, *83*, 735.

(182) Reiher, M. *Faraday Discuss.* **2007**, *135*, 97.

(183) Reiher, M.; Salomon, O.; Hess, B. A. *Theor. Chem. Acc.* **2001**, *107*, 48.

(184) Renger, G. *Angew. Chem. Int. Edit.* **1987**, *26*, 643.

(185) Roos, B. O. In *Theory and Applications of Computational Chemistry: The First Forty Years*; Dykstra, C. A., Frenking, G., Kim, K. S., Scuseria, G. E., Eds.; Elsevier: Amersterdam, 2005, p 729.

(186) Roos, B. O.; Lindh, R.; Malmqvist, P. A.; Veryazov, V.; Widmark, P. O. *J. Phys. Chem. A* **2005**, *109*, 6575.

(187) Roothaan, C. C. J. *Rev. Mod. Phys.* **1951**, *23*, 69.

(188) Ruiz, E.; Rodriguez-Fortea, A.; Cano, J.; Alvarez, S.; Alemany, P. *J. Comput. Chem.* **2003**, *24*, 982.

(189) Ruiz-Diaz, P.; Dorantes-Davila, J.; Pastor, G. M. *Eur. Phys. J. D* **2009**, *52*, 175.

(190) Sandratskii, L. M.; Guletskii, P. G. *J. Phys. F* **1986**, *16*, L43.

(191) Sarneski, J. E.; Thorp, H. H.; Brudvig, G. W.; Crabtree, R. H.; Schulte, G. K. *J. Am. Chem. Soc.* **1990**, *112*, 7255.

(192) Sattelmeyer, K. W.; Tirado-Rives, J.; Jorgensen, W. L. *J. Phys. Chem. A* **2006**, *110*, 13551.

(193) Scalmani, G.; Frisch, M. J. *J. Chem. Theory Comput.* **2012**, *8*, 2193.

(194) Schimka, L.; Harl, J.; Stroppa, A.; Gruneis, A.; Marsman, M.; Mittendorfer, F.; Kresse, G. *Nat. Mater.* **2010**, *9*, 741.

(195) Schinzel, S.; Schraut, J.; Arbuznikov, A. V.; Siegbahn, P. E. M.; Kaupp, M. *Chem.-Eur. J.* **2010**, *16*, 10424.

(196) Schmider, H. L.; Becke, A. D. *J. Chem. Phys.* **1998**, *108*, 9624.

(197) Schultz, N. E.; Zhao, Y.; Truhlar, D. G. *J. Phys. Chem. A* **2005**, *109*, 11127.

(198) Schwabe, T.; Grimme, S. *Phys. Chem. Chem. Phys.* **2006**, *8*, 4398.

(199) Seeger, R.; Pople, J. A. *J. Chem. Phys.* **1977**, *66*, 3045.

(200) Seidl, A.; Gorling, A.; Vogl, P.; Majewski, J. A.; Levy, M. *Phys. Rev. B* **1996**, *53*, 3764.

(201) Sharma, S.; Dewhurst, J. K.; Ambrosch-Draxl, C.; Kurth, S.; Helbig, N.; Pittalis, S.; Shallcross, S.; Nordstrom, L.; Gross, E. K. U. *Phys. Rev. Lett.* **2007**, *98*.

(202) Shoji, M.; Koizumi, K.; Kitagawa, Y.; Kawakami, T.; Yamanaka, S.; Okumura, M.; Yamaguchi, K. *Chem. Phys. Lett.* **2006**, *432*, 343.

(203) Shoji, M.; Koizumi, K.; Takeda, R.; Kitagawa, Y.; Yamanaka, S.; Okumura, M.; Yamaguchi, K. *Polyhedron* **2007**, *26*, 2335.

(204) Slater, J. C. *Phys. Rev.* **1929**, *34*, 1293.

(205) Slater, J. C. *Quantum Theory of Molecular and Solids*; McGraw-Hill: New York, 1974; Vol. 4.

(206) Soler, J. M.; Artacho, E.; Gale, J. D.; Garcia, A.; Junquera, J.; Ordejon, P.; Sanchez-Portal, D. *J. Phys. Condens. Mat.* **2002**, *14*, 2745.

(207) Soncini, A.; Chibotaru, L. F. *Phys. Rev. B* **2010**, *81*, 132403/1.

(208) Sproviero, E. M.; Gascon, J. A.; McEvoy, J. P.; Brudvig, G. W.; Batista, V. S. *J. Inorg. Biochem.* **2006**, *100*, 786.

(209) Sproviero, E. M.; Gascon, J. A.; McEvoy, J. P.; Brudvig, G. W.; Batista, V. S. *Coordin. Chem. Rev.* **2008**, *252*, 395.

(210) Staroverov, V. N.; Scuseria, G. E.; Tao, J. M.; Perdew, J. P. *J. Chem. Phys.* **2003**, *119*, 12129.

(211) Stephens, P. J.; Devlin, F. J.; Chabalowski, C. F.; Frisch, M. J. *J. Phys. Chem.* **1994**, *98*, 11623.

(212) Sticht, J.; Hock, K. H.; Kubler, J. *J. Phys. Condens. Mat.* **1989**, *1*, 8155.

(213) Stroppa, A.; Kresse, G. *New J. Phys.* **2008**, *10*, 063020.

(214) Stroppa, A.; Termentzidis, K.; Paier, J.; Kresse, G.; Hafner, J. *Phys. Rev. B* **2007**, *76*, 195440.

(215) Sun, J. W.; Marsman, M.; Ruzsinszky, A.; Kresse, G.; Perdew, J. P. *Phys. Rev. B* **2011**, *83*, 121410.

(216) Tao, J. M.; Perdew, J. P.; Staroverov, V. N.; Scuseria, G. E. *Phys. Rev. Lett.* **2003**, *91*, 146401.

(217) te Velde, G.; Bickelhaupt, F. M.; Baerends, E. J.; Guerra, C. F.; Van Gisbergen, S. J. A.; Snijders, J. G.; Ziegler, T. *J. Comput. Chem.* **2001**, *22*, 931.

(218) Thakkar, A. J.; McCarthy, S. P. *J. Chem. Phys.* **2009**, *131*, 134109.

(219) Truhlar, D. G. *J. Comput. Chem.* **2007**, *28*, 73.

(220) Tsuchiya, T.; Abe, M.; Nakajima, T.; Hirao, K. *J. Chem. Phys.* **2001**, *115*, 4463.

(221) Uhl, M.; Sandratskii, L. M.; Kubler, J. *J. Magn. Magn. Mater.* **1992**, *103*, 314.

(222) Valero, R.; Costa, R.; Moreira, I. D. P. R.; Truhlar, D. G.; Illas, F. *J. Chem. Phys.* **2008**, *128*, 114103.

(223) Van Voorhis, T.; Scuseria, G. E. *J. Chem. Phys.* **1998**, *109*, 400.

(224) van Wullen, C. *J. Comput. Chem.* **2002**, *23*, 779.

(225) Vilhelmsen, L. B.; Hammer, B. *Phys. Rev. Lett.* **2012**, *108*, 126101.

(226) Vitos, L.; Ruban, A. V.; Skriver, H. L.; Kollar, J. *Surf. Sci.* **1998**, *411*, 186.

(227) Vosko, S. H.; Wilk, L.; Nusair, M. *Can. J. Phys.* **1980**, *58*, 1200.

(228) Vydrov, O. A.; Heyd, J.; Krukau, A. V.; Scuseria, G. E. *J. Chem. Phys.* **2006**, *125*, 074106.

(229) Vydrov, O. A.; Scuseria, G. E. *J. Chem. Phys.* **2006**, *125*, 234109.

(230) Weinhold, F.; Carpenter, J. E. *The Structure of Small Molecules and Ions*; Plenum: New York, 1988.

(231) Werner, H. J.; Knowles, P. J.; Knizia, G.; Manby, F. R.; Schutz, M. *WIRES Comput. Mol. Sci.* **2012**, *2*, 242.

(232) Werner, H.-J.; Knowles, P. J.; Manby, F. R.; Schutz, M.; Celani, P.; Knizia, G.; Korona, T.; Lindh, R.; Mitrushenkov, A.; Rauhut, G.; Adler, T. B.; Amos, R. D.; Bernhardsson, A.; Berning, A.; Cooper, D. L.; Deegan, M. J. O.; Dobbyn, A. J.; F. Eckert; Goll, E.; Hampel, C.; Hesselmann, A.; Hetzer, G.; Hrenar, T.; Jansen, G.;

Koppl, C.; Liu, Y.; Lloyd, A. W.; R. A. Mata; May, A. J.; McNicholas, S. J.; Meyer, W.; Mura, M. E.; Nicklaß, A.; Palmieri, P.; Pfluger, K.; Pitzer, R.; Reiher, M.; Shiozaki, T.; Stoll, H.; Stone, A. J.; Tarroni, R.; Thorsteinsson, T.; Wang, M.; Wolf, A.; 2010 ed.; University College Cardiff: Cardiff, 2010.

(233) Wilson, P. J.; Bradley, T. J.; Tozer, D. J. *J. Chem. Phys.* **2001**, *115*, 9233.

(234) Xie, Y. N.; Blackman, J. A. *Phys. Rev. B* **2006**, *73*, 214436.

(235) Yamaguchi, K.; Takahara, Y.; Fueno, T. *Applied Quantum Chemistry*; D. Reidel: Boston, 1986.

(236) Yamaguchi, K.; Yamanaka, S.; Nishino, M.; Takano, Y.; Kitagawa, Y.; Nagao, H.; Yoshioka, Y. *Theor. Chem. Acc.* **1999**, *102*, 328.

(237) Yamanaka, S.; Yamaguchi, K. *B. Chem. Soc. Jpn.* **2004**, *77*, 1269.

(238) Yamanaka, S.; Yamaki, D.; Shigeta, Y.; Nagao, H.; Yamaguchi, K. *Int. J. Quantum Chem.* **2001**, *84*, 670.

(239) Yanagisawa, S.; Tsuneda, T.; Hirao, K. *J. Chem. Phys.* **2000**, *112*, 545.

(240) Yanai, T.; Tew, D. P.; Handy, N. C. *Chem. Phys. Lett.* **2004**, *393*, 51.

(241) Yang, K.; Peverati, R.; Truhlar, D. G.; Valero, R. *J. Chem. Phys.* **2011**, *135*, 044118.

(242) Yang, K.; Zheng, J. J.; Zhao, Y.; Truhlar, D. G. *J. Chem. Phys.* **2010**, *132*, 164117.

(243) Zhao, Y.; Gonzalez-Garcia, N.; Truhlar, D. G. *J. Phys. Chem. A* **2005**, *109*, 2012.

(244) Zhao, Y.; Lynch, B. J.; Truhlar, D. G. *J. Phys. Chem. A* **2004**, *108*, 4786.

(245) Zhao, Y.; Lynch, B. J.; Truhlar, D. G. *Phys. Chem. Chem. Phys.* **2005**, *7*, 43.

(246) Zhao, Y.; Schultz, N. E.; Truhlar, D. G. *J. Chem. Phys.* **2005**, *123*, 161103.

(247) Zhao, Y.; Schultz, N. E.; Truhlar, D. G. *J. Chem. Theory Comput.* **2006**, *2*, 364.

(248) Zhao, Y.; Tishchenko, O.; Gour, J. R.; Li, W.; Lutz, J. J.; Piecuch, P.; Truhlar, D. G. *J. Phys. Chem. A* **2009**, *113*, 5786.

(249) Zhao, Y.; Truhlar, D. G. *J. Phys. Chem. A* **2004**, *108*, 6908.

(250) Zhao, Y.; Truhlar, D. G. *J. Phys. Chem. A* **2005**, *109*, 5656.

(251) Zhao, Y.; Truhlar, D. G. *J. Chem. Phys.* **2006**, *125*, 194101.

(252) Zhao, Y.; Truhlar, D. G. *J. Phys. Chem. A* **2006**, *110*, 13126.

(253) Zhao, Y.; Truhlar, D. G. *J. Chem. Theory Comput.* **2008**, *4*, 1849.

(254) Zhao, Y.; Truhlar, D. G. *Accounts. Chem. Res.* **2008**, *41*, 157.

(255) Zhao, Y.; Truhlar, D. G. *J. Chem. Phys.* **2008**, *128*, 184109.

(256) Zhao, Y.; Truhlar, D. G. *Theor. Chem. Acc.* **2008**, *120*, 215.

(257) Zhao, Y.; Truhlar, D. G. *Chem. Phys. Lett.* **2011**, *502*, 1.

(258) Zheng, J. J.; Yu, T.; Papajak, E.; Alecu, I. M.; Mielke, S. L.; Truhlar, D. G. *Phys. Chem. Chem. Phys.* **2011**, *13*, 10885.